

# NOTE TO USERS

This reproduction is the best copy available.

**UMI<sup>®</sup>**



# Thermodynamic Modeling of the Mg-Al-Sb System

Thevika Thangarajah

A Thesis

in

The Department

of

Mechanical and Industrial Engineering

Presented in Partial Fulfillment of the Requirements  
for the Degree of Master of Applied Science (Mechanical Engineering) at  
Concordia University  
Montreal, Quebec, Canada.

December 2004

© Thevika Thangarajah, 2004



Library and  
Archives Canada

Bibliothèque et  
Archives Canada

Published Heritage  
Branch

Direction du  
Patrimoine de l'édition

395 Wellington Street  
Ottawa ON K1A 0N4  
Canada

395, rue Wellington  
Ottawa ON K1A 0N4  
Canada

*Your file    Votre référence*

*ISBN: 0-494-04433-0*

*Our file    Notre référence*

*ISBN: 0-494-04433-0*

#### NOTICE:

The author has granted a non-exclusive license allowing Library and Archives Canada to reproduce, publish, archive, preserve, conserve, communicate to the public by telecommunication or on the Internet, loan, distribute and sell theses worldwide, for commercial or non-commercial purposes, in microform, paper, electronic and/or any other formats.

The author retains copyright ownership and moral rights in this thesis. Neither the thesis nor substantial extracts from it may be printed or otherwise reproduced without the author's permission.

#### AVIS:

L'auteur a accordé une licence non exclusive permettant à la Bibliothèque et Archives Canada de reproduire, publier, archiver, sauvegarder, conserver, transmettre au public par télécommunication ou par l'Internet, prêter, distribuer et vendre des thèses partout dans le monde, à des fins commerciales ou autres, sur support microforme, papier, électronique et/ou autres formats.

L'auteur conserve la propriété du droit d'auteur et des droits moraux qui protègent cette thèse. Ni la thèse ni des extraits substantiels de celle-ci ne doivent être imprimés ou autrement reproduits sans son autorisation.

---

In compliance with the Canadian Privacy Act some supporting forms may have been removed from this thesis.

Conformément à la loi canadienne sur la protection de la vie privée, quelques formulaires secondaires ont été enlevés de cette thèse.

While these forms may be included in the document page count, their removal does not represent any loss of content from the thesis.

Bien que ces formulaires aient inclus dans la pagination, il n'y aura aucun contenu manquant.

  
**Canada**

# ABSTRACT

## Thermodynamic modeling of the Mg-Al-Sb system

Thevika Thangarajah

Thermodynamic modeling of the Mg-Al-Sb system is carried out as a part of thermodynamic database construction for Mg-Al based alloys. This system was modeled by combining the thermodynamic descriptions of the constituent binaries Mg-Al, Al-Sb, and Mg-Sb. The Mg-Al system has been already studied thoroughly and its database is readily available. Hence, only Al-Sb and Mg-Sb were modeled in the present work considering all available experimental phase diagrams and thermodynamic data in the literature. Liquid phases in both systems were described by the Redlich-Kister polynomial model. High temperature modification of the  $\text{Mg}_3\text{Sb}_2$  compound in the Mg-Sb system was described by the sublattice model.

The constructed database provides a basis to understand the alloys in the Mg-Al-Sb system. It was used to calculate and predict thermodynamic properties, binary phase diagrams of Al-Sb and Mg-Sb, and liquidus projections of the ternary Mg-Al-Sb. The calculated phase diagrams, the thermodynamic properties such as enthalpy, entropy, and Gibbs free energy of mixing, and activity of liquid Al-Sb and Mg-Sb alloys were found to be in good agreement with the experimental data reported in the literature. Moreover, isothermal sections, vertical sections, and phase assemblage diagrams were calculated for the Mg-Al-Sb ternary system, and the invariant reaction points were predicted. The predicted critical points in the Mg-Al-Sb system were 6 ternary eutectics, 2 ternary peritectics, one saddle point and 4 plait points. Mg-Al-Sb ternary phase diagram was modeled for the first time in this work.

# ACKNOWLEDGEMENTS

First of all, I would like to express my deep sense of gratitude to my supervisor Dr. Mamoun Medraj who offered me an opportunity to be a graduate student at Concordia University, and conduct research under his guidance. He gave me all the support and confidence needed to complete this work. I sincerely thank him for spending countless hours discussing my work.

I would like to thank all staff members of our department for their kind help in solving my non-academic and technical problems. Especially, I would like to thank William Wong who solved my computer related problems. Further, I would like to thank Andie Zeliger who was very kind and helpful in every aspect.

I thank the fellow graduate students in my office, who provided me with a perfect research environment to work in with all the fun and offered support whenever needed. Especially, I thank Saher Shakhshir for his help and support during the course of my studies. Our research lab remains one of the most peaceful places in the world.

I thank my parents for their endless love and support. I thank my brother, Ahilan, who constantly wrote me letters and encouraged my studies. And, finally, I would like to thank my husband, Balakumar, for being a part of my success.

# TABLE OF CONTENTS

LIST OF FIGURES.....	viii
LIST OF TABLES.....	xii
<b>CHAPTER 1: INTRODUCTION.....</b>	<b>1</b>
1.1 THE IMPORTANCE OF THERMODYNAMIC MODELING.....	1
1.2 THE IMPORTANCE OF Mg-Al-Sb SYSTEM.....	2
1.3 AN INTRODUCTION TO THE CONSTITUENT BINARIES IN THE Mg-Al-Sb SYSTEM.....	5
1.3.1 Al-Sb binary system.....	5
1.3.2 Mg-Sb binary system.....	6
1.3.3 Mg-Al binary system.....	8
<b>CHAPTER 2: DATA ANALYSIS.....</b>	<b>10</b>
2.1 Al-Sb BINARY SYSTEM.....	10
2.1.1 Phase diagram data.....	10
2.1.2 Thermodynamic data.....	13
2.2 Mg-Sb BINARY SYSTEM.....	16
2.2.1 Phase diagram data.....	16
2.2.2 Thermodynamic data.....	18
2.2.3 Crystal structure data.....	22
2.3 Mg-Al BINARY SYSTEM.....	23

2.3.1	Phase diagram data.....	23
2.3.2	Thermodynamic data.....	26
2.4	Mg-Al-Sb TERNARY SYSTEM.....	29
2.5	THE AIMS OF THIS WORK.....	31
<b>CHAPTER 3: THERMODYNAMIC MODELING.....</b>		<b>32</b>
3.1	THEORY.....	32
3.2	THE GIBBS FREE ENERGY EQUATIONS OF DIFFERENT PHASES IN BINARIES Al-Sb AND Mg-Sb.....	36
3.2.1	Unary phase.....	36
3.2.2	Disordered solution phase.....	36
3.2.3	Stoichiometric compound phase.....	37
3.2.4	Non-stoichiometric phase.....	37
3.3	METHODOLOGY.....	42
3.4	CONSTRUCTION OF BINARY PHASE DIAGRAM.....	45
3.5	TERNARY PHASE DIAGRAM.....	49
<b>CHAPTER 4: RESULTS AND DISCUSSIONS.....</b>		<b>53</b>
4.1	Al-Sb BINARY SYSTEM.....	53
4.1.1	Phase diagram.....	54
4.1.2	Thermodynamic properties.....	55
4.2	Mg-Sb BINARY SYSTEM.....	60
4.2.1	Phase diagram.....	61



4.2.2	Thermodynamic properties.....	62
4.3	Mg-Al-Sb TERNARY SYSTEM.....	66
4.3.1	Polythermal projections of liquidus surfaces.....	66
4.3.2	Ternary isothermal sections.....	71
4.3.3	Pseudo-binary phase diagrams.....	73
4.3.4	Ternary isopleths (at constant composition of one component)	76
4.3.5	Phase assemblage diagrams.....	79
 <b>CHAPTER 5: CONCLUSIONS, CONTRIBUTIONS AND SUGGESTIONS FOR FUTURE WORK.....</b>		 85
5.1	CONCLUSIONS.....	85
5.2	CONTRIBUTIONS.....	86
5.3	SUGGESTIONS FOR FUTURE WORK.....	87
 <b>REFERENCES.....</b>		 88

# LIST OF FIGURES

Figure 1.1:	TEM micrograph of creep specimen of Mg-9Al-0.8Zn-0.2Mn-0.35Sb for 50h at 473 K and 50MPa [7].....	3
Figure 1.2:	Creep curves of the alloys containing Sb tested at 473 K, and 50MPa [7].....	4
Figure 1.3:	Calculated Al-Sb phase diagram [8].....	5
Figure 1.4:	Calculated Mg-Sb phase diagram [12].....	7
Figure 1.5:	Calculated Mg-Al phase diagram [15].....	8
Figure 2.1:	Assessed Al-Sb phase diagram by Redlich-Kister model [10].....	11
Figure 2.2:	Assessed Al-Sb phase diagram by associated solution model [10].....	11
Figure 2.3:	Al-Sb phase diagram [8].....	12
Figure 2.4:	Comparison between calculated and experimental values of heat and entropy of mixing of the Al-Sb system at 1350 K [8].....	14
Figure 2.5:	Comparison between calculated and experimental values of Gibbs free energy of mixing of the Al-Sb system at 1350 K [8].....	15
Figure 2.6:	Activity of components in the liquid Al-Sb alloys.....	16
Figure 2.7:	Experimental Mg-Sb phase diagram [35] .....	17
Figure 2.8:	Activity of Mg in liquid Mg-Sb alloys at 1073 K [37].....	19
Figure 2.9:	Relative integral molar quantities of liquid Mg-Sb alloys at 1073 K [37].....	19
Figure 2.10:	[100] view of the structure of Mg <sub>3</sub> Sb <sub>2</sub> with the unit cell outlined [47]	22

Figure 2.11:	Calculated Al-Mg phase diagram [19].....	24
Figure 2.12:	Optimized Al-Mg phase diagram [21].....	25
Figure 2.13:	Calculated heat of mixing for the liquid phase in Al-Mg [19].....	26
Figure 2.14:	Calculated enthalpy of mixing of Al-Mg liquid alloys at 948 K [21]...	27
Figure 2.15:	Integral enthalpies in liquid Al-Mg alloys [22].....	28
Figure 2.16:	Quasibinary system: Al-Mg <sub>3</sub> Sb <sub>2</sub> [50].....	29
Figure 2.17:	An approximate picture of primary phase distribution in Al-Sb-Mg system [50].....	30
Figure 3.1:	A schematic variation of Gibbs free energy with the arrangement of atoms.....	34
Figure 3.2:	$\beta$ -Mg <sub>3</sub> Sb <sub>2</sub> crystal structure projected on (010).....	39
Figure 3.3:	$\beta$ -Mg <sub>3</sub> Sb <sub>2</sub> crystal structure projected on (111).....	39
Figure 3.4:	Neighboring atoms around Sb1, Sb2, and Mg.....	40
Figure 3.5:	CHALPHAD assessment procedure [59].....	43
Figure 3.6:	CHALPHAD methodology. The assessed excess Gibbs free energies of the constituent subsystems are for extrapolation to a higher component system [1].....	44
Figure 3.7:	The assessment strategy of Mg-Al-Sb ternary system.....	45
Figure 3.8:	Derivation of the eutectic phase diagram from the Gibbs free energy curves for the liquid, $\alpha$ and $\beta$ phases [62].....	47
Figure 3.9:	Common tangent construction in two phase equilibrium.....	48
Figure 3.10:	Gibbs triangle with components A, B and C.....	50
Figure 3.11:	Diagram of a ternary system containing one ternary eutectic [64].....	51

Figure 3.12:	The plan view of the liquidus surface of system shown in Figure 3.11	52
Figure 4.1:	Calculated Al-Sb Phase diagram with experimental data from the literature.....	54
Figure 4.2:	Activity of components in the liquid Al-Sb alloys at 1350 K: comparison between calculated values and the experimental data.....	56
Figure 4.3:	Enthalpy of mixing of liquid Al-Sb alloys at 1350 K: comparison between calculated values and the experimental data.....	57
Figure 4.4:	Entropy of mixing of liquid Al-Sb alloys at 1350 K: comparison between calculated values and the experimental data.....	58
Figure 4.5:	Gibbs free energy of mixing of liquid Al-Sb alloys at 1350 K: comparison between calculated values and the experimental data.....	59
Figure 4.6:	Calculated Mg-Sb Phase diagram with experimental data from the literature.....	61
Figure 4.7:	Activity of component Mg in the liquid Mg-Sb alloys at 1073 K: comparison between calculated values and the experimental data.....	63
Figure 4.8:	Entropy of mixing of liquid Mg-Sb alloys at 1073 K: comparison between calculated values and the experimental data.....	63
Figure 4.9:	Enthalpy of mixing of liquid Mg-Sb alloys at 1073 K: comparison between calculated values and the experimental data.....	64
Figure 4.10:	Gibbs free energy of mixing of liquid Mg-Sb alloys at 1073 K: comparison between calculated values and the experimental data.....	65
Figure 4.11:	Projection of the liquidus surface of the Mg-Al-Sb system onto a	

ternary composition triangle.....	68
Figure 4.12: Different phase fields around the plait points in the Mg-Al-Sb ternary system.....	70
Figure 4.13: Isothermal section of the Mg-Al-Sb system at 1300 K.....	71
Figure 4.14: Isothermal section of the Mg-Al-Sb system at 1400 K.....	72
Figure 4.15: Pseudo-binary diagram of Al-AlSb phase diagram.....	74
Figure 4.16: Pseudo-binary AlSb-Mg <sub>3</sub> Sb <sub>2</sub> phase diagram.....	75
Figure 4.17: Calculated pseudo-binary Al-Mg <sub>3</sub> Sb <sub>2</sub> phase diagram.....	76
Figure 4.18: Isopleth of the Mg-Al-Sb system at $X_{Sb} = 0.5$ .....	77
Figure 4.19: Isopleth of the Mg-Al-Sb system at $X_{Sb} = 0.2$ .....	78
Figure 4.20: Phase assemblage diagram of 40wt% Mg, 30wt% Al, and 30wt% Sb	79
Figure 4.21: Isopleth of the Mg-Al-Sb system at 0.35wt% Sb.....	80
Figure 4.22: Isopleth of the Mg-Al-Sb system at 0.7wt% Sb.....	81
Figure 4.23: Phase assemblage diagram of Mg-9Al-0.35Sb.....	82
Figure 4.24: Phase assemblage diagram of Mg-9Al-0.7Sb.....	83

# LIST OF TABLES

Table 2.1:	Relative integral molar properties, $\Delta G^M$ , $\Delta S^M$ , and $\Delta H^M$ of liquid Mg-Sb alloys [37, 41].....	21
Table 2.2:	Crystal structure and lattice parameter [12].....	23
Table 3.1:	Crystal structure data of $\beta$ -Mn <sub>2</sub> O <sub>3</sub> [54].....	38
Table 4.1:	The optimized model parameters for the liquid and AlSb phases.....	53
Table 4.2:	Comparison between different works (calculations) on the equilibria in the Al-Sb system.....	55
Table 4.3:	Calculated enthalpy and entropy of formation of AlSb with the reported literature data.....	59
Table 4.4:	The optimized parameters for the liquid, $\alpha$ -Mg <sub>3</sub> Sb <sub>2</sub> , and $\beta$ -Mg <sub>3</sub> Sb <sub>2</sub> ....	60
Table 4.5:	Comparison between different works (calculations) on the equilibria in the Mg-Sb system.....	62
Table 4.6:	Calculated enthalpy and entropy of formation of $\alpha$ -Mg <sub>3</sub> Sb <sub>2</sub> with the reported literature data.....	65
Table 4.7:	Calculated invariants points and reactions.....	69

# **CHAPTER 1**

---

## **INTRODUCTION**

### **1.1 THE IMPORTANCE OF THERMODYNAMIC MODELING**

Phase diagrams are the primary visualizing tools in materials science. They represent the state of a material as a function of temperature, pressure, and concentrations of the constituent components and allow one to predict and interpret the change in composition of a material from phase to phase. Hence, phase diagrams play an important role in alloy design, development, processing, and understanding. However, experimental determination of phase diagrams is a time-consuming and expensive task. This becomes more pronounced as the number of components increases. In a multi-component system, the calculation of phase diagrams reduces the effort required to determine the equilibrium conditions.

The foundation for the calculation of phase diagrams was laid by J. W. Gibbs more than a century ago [1]. Since then many researchers continued working in this field and developed solution models, numerical methods, and computer software to permit a quantitative application of thermodynamic principles to phase diagram analysis. Now, for a great many systems, it is possible to perform a simultaneous critical evaluation of available phase diagram measurements and of available thermodynamic data (enthalpy,

entropy, Gibbs free energy, activity, etc.) with a view to obtain optimized equations for the Gibbs free energies for each phase which best represent all data [2]. These equations are consistent with the thermodynamic principles and with theories of solution behavior. Hence, one set of self-consistent equations is enough to describe all the thermodynamic properties and the phase diagram of a multi-component system. Moreover, these sets of self-consistent equations allow both more accurate interpolation and extrapolation of data and calculation of meta-stable phase boundaries. As the present research is a part of an analysis of a multi-component alloy system, it is focused on thermodynamic modeling.

## **1.2 THE IMPORTANCE OF Mg-Al-Sb SYSTEM**

The current need for higher fuel efficient vehicles increases the demand for magnesium alloys due to their light weight and good specific mechanical properties. However, the use of magnesium alloys has been limited due to their poor creep resistance. Hence, new magnesium alloys are needed to meet the automobile and aerospace requirements for elevated temperature strength.

Approximately 90% of all magnesium cast products are being made out of the standard magnesium die-casting alloy AZ91 (Mg- 9.2 Al- 0.88 Zn- 0.34 Mn) [3]. This magnesium alloy has excellent castability and in its high purity form (AZ91E) shows good corrosion resistance. However, it suffers from low creep resistance at temperatures in excess of 393 K which makes it unsuitable for many of the components in automobile engines [3].



Plastic deformation at higher temperature is known as creep. Creep takes different forms such as: logarithmic creep (up to  $0.3T_M$ ), high temperature creep (around  $0.6T_M$ ), and diffusional creep (above  $0.9T_M$ ). For components used in automotive or aerospace applications, the most important type of creep is high temperature creep. It is found that, in the specific case of magnesium and its alloys, grain boundary sliding makes the major contribution to creep strain [4-6].

The resistance to grain boundary sliding can be improved by producing thermally stable grain boundary phases. It is found that small amount of Sb additions to AZ91 based alloys significantly increases the yield strength and creep resistance at elevated temperature up to 473 K [7]. Moreover, the work of Guangyin *et al.* [7] indicated, as shown in Figure 1.1, that the addition of Sb causes the formation of some rod-shaped  $Mg_3Sb_2$  precipitates with hexagonal  $D5_2$  structure which strengthen both matrix and grain boundaries effectively.



**Figure 1.1:** TEM micrograph of creep specimen of Mg-9Al-0.8Zn-0.2Mn-0.35Sb for 50h at 473 K and 50MPa [7]

Figure 1.1 shows that, even after 50 hours of creep at 473 K and 50MPa, fine precipitates of  $Mg_3Sb_2$  were observed in the alloy Mg-9Al-0.8Zn-0.2Mn-0.35Sb. Hence these precipitates are thermally stable. Moreover, it can be observed from Figure 1.2 that addition of Sb increases the creep resistant significantly. Therefore, studying Mg-Al-Sb system is important for understanding and developing creep resistance magnesium alloys in this system.

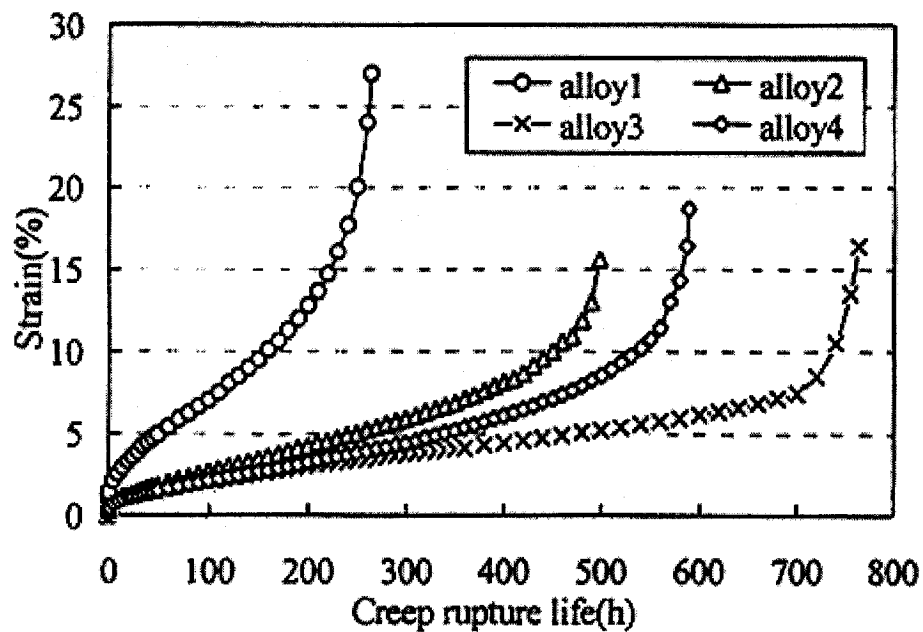


**Figure 1.2:** Creep curves of the alloys containing Sb tested at 473K, and 50MPa [7]. Where alloy1: Mg-9Al-0.8Zn-0.2Mn, alloy2: Mg-9Al-0.8Zn-0.2Mn-0.15Sb, alloy3: Mg-9Al-0.8Zn-0.2Mn-0.35Sb, and alloy4: Mg-9Al-0.8Zn-0.2Mn-0.7Sb

### 1.3 AN INTRODUCTION TO THE CONSTITUENT BINARIES IN Mg-Al-Sb SYSTEM

The Constituent binaries in the Mg-Al-Sb system are: Mg-Al, Al-Sb, and Mg-Sb. The following sections describe the different phases present in each binary and give a brief summary about the previous work on these binary systems.

#### 1.3.1 Al-Sb binary system

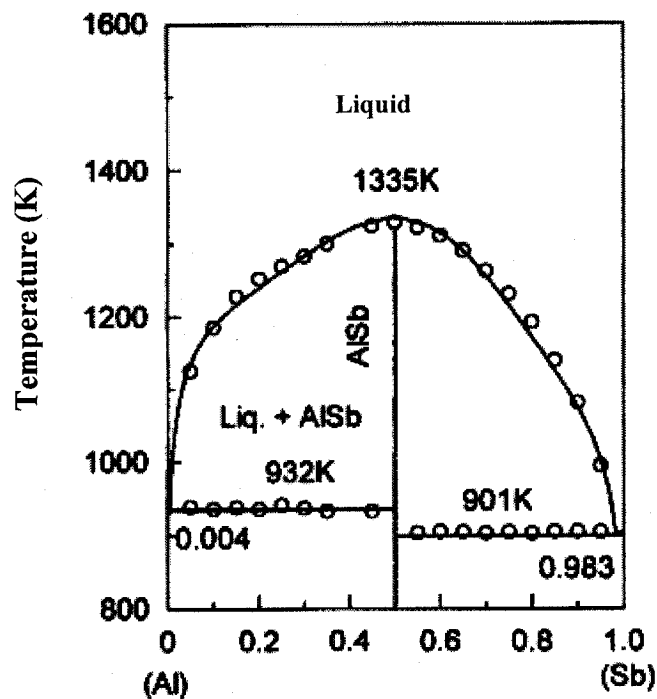
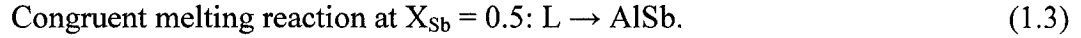
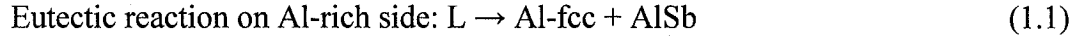


*Figure 1.3: Calculated Al-Sb phase diagram [8]*

Figure 1.3 shows the Al-Sb binary phase diagram. It is a simple phase diagram with two eutectic points and an intermediate line compound AlSb. There is no evidence found in the literature for mutual solubility between Al and Sb. The different phases in this system

are: Al-fcc, Sb-rhombo, AlSb, and liquid. There are three invariant reactions in this system. These reactions are described by equations 1.1, 1.2, and 1.3.



It can be observed from Figure 1.3 that the intermediate compound AlSb shows a higher melting point than that of pure constituents Al and Sb. This is one of the interesting features which drives this research on Mg-Al-Sb.

The latest assessment of Al-Sb system was carried out by Yamaguchi *et al.* [9], they used an associated solution model to describe the liquid phase. Yamaguchi *et al.* [8], Coughanowr *et al.* [10], and Zajackowski and Botor [11] also studied this system and calculated the phase diagram and thermodynamic properties. Among these works Coughanowr *et al.* [10], did only a thermodynamic assessment using the Lukas optimization program.

### 1.3.2 Mg-Sb binary system

Figure 1.4 shows the Mg-Sb binary phase diagram. Different phases in the Mg-Sb system are: liquid, Mg-hcp, Sb-rhombo, and the intermediate compound  $\text{Mg}_3\text{Sb}_2$ . The intermediate compound has two crystalline modifications. They are:  $\alpha\text{-Mg}_3\text{Sb}_2$  and  $\beta\text{-Mg}_3\text{Sb}_2$ . As can be seen from Figure 1.4, these crystalline modifications show very

narrow solubility ranges. Hence, in the present research, the low temperature modification  $\alpha$ - $\text{Mg}_3\text{Sb}_2$  is treated as a stoichiometric compound. However, for the high temperature modification  $\beta$ - $\text{Mg}_3\text{Sb}_2$ , it is necessary to apply a model that allows a variable composition. Otherwise, invariant reactions on the right- and left- hand sides of the  $\beta$ - $\text{Mg}_3\text{Sb}_2$  will occur at the same temperature. Hence, in the present research, the  $\beta$ - $\text{Mg}_3\text{Sb}_2$  is treated as a non-stoichiometric compound with a narrow range of composition towards the Mg-rich side. In this case, there is no evidence available on the types of defects which make the deviation from stoichiometry. Furthermore, it is assumed that there is no solubility between Mg and Sb in this system. Although this system looks simple, it is extremely difficult to get the optimized model parameters due to the unusual liquidus shape of the  $\beta$ - $\text{Mg}_3\text{Sb}_2$ .

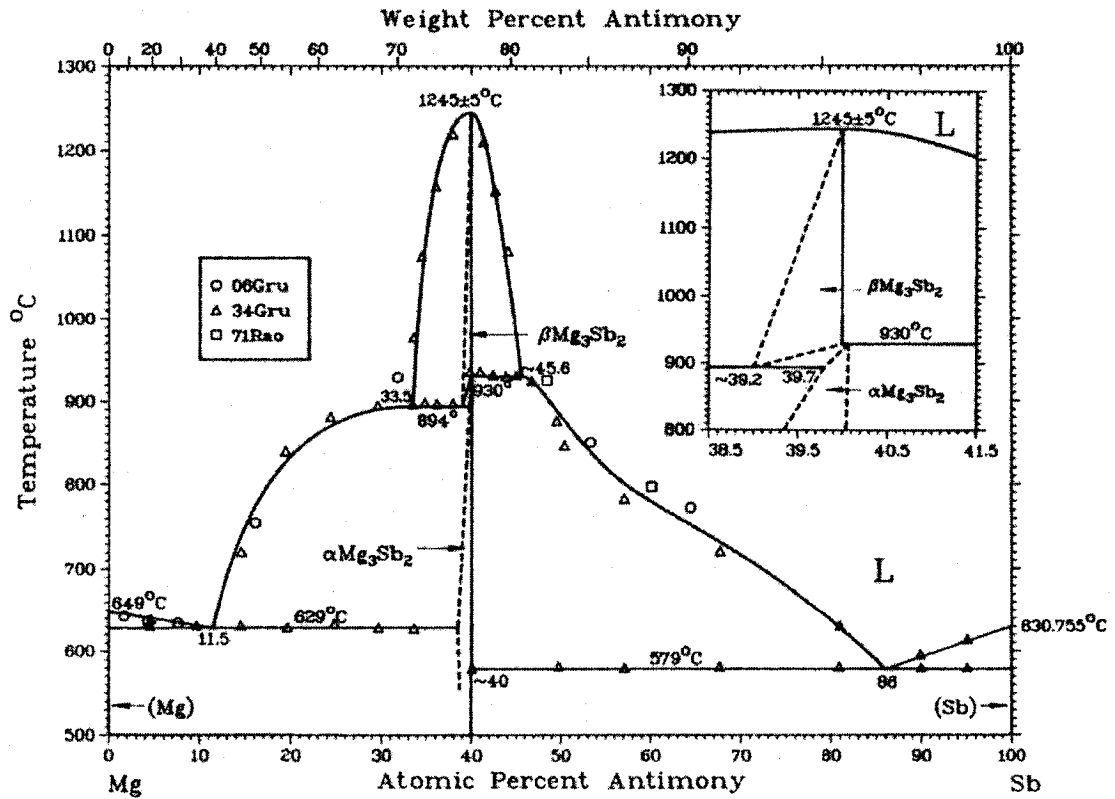
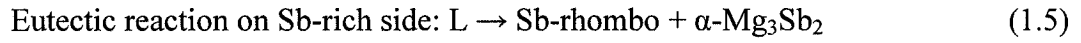


Figure 1.4: Calculated Mg-Sb phase diagram [12]

There are two eutectic points observed. The eutectic reactions are described by equations 1.4, and 1.5.



The Mg-Sb system was previously assessed by Nayeb-Hashemi and Clark [12], and Jönsson and Ågren [13]. Among these two assessments, the latter used a computer operated method developed by Jansson [14] to obtain the thermodynamic descriptions.

### 1.3.3 Mg-Al binary system

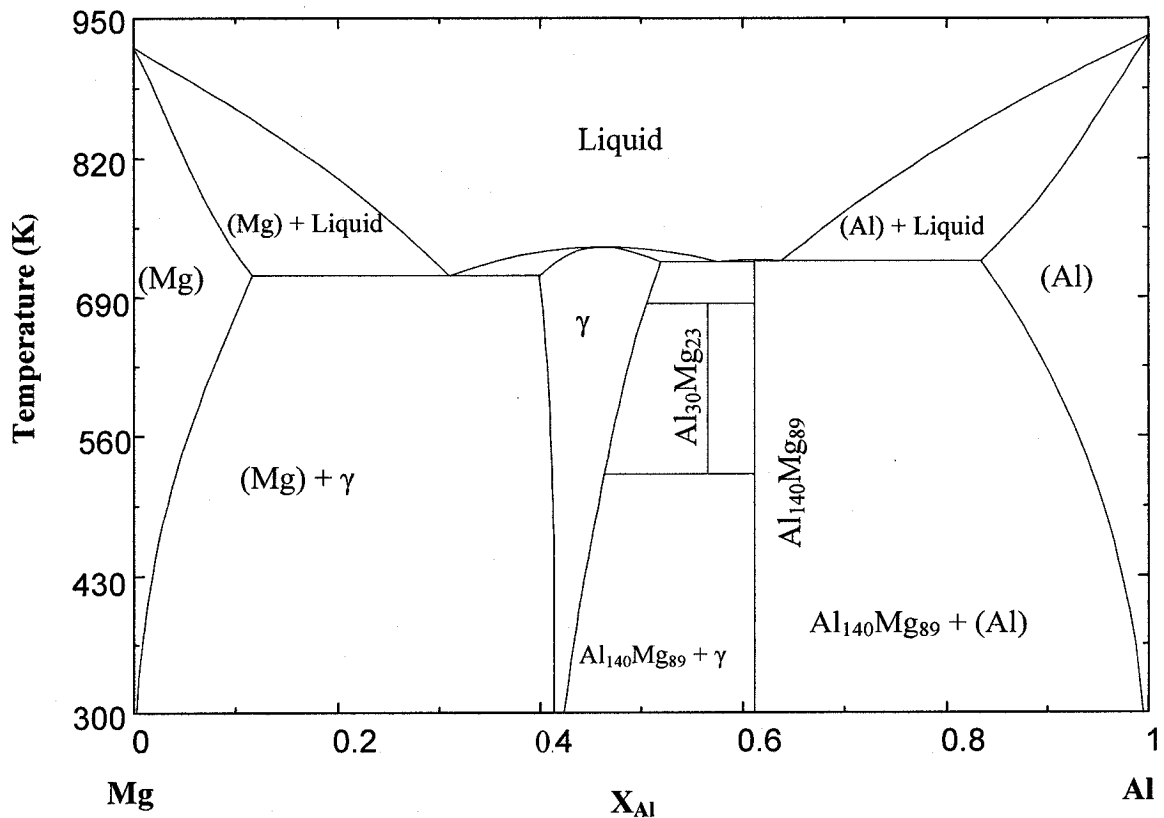
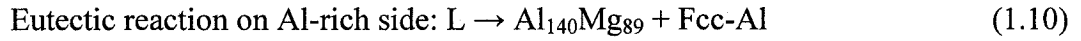
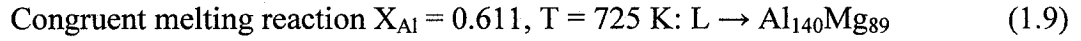
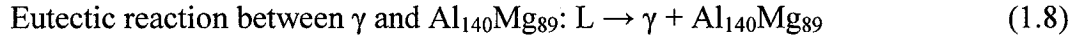
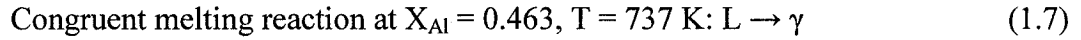


*Figure 1.5: Calculated Mg-Al phase diagram [15]*

Figure 1.5 shows the Mg-Al binary phase diagram. This system has two terminal solid solutions. They are Mg-Hcp and Al-Fcc at the Mg end and Al end respectively. This binary system has two line compounds,  $\text{Al}_{30}\text{Mg}_{23}$  and  $\text{Al}_{140}\text{Mg}_{89}$  and a non-stoichiometric compound Gamma ( $\gamma$ ). The line compound  $\text{Al}_{30}\text{Mg}_{23}$  is stable only in the temperature range of 523 K to 683 K. There are four invariant reactions and they are described by equation 1.6 – 1.10.



This system was thermodynamically modeled by several authors [16-21] and experimentally studied for new thermodynamic data by Moser *et al.* [22]. Moreover, Czeppe *et al.* [23], and Liang *et al.* [24] performed experimental investigation in the central part of the Mg-Al phase diagram. In addition to the experimental investigation, Liang *et al.* [24] carried out thermodynamic calculations too.

The COST 507 project, which aimed at generating a thermochemic database for light metal alloys, was carried out by Ansara *et al.* [15]. In establishing the database for the Mg-Al system, they used the experimental investigation results from Liang *et al.* [24] and this database is found to be the most recent and reliable one for Mg-Al system. Hence, the present research used this database for the Mg-Al binary system.

# CHAPTER 2

---

## DATA ANALYSIS

The accuracy of the thermodynamic model of a system depends on the reliability of the data used in the thermodynamic model parameters optimization. Hence, it is important to select reliable experimental data from the literature for this purpose. The following sections analyze the previous research work on Al-Sb, Mg-Sb, Mg-Al, and Mg-Al-Sb systems, show how reliable data are extracted from a pool of available data and derive the aim of the present research.

### 2.1 Al-Sb BINARY SYSTEM

#### 2.1.1 Phase diagram data

Coughanowr *et al.* [10] reviewed the previous work on the Al-Sb system and carried out an assessment of thermodynamic properties and phase diagram data using the Lukas optimization program. They used Redich-Kister and associated solution models separately and compared the optimized results. It can be observed from Figures 2.1 and 2.2 that, the two models gave slightly different liquidus and eutectic temperatures.



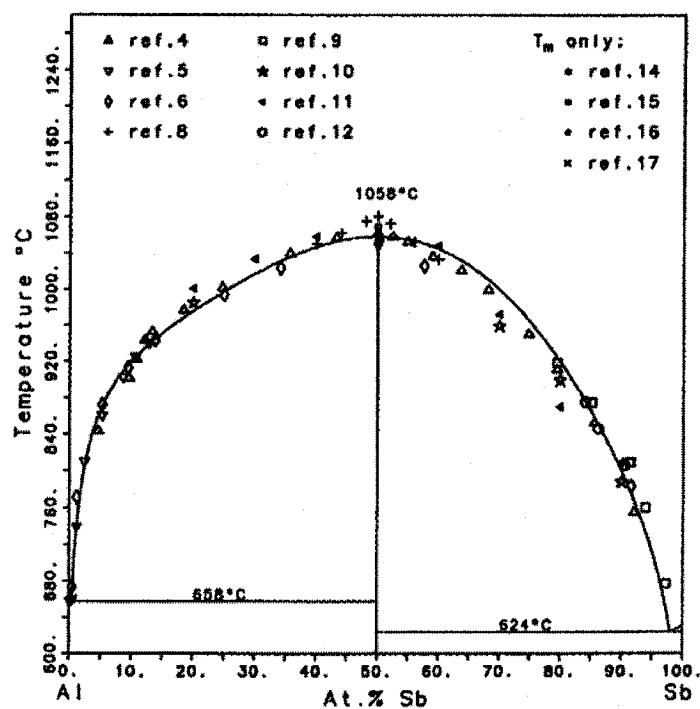


Figure 2.1: Assessed Al-Sb phase diagram by Redlich-Kister model [10]

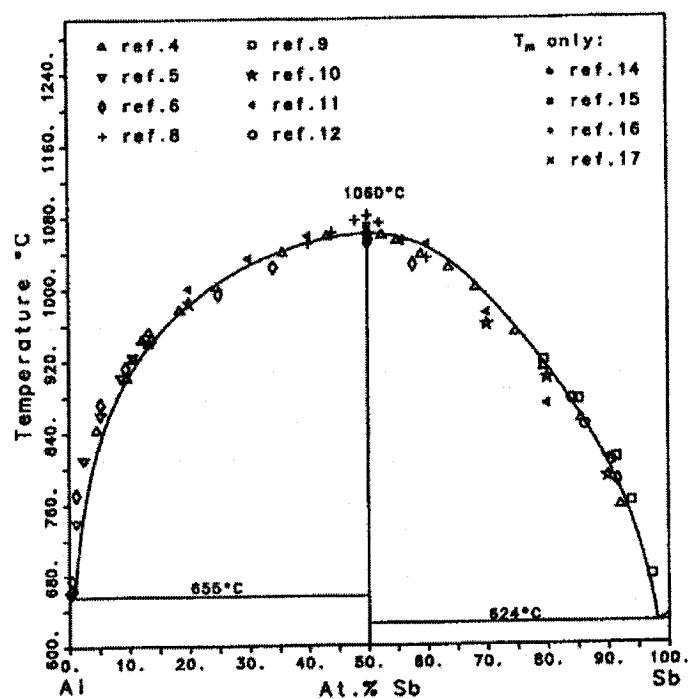


Figure 2.2: Assessed Al-Sb phase diagram by associated solution model [10]

Later Yamaguchi *et al.* [8] measured the heat content of the Al-Sb alloys using drop calorimetry in a temperature range of 800 K-1450 K and in a concentration range of  $0.05 \leq X_{Sb} \leq 0.95$ . They determined the Al-Sb phase diagram from the heat content-temperature-composition relationships. Moreover, they measured heat and entropy of formation of AlSb using a twin solution calorimeter and an adiabatic calorimeter, respectively, and calculated the Al-Sb system using the Redlich-Kister polynomial equation. As shown in Figure 2.3, their calculated phase diagram was found to be in good agreement with their experimental work as well as with other experimental data reported in the literature. Especially, the liquidus line of the Al-rich side agrees with Guertler and Bergmann [25] and the Sb-rich side agrees with Linnebach and Benz [26]. Hence, the present work adopts the liquidus points reported in Yamaguchi *et al.* [8].

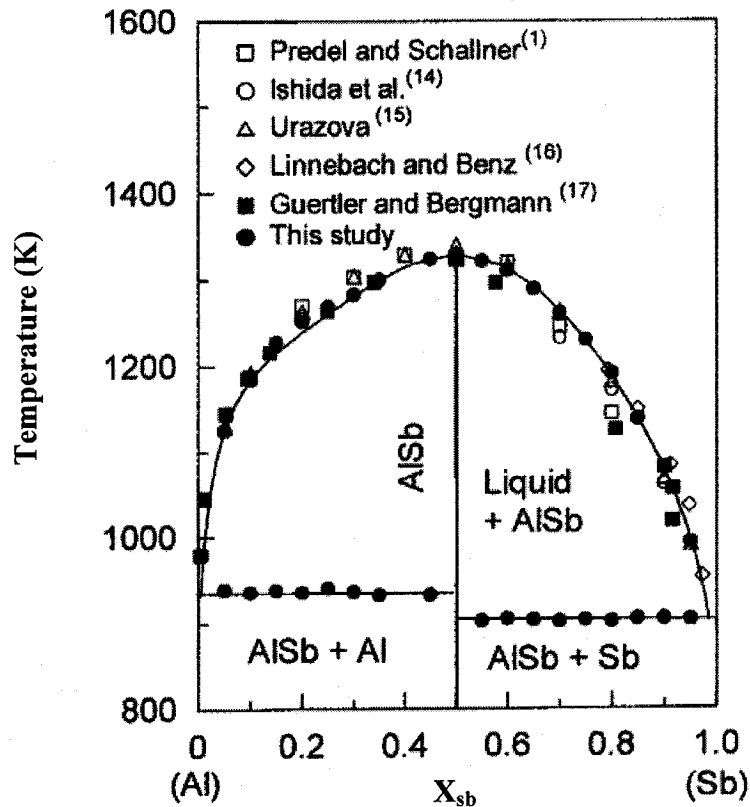
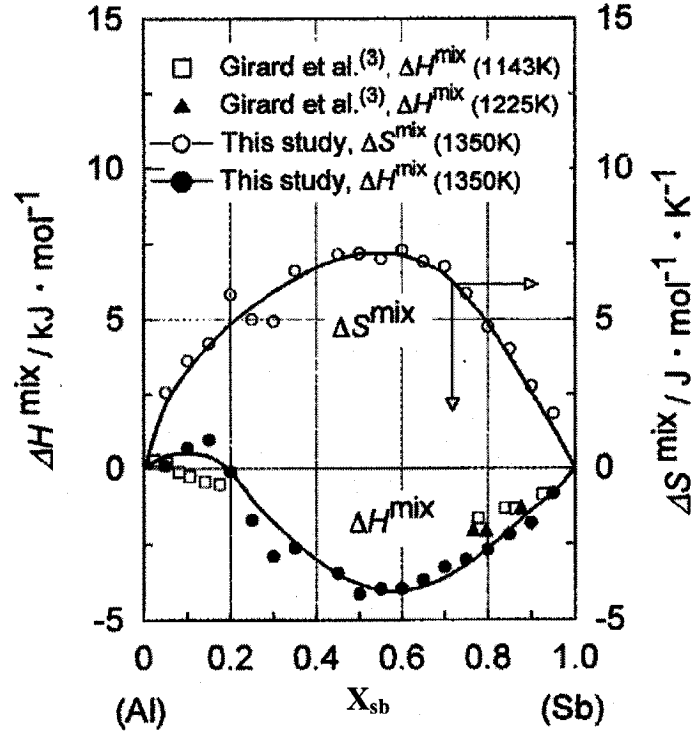


Figure 2.3: Al-Sb phase diagram [8]

Zajackowski and Botor [11] also studied the Al-Sb system using vapor pressure measurements and calculated the system using a regular associate solution model and determined the Al-Sb phase diagram. The invariant points reported in Yamaguchi *et al.* [8] and Zajackowski and Botor [11] showed slight difference in temperature and composition. Lichter and Sommelet [27] measured the high temperature heat content and heat of fusion of the AlSb, and determined the melting point of AlSb as  $1330 \pm 5$  K.

### 2.1.2 Thermodynamic data

The Al-Sb system is found to be less investigated with regard to experimental determination of its thermodynamic properties. There are only scarce literature data available on the enthalpy and Gibbs free energy of the liquid phase of this system. Yamaguchi *et al.* [8] derived the integral molar quantities of the liquid Al-Sb alloys from the heat content for the Al-Sb system and the heat and entropy of formation of the AlSb compound which were obtained by calorimetric measurements. They conducted their experiments using different mole fractions of Sb in the range of  $0.05 \leq X_{\text{Sb}} \leq 0.95$  within the temperature range 800 K to 1450 K. Figure 2.4 shows their reported results on the entropy and enthalpy of mixing of liquid Al-Sb alloys at 1350 K.



**Figure 2.4:** Comparison between calculated and experimental values of heat and entropy of mixing of the Al-Sb system at 1350 K [8]

Previously Girard *et al.* [28] measured the enthalpy of mixing for liquid Al-Sb alloys in the temperature range of 968 K-1227 K by drop calorimetric method using a calvet micro calorimeter. However, they did not cover the complete composition range, and they reported the enthalpy of liquid Al-Sb in the composition ranges of  $0 < X_{Sb} < 0.2$  and  $0.7 < X_{Sb} < 1.0$ . On the Al-rich side, the reported enthalpy of mixing values of Girard *et al.* [28] showed very big deviation from those of Yamaguchi *et al.* [8]. On the other hand, their values show fairly good agreement on the Sb-rich side. Another work by Batalin *et al.* [29] on the enthalpy of mixing of liquid Al-Sb alloys show complete disagreement with other authors' results. The Gibbs free energy of mixing and the

entropy of mixing values for liquid Al-Sb alloys were only reported by Yamaguchi *et al.* [8] at 1350 K. Figure 2.5 shows their reported Gibbs free energy of mixing at 1350 K.

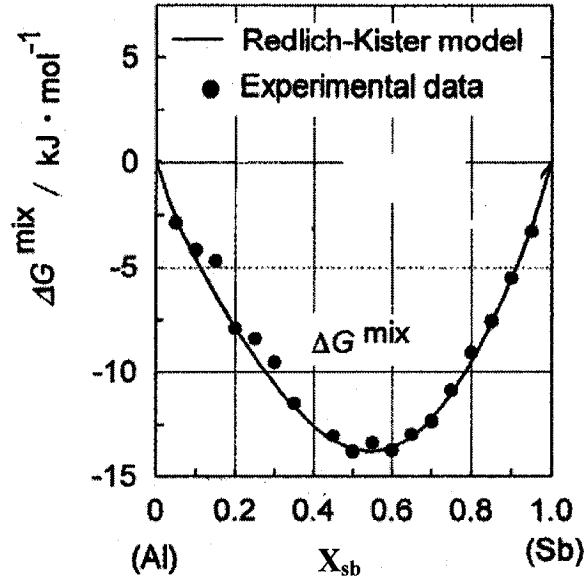


**Figure 2.5:** Comparison between calculated and experimental values of Gibbs free energy of mixing of the Al-Sb system at 1350 K [8]

There are very few measurements reported in the literature on the thermodynamic activities of Al and Sb in liquid Al-Sb alloys. Zajackowski and Botor [11] determined the thermodynamic activity of Al and Sb by measuring the vapor pressure of Sb in liquid Al-Sb alloys in the composition range of  $0.0264 \leq X_{Sb} \leq 0.9858$  and in the temperature range of 950 K to 1461 K. Predel and Schallner [30] also studied the thermodynamic activities of Al and Sb in liquid Al-Sb alloys. The reported activity data of Al-Sb system by Zajackowski and Botor [11] are shown in Figure 2.6.

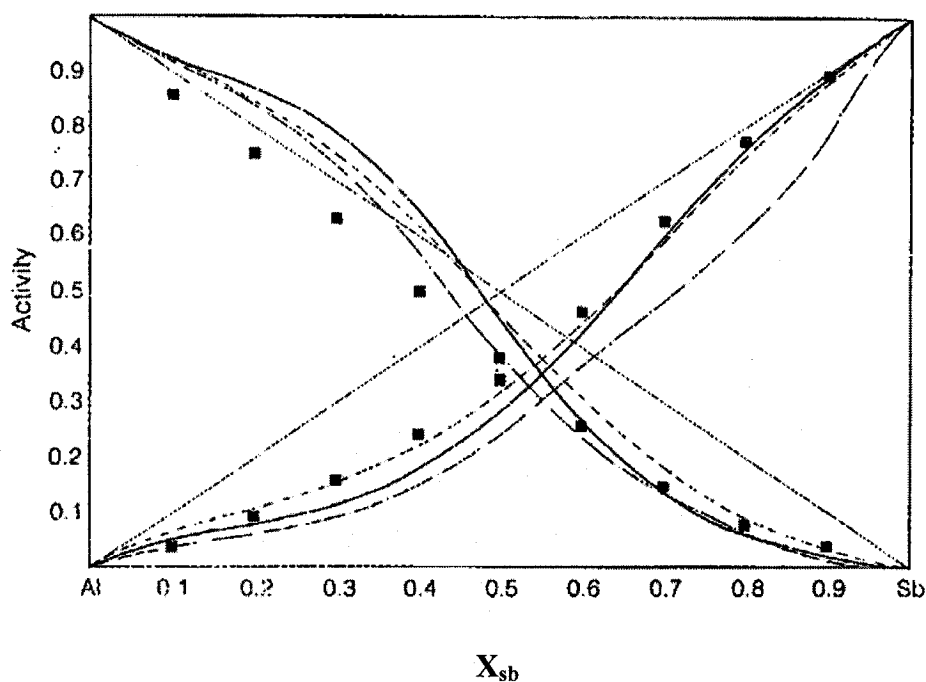


**Figure 2.6:** Activity of components in the liquid Al-Sb alloys:  
 — 1350 K, [11]; - - - 1350 K, Botor *et al.* [31];  
 ..... 1350K, Coughanowr *et al.* [10]; ▪ 1400 K, Predel and  
 Schallner [30]

From the above thermodynamic data analysis, the present work considers the thermodynamic properties reported by Yamaguchi *et al.* [8] and Zajaczkowski and Botor [11] in the thermodynamic model parameters optimization.

## 2.2 Mg-Sb BINARY SYSTEM

### 2.2.1 Phase diagram data

The work on Mg-Sb phase diagram development was first started in 1906 by Grube [32], when he determined the liquidus temperature across the whole concentration range.

However, the reported liquidus values were found to be unreliable and it was re-determined later in 1934 by Grube himself and Bornhak [33] using thermal analysis. Moreover, Jones and Powel [34] performed thermal analysis on Mg-rich side, in the composition range of  $0 \leq X_{\text{Sb}} \leq 0.014$ , and determined the liquidus line. Later on, Hansen and Anderko [35] also reported the liquidus points of Mg-Sb system for the complete composition range. Figure 2.7 shows the experimental phase diagram of Mg-Sb by Hansen and Anderko [35].

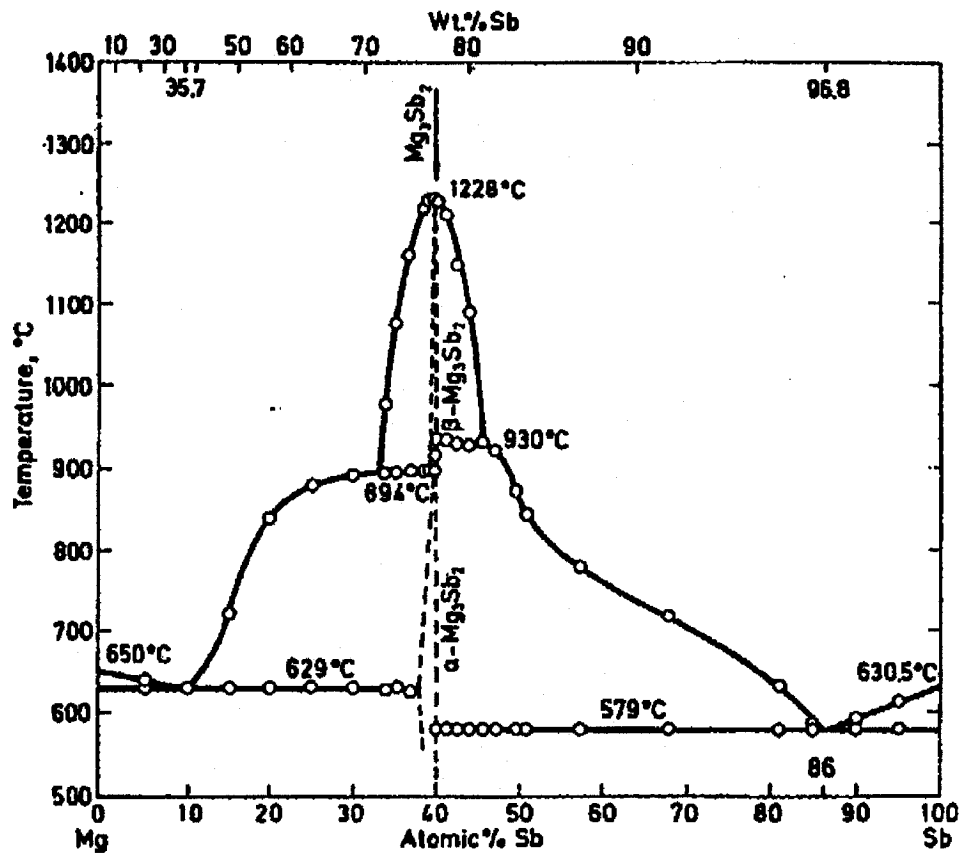


Figure 2.7: Experimental Mg-Sb phase diagram [35]

Since the work of Hansen and Anderko [35] is more recent than the other works, the present research considers their results for the liquidus points in this system. Zabdyr and Moser [36] investigated the dilute solutions of Mg in Mg-Sb system using an emf technique and calculated part of the liquidus in the Sb-rich side of Mg-Sb phase diagram. Rao and Patil [37] also reported liquidus points for the Sb-rich side. Their reported values are found to be in good agreement with Zabdyr and Moser [36].

The melting point of  $\beta$ -Mg<sub>3</sub>Sb<sub>2</sub> phase was re-determined by Bolshakov *et al.* [38] using differential thermal analysis (DTA) measurements. They reported the melting point of  $\beta$ -Mg<sub>3</sub>Sb<sub>2</sub> as  $1518 \pm 5$  K. This value is 17 K higher than that of both Grube and Bornhak [33], and Hansen and Anderko [35]. Bolshakov *et al.* [38] reported the transformation temperature of the  $\alpha$ -Mg<sub>3</sub>Sb<sub>2</sub> to  $\beta$ -Mg<sub>3</sub>Sb<sub>2</sub> as  $1198 \pm 5$  K. The upper limit of this value is in accord with the value reported by Grube and Bornhak [33].

Only Jones and Powel [34] reported a very small solubility of Sb in Mg. Hence, the present work is carried out by assuming no mutual solubility between Mg and Sb.

### 2.2.2 Thermodynamic data

The thermodynamic properties of Mg in liquid Mg-Sb alloys such as activities, relative partial molar free energies, entropies and enthalpies were determined by Rao and Patil [37] using emf measurements. They determined these thermodynamic properties in the temperature range of 980 K to 1250 K and in the composition range of  $0.4 \leq X_{\text{Sb}} \leq 1.0$ . Figures 2.8 and 2.9 show these thermodynamic properties.



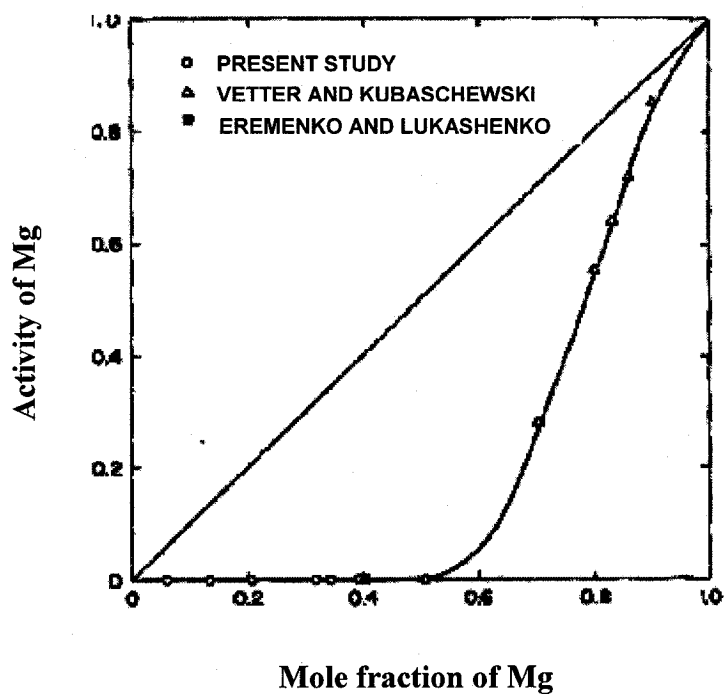


*Figure 2.8: Activity of Mg in liquid Mg-Sb alloys at 1073 K [37]*

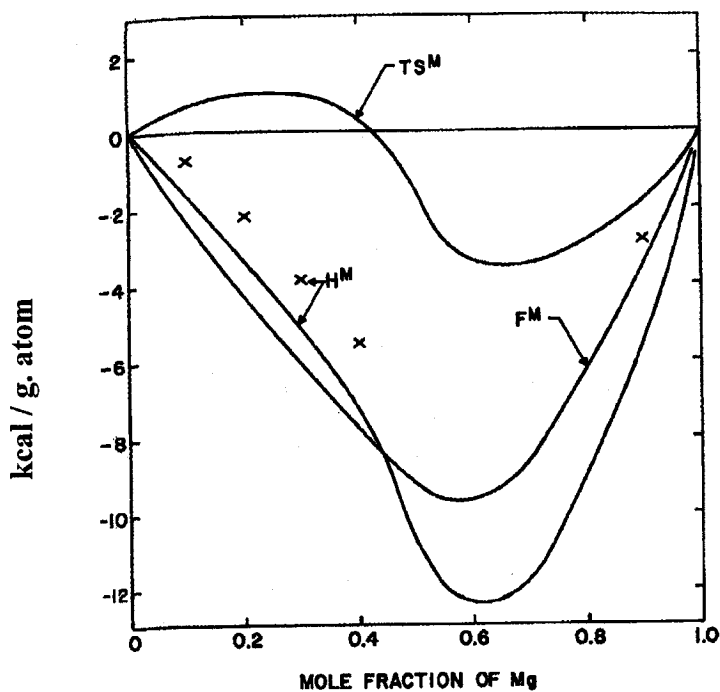


*Figure 2.9: Relative integral molar quantities of liquid Mg-Sb alloys at 1073 K [37]*

Another emf measurement on the Mg-Sb system was carried out by Egan [39] at 1123 K in the composition range of  $0.1 \leq X_{\text{Sb}} \leq 0.9$ . From the emf measurement, he determined the relative partial molar energy of Mg in liquid Mg-Sb alloys at 1123 K. The thermodynamic properties which were reported by both Rao and Patil [37] and Egan [39] are found to be in fair agreement. Also, Eremenko and Lukashenko [40] conducted an emf measurement in the temperature range of 673 K to 823 K. However, their values are found to be scattered. Vetter and Kubaschewski [41] measured the vapor pressure of Mg over liquid Mg-Sb alloys at the temperatures of 1133 K and 1193 K in the composition range of  $0 \leq X_{\text{Sb}} \leq 0.66$ . They measured the vapor pressure using a carrier gas entrainment method, and obtained the equilibrium pressure by extrapolation to zero flow rate. Their vapor pressure measurements are found to be unreliable beyond the composition of  $X_{\text{Sb}} > 0.3$ , as they have neglected the Sb content in the vapor. Hence, the present work considers the reported thermodynamic properties of Vetter and Kubaschewski [41] in the composition range of  $0 < X_{\text{Sb}} < 0.3$  and that of Rao and Patil [37] in the composition range of  $0.3 < X_{\text{Sb}} < 1.0$ . These values are shown in Table 2.1.

In addition, Eckert *et al.* [42] measured the thermodynamic activity of Mg in liquid Mg-Sb alloys at 1123 K across the whole concentration range using the emf technique. Their reported values are found to be in accord with Rao and Patil [37] and Vetter and Kubaschewski [41]. Hence, the present work considers their reported activity values too. Furthermore, Zabdyr and Moser [36] also employed an emf technique and reported activity coefficients of Mg in its dilute solution with Sb and mentioned that their results were in good agreement with previously reported data.

**Table 2.1:** Relative integral molar properties,  $\Delta G^M$ ,  $\Delta S^M$ , and  $\Delta H^M$  of liquid Mg-Sb alloys [37, 41]

$X_{Sb}$	$\Delta G^M$ at 1073 K (J/ mole-atom)	$\Delta S^M$ at 1073 K (J/ mole-atom-K)	$\Delta H^M$ at 1073 K (J/ mole-atom)
0.100*	-14616	-6.930	-22092
0.140*	-19866	-9.072	-29400
0.170*	-21504	-10.458	-32739
0.200*	-26712	-11.298	-38808
0.295*	-35742	-13.860	-50610
0.489	-39396	-7.392	-47334
0.602	-32214	1.344	-30765
0.606	-31962	1.512	-30345
0.656	-28602	3.108	-25284
0.681	-26838	3.570	-23016
0.795	-18312	4.074	-13923
0.866	-12684	3.318	-9114
0.942	-6006	1.764	-4095
0.996	-462	0.168	-273

\* Data of Vetter and Kubaschewski [41]

Among available thermodynamic data on  $Mg_3Sb_2$ , much information are on the low temperature modification  $\alpha$ - $Mg_3Sb_2$ . Rao and Patil [37] obtained the heat of formation, and entropy of formation of the  $\alpha$ - $Mg_3Sb_2$  relative to pure liquid components in the temperature range of 980 K to 2000 K. The reported values are  $-365 \pm 3$  kJ/mol and  $-132 \pm 4$  J/mol.K, respectively. They also obtained these values relative to pure solid components at 900 K and reported them as  $-299 \pm 3$  kJ/mol and  $-59.5 \pm 5$  J/mol.K, respectively. Furthermore, the heat of formation of  $\alpha$ - $Mg_3Sb_2$  relative to pure solid component was also determined by several other authors [40, 43-46]. Hultgren *et al.* [45] also reported the entropy of formation of  $\alpha$ - $Mg_3Sb_2$  as  $-91 \pm 52$  J/mol.K. However, there is no such information available for  $\beta$ - $Mg_3Sb_2$  except the information on the heat capacity reported by Barin *et al.* [46] as  $c_p = 160.7$  J/mol.K.

### 2.2.3 Crystal structure data

Ganguli *et al.* [47] reported a single crystal investigation on  $\alpha$ - $\text{Mg}_3\text{Sb}_2$ . They reported that the  $\alpha$ - $\text{Mg}_3\text{Sb}_2$  is a classical example of a Zintl phase and was first studied by Zintl himself. Figure 2.10 shows the [100] view of the  $\alpha$ - $\text{Mg}_3\text{Sb}_2$  structure

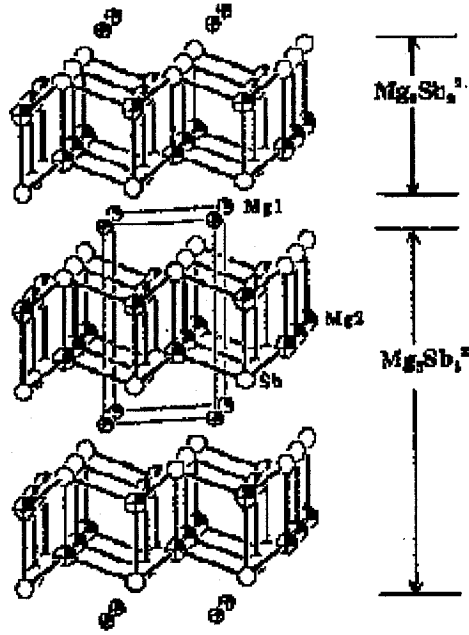


**Figure 2.10:** [100] view of the structure of  $\alpha$ - $\text{Mg}_3\text{Sb}_2$  with the unit cell outlined [47]

The crystal structures and lattice parameters of  $\alpha$ - $\text{Mg}_3\text{Sb}_2$  and  $\beta$ - $\text{Mg}_3\text{Sb}_2$  are summarized in Table 2.2.

**Table 2.2:** Crystal structure and lattice parameter of  $Mg_3Sb_2$  [12]

Phase	Approximate composition(a) (at.% Sb)	Pearson symbol	Space group	Proto type	Lattice parameter, nm	
					a	c
$\beta$ - $Mg_3Sb_2$	40	cI 80	Ia3	$\beta$ Mn <sub>2</sub> O <sub>3</sub>	-	-
$\alpha$ - $Mg_3Sb_2$	40	hP 5	$P\bar{3}m_1$	La <sub>2</sub> O <sub>3</sub>	0.45822	0.72436

(a) From the phase diagram

It can be seen from Table 2.2 that the lattice parameters for  $\beta$ - $Mg_3Sb_2$  are not available.

## 2.3 Mg-Al BINARY SYSTEM

### 2.3.1 Phase diagram data

Saunders [19] reviewed the work on the Mg-Al system prior to 1989 and found that there is no doubt in the existence of two intermediate compounds such as  $\beta$  ( $Al_{140}Mg_{89}$ ) and  $\gamma$ . Moreover he was certain that  $\beta$  phase has a narrow range of homogeneity which is centered at  $X_{Mg} = 0.385$  and the  $\gamma$  phase has extensive solubility. However, he found that the central part of the Mg-Al phase diagram in the composition range of  $0.4 < X_{Mg} < 0.6$  needs to be further investigated. Hence, he carried out a thermodynamic assessment on Mg-Al system based on the results of Schuermann and Geissler [48]. Saunders [19] modeled the  $\gamma$  phase which has  $\alpha$ -Mn structure by a sublattice model with 4 sublattices. His calculated Al-Mg phase diagram is shown in Figure 2.11.

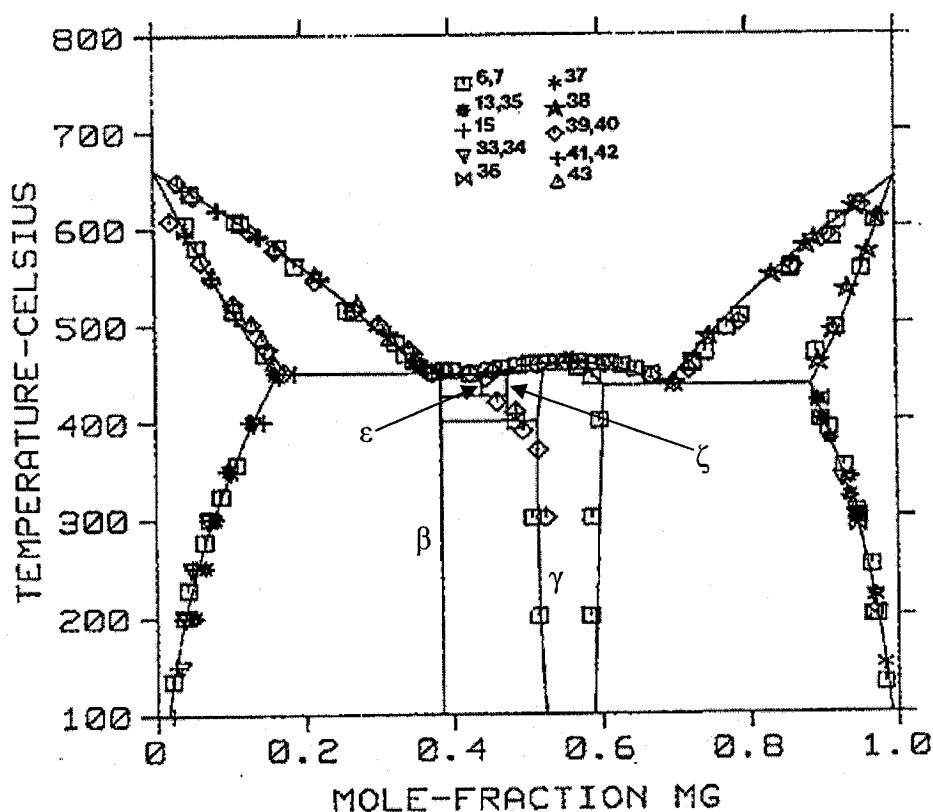


**Figure 2.11:** Calculated Al-Mg phase diagram [19]

The calculated Al-Mg phase diagram of Saunders [19] showed good agreement with the reported experimental literature data. As it can be seen from Figure 2.11, Saunders [19] predicted two other compounds  $\epsilon$  and  $\zeta$  between  $\beta$  and  $\gamma$ . This was contradictory with Murray [16] who predicted only one compound R ( $\text{Al}_{30}\text{Mg}_{23}$ ) between  $\beta$  and  $\gamma$ . Hence, Goel *et al.* [49] studied the Mg-Al system by diffusion couple investigation and concluded that there is an R phase in Mg-Al system and it is only stable in the temperature range of  $305 \pm 5$  to  $405 \pm 5$  °C.

As there was new thermodynamic data available for this system, Chartrand and Pelton [21] decided to re-optimize this system in order to obtain more complete and

precise results. They used a modified quasichemical model for the liquid phase. In their thermodynamic modeling, they assumed that the compound  $\beta$  has a hypothetical stoichiometry of  $\text{Al}_{45}\text{Mg}_{28}$ . The optimized Al-Mg phase diagram by Chartrand and Pelton [21] is given in Figure 2.12.

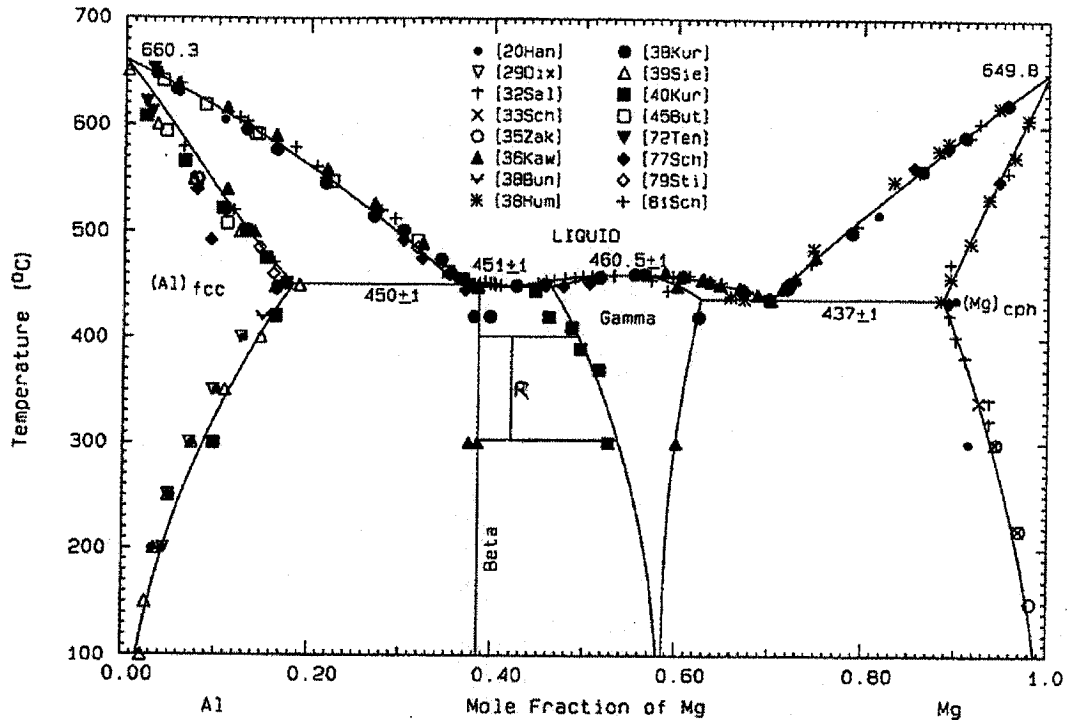


**Figure 2.12:** Optimized Al-Mg phase diagram [21]

Chartrand and Pelton [21] concluded that the principle difference between their optimization and those of Saunders [19] and Zuo and Chang [20] was that these authors included  $\zeta$  phase in their analysis. Here it can be noted that, the location of  $\varepsilon$  phase predicted by Saunders [19] is equivalent to the R phase in Figure 2.12.

Until now, there is no doubt regarding the existence of two intermediate phases:  $\beta$  ( $\text{Al}_{140}\text{Mg}_{89}$ ) and  $\gamma$  ( $\text{Al}_{12}\text{Mg}_{17}$ ) in the Mg-Al phase diagram. But the existence of other

phases; stable or metastable in nature suggested by experimental observations were still doubtful. Hence, recently Czepe *et al.* [23] presented a work to verify the temperature and concentration ranges of the  $\beta$ ,  $\gamma$ , and  $\varepsilon$  phases, thermal stability of these phases, and possible appearance of other phases in the central part of the Mg-Al phase diagram. They studied the Mg-Al phase diagram in the composition range of  $0.48 < X_{Al} < 0.61$  by Differential Scanning Calorimetry (DSC).

### 2.3.2 Thermodynamic data

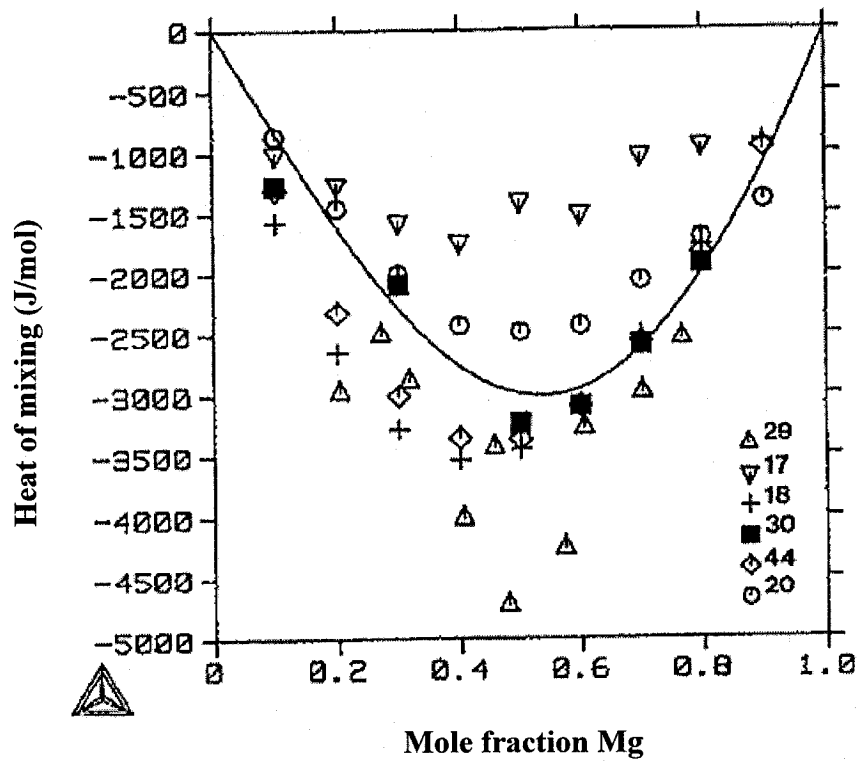


**Figure 2.13:** Calculated heat of mixing for the liquid phase in the Al-Mg system [19]



Figure 2.13 shows the calculated heat of mixing of liquid Al-Mg by Saunders [19]. He observed that his calculated values of the heat of mixing of liquid Al-Mg were in broad agreement with previous calorimetric measurements. On the other hand the calculated enthalpy of mixing values for liquid Al-Mg by Chartrand and Pelton [21] is shown in Figure 2.14

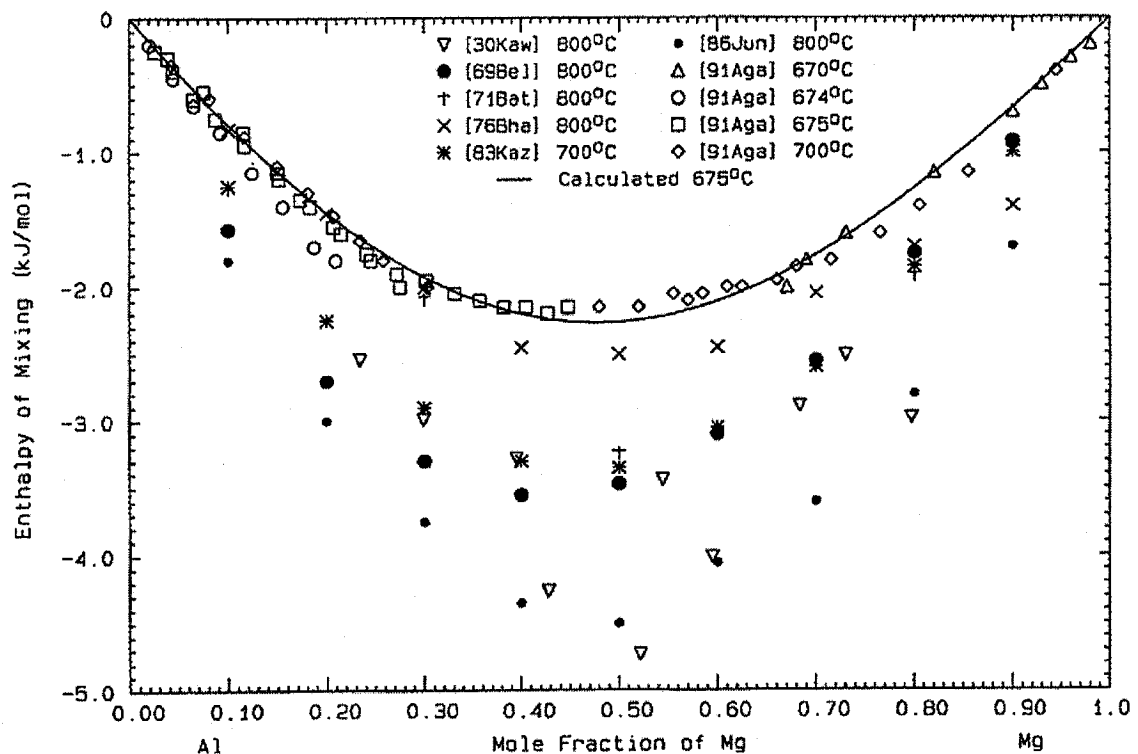


**Figure 2.14:** Calculated enthalpy of mixing of Al-Mg liquid alloys at 948 K [21]

It can be observed that the calculated enthalpy values for liquid Al-Mg alloys of Chartrand and Pelton [21] are higher than those of Saunders [19]. It is because of their different selection of experimental data for the optimization. Chartrand and Pelton [21]

used the experimental data which were obtained by three different calorimetric methods in order to minimize systematic error.

Though extensive thermodynamic data were available in the literature for, liquid Mg-Al alloys, results from various techniques were not in agreement. Hence, in 1998 Moser *et al.* [22] carried out a multi technique research on Mg-Al alloys to determine the consistent thermodynamic data among participating laboratories for the liquid phase and to use those results with the selected information from various references for optimization and, ultimately, for phase diagram calculations. They reported new thermodynamic data for liquid Mg-Al alloys from emf, vapor pressures, and calorimetric studies and then optimized their results together with the thermodynamic information reported in the literature using the Redlich-Kister model. Figure 2.15 shows the experimental and calculated integral enthalpies in liquid Al-Mg alloys by Moser *et al.* [22].

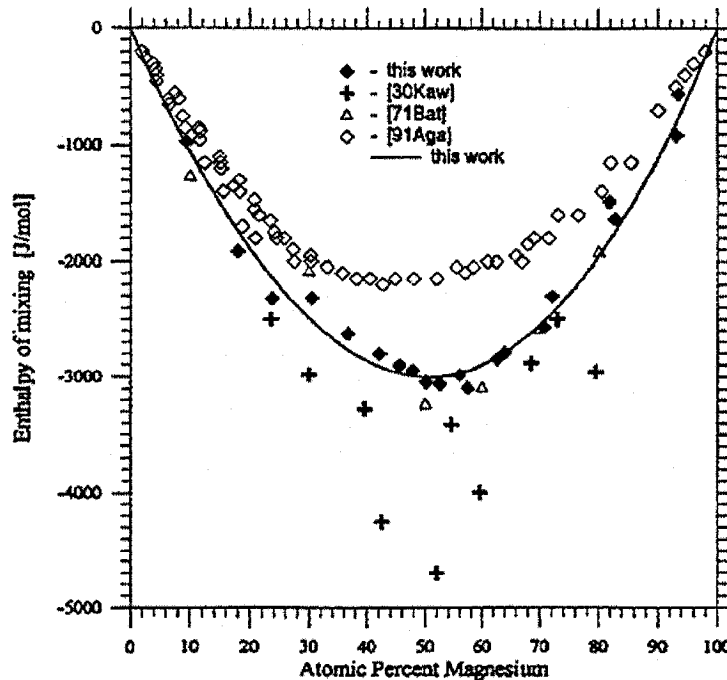


**Figure 2.15:** Integral enthalpies in liquid Al-Mg alloys [22]

During the vapor pressure studies, they assumed that the gas consists solely of magnesium vapor. It can be observed from Figures 2.13 and 2.15 that the calculated values for enthalpy of mixing of Al-Mg liquid alloys by Moser *et al.* [22] and Saunders [19] are similar with the minimum value of -3000 J/mol (approximately) being achieved around  $X_{\text{Mg}} = 0.5$ .

## 2.4 Mg-Al-Sb TERNARY SYSTEM

The Mg-Al-Sb ternary has not been investigated completely. Guertler and Bergman [25, 50], and Loofs-Rassow [51] carried out microscopical and thermal examination on the Al-Sb-Mg system. Guertler and Bergman [50] performed thermal analysis on the quasibinary Al-Mg<sub>3</sub>Sb<sub>2</sub> and their reported quasibinary is shown in Figure 2.16.

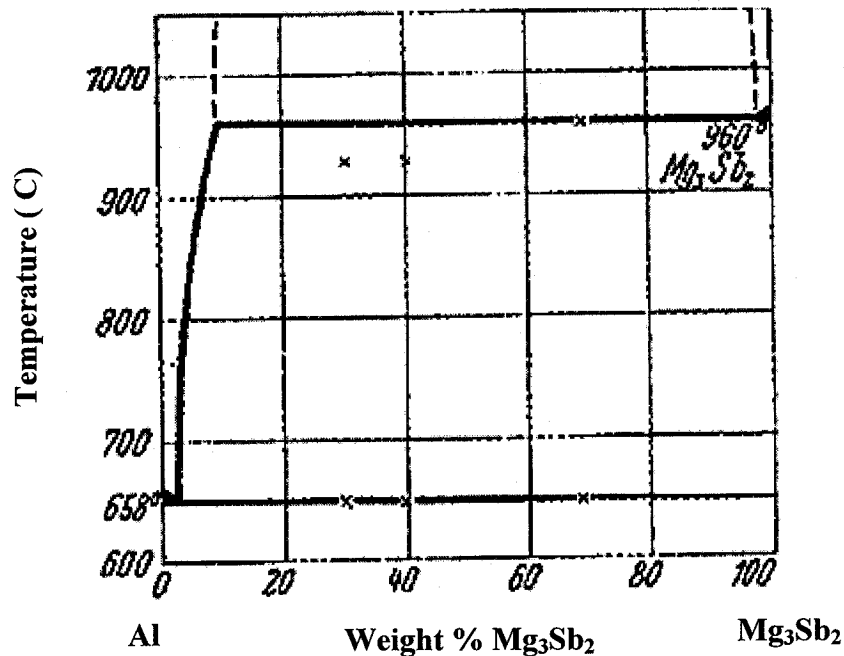
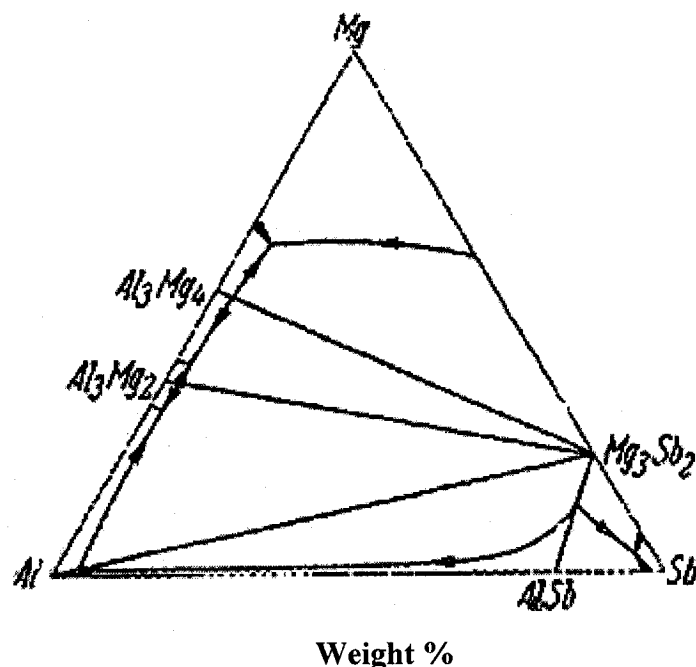


Figure 2.16: Quasibinary system: Al-Mg<sub>3</sub>Sb<sub>2</sub> [50]

Moreover they reported an approximate picture of primary phase distribution in Al-Sb-Mg ternary system (Figure 2.17).



**Figure 2.17:** An approximate picture of primary phase distribution in Al-Sb-Mg system [50]

Guertler and Bergman [50] reported that in the quasibinary Al-Mg<sub>3</sub>Sb<sub>2</sub>, the liquid miscibility gap extends from 9% to 98% Mg<sub>3</sub>Sb<sub>2</sub>. Loofs-Rassow [51] reported that the binary Al-AlSb, Al-Mg<sub>3</sub>Sb<sub>2</sub>, and AlSb-Mg<sub>3</sub>Sb<sub>2</sub> exhibit binary or quasibinary eutectics. They also found that Al-AlSb and AlSb-Mg<sub>3</sub>Sb<sub>2</sub> are completely miscible in the liquid state while Al-Mg<sub>3</sub>Sb<sub>2</sub> shows a miscibility gap. Later, the existence of this miscibility gap was supported by the experimental work of Guertler and Bergman [50].

For the Mg-Al-Sb system, neither ternary compound nor thermodynamic data were reported in the literature.

## 2.5 THE AIMS OF THIS WORK

The significance of studying Mg-Al-Sb system stems from the importance of Sb addition to Mg based alloys to improve their creep resistance. Hence, the current research is aimed at establishing the equilibria in the Mg-Al-Sb system through:

- Thermodynamic modeling of the different phases in the Al-Sb and Mg-Sb systems.
- Calculation of the phase diagrams and the thermodynamic properties of the Al-Sb and Mg-Sb systems and comparison of the results with the experimental data reported in the literature.
- Construction of a database for the Mg-Al-Sb ternary alloy system by combining the databases of the constituent binaries Mg-Al, Al-Sb, and Mg-Sb, where, the database of Mg-Al is obtained from the COST 507 project [15].
- Estimation of the Mg-Al-Sb ternary phase diagram from the constructed database for this system.
- Identification of the critical points in the Mg-Al-Sb ternary system.
- Calculation of isothermal sections and identification of the primary crystallization fields.
- Application of the current understanding of the phase equilibria in Mg-Al-Sb system to explain the experimental observations of some alloys in this system.

# CHAPTER 3

---

## THERMODYNAMIC MODELING

Thermodynamic modeling of an alloy system is a process of finding Gibbs free energy equations for different phases in terms of temperature and compositions of the constituents of the alloy system. Different thermodynamic models are needed to represent different phases such as liquid, solid solution, and stoichiometric compound. However, the fundamental equation for different thermodynamic models is the Gibbs free energy equation of a system established by J. W. Gibbs and it is given in equation 3.1.

$$G = H - TS \quad (3.1)$$

Where,  $G$  is the Gibbs free energy,  $H$  is the enthalpy,  $T$  is the absolute temperature, and  $S$  is the entropy.

### 3.1 THEORY

The main use of thermodynamics in physical metallurgy is to allow the prediction of whether an alloy is in equilibrium [52]. In considering phase transformations we are always concerned with changes towards equilibrium. The reason why a transformation occurs at all is because the initial state of the alloy is unstable relative to the final state. The relative stability of a system at constant temperature and pressure is determined by

its Gibbs free energy (G) given by the equation 3.1. where enthalpy is a measure of the heat content of the system and is given by the equation 3.2.

$$H = U + PV \quad (3.2)$$

where, U is the internal energy of the system, P is the pressure, and V is the volume. It can be seen from equation 3.2 that, at constant pressure, the heat absorbed or evolved is given by the change in H (i.e.  $\Delta H$ ). In solid and liquid phases the change in term PV (i.e.  $P\Delta V$ ) is very small compared to  $\Delta U$ , that is

$$\Delta H \approx \Delta U \quad (3.3)$$

The other term in the expression for the G in equation 3.1 is entropy (S), which is a measure of the randomness of the system.

A system is said to be in equilibrium when it is in the most stable state, that is, when it shows no desire to change. An important result of the classical thermodynamics is that at constant temperature and pressure, a closed system (fixed mass and composition) will be in stable equilibrium if it has the lowest possible value of the Gibbs free energy. That is in mathematical terms

$$dG = 0 \quad (3.4)$$

and this can be explained by Figure 3.1.

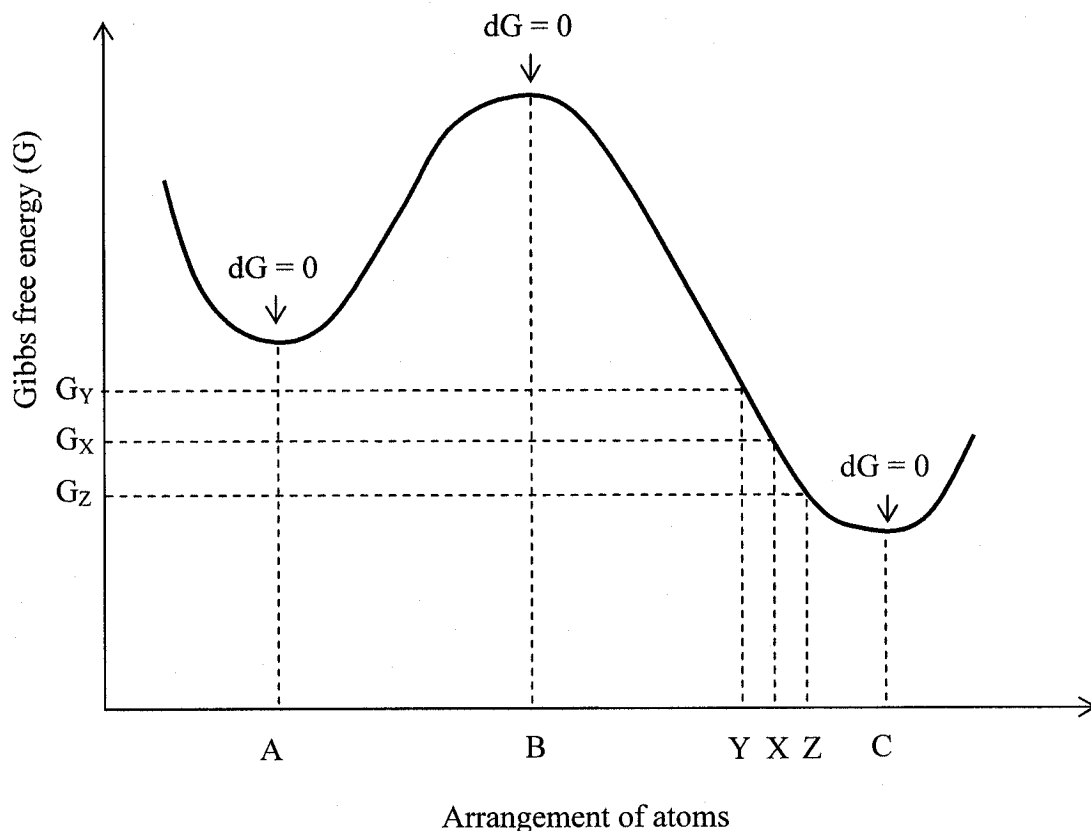


**Figure 3.1:** A schematic variation of Gibbs free energy with the arrangement of atoms

It can be seen from Figure 3.1 that, when the atomic arrangement (configuration) is A or B or C,  $dG = 0$ . When the configuration is A or C, the system is with minimum Gibbs free energy. However, when the configuration is B, the system is with maximum Gibbs free energy. Among these three critical configurations, the system is with lowest Gibbs free energy when the configuration is C. Hence from the results of thermodynamic laws, C is the stable equilibrium configuration. Configuration B is called a metastable equilibrium state.



For multi-component solution phases, Gibbs free energy is expressed by the equation 3.5.

$$G_m = G_m^0 + G_{mix}^{ideal} + G_{mix}^{ex} \quad (3.5)$$

Where,  $G_m^0$  is the contribution from the mechanical mixing of pure components,  $G_{mix}^{ideal}$  is the ideal mixing contribution, and  $G_{mix}^{ex}$  is the excess Gibbs free energy contribution due to the interactions between the components. To expand the individual terms in equation 3.5, let us consider a binary system with components A and B

$$G_m^0 = X_A G_A^0 + X_B G_B^0 \quad (3.6)$$

$$\begin{aligned} G_{mix}^{ideal} &= H_{mix}^{ideal} - TS_{mix}^{ideal} \\ &= 0 - RT (X_A \ln X_A + X_B \ln X_B) \\ &= - RT (X_A \ln X_A + X_B \ln X_B) \end{aligned} \quad (3.7)$$

A mixing is said to be ideal when there is no change in bond energy or volume upon mixing. This means that in ideal mixing the enthalpy of mixing is zero which leads to the term in equation 3.7. However, real solutions deviate from the ideal behavior and an excess term must be added, this term can take the form of equation 3.8.

$$G_{mix}^{ex} = \alpha_{AB} X_A X_B \quad (3.8)$$

Where,  $X_A$ ,  $X_B$  are the compositions of the components A and B respectively, and  $\alpha_{AB}$  is a parameter which, under the assumptions of regular solution theory can be expressed by the equation 3.9.

$$\alpha_{AB} = \sum_{i \geq 0} \sum_{j \geq 0} q_{AB}^{ij} X_A^i X_B^j \quad (3.9)$$

Where the  $q_{AB}^{ij}$  are empirical coefficients which may be temperature independent.

## 3.2 THE GIBBS FREE ENERGY EQUATIONS OF DIFFERENT PHASES IN BINARIES Al-Sb AND Mg-Sb

### 3.2.1 Unary phase

The Gibbs free energy of the pure element,  $i$ , with a certain structure,  $\phi$ , referred to the enthalpy of its standard state,  $H_{i, \text{SER}}$ , at 298.15K is described in terms of temperature as in equation 3.10

$${}^0G_i^\phi(T) = a + bT + CT \ln T + dT^2 + eT^3 + fT^{-1} + gT^7 + hT^{-9} \quad (3.10)$$

where  $a, b, \dots, h$  are coefficients and the values are assigned from the SGTE database [53].

### 3.2.2 Disordered solution phase

The molar Gibbs free energy of the liquid phase in the Al-Sb and Mg-Sb systems is described using equation 3.11.

$$G^{\text{Liquid}} = X_i {}^0G_i^{\text{Liquid}} + X_j {}^0G_j^{\text{Liquid}} + RT[X_i \ln(X_i) + X_j \ln(X_j)] + {}^{\text{ex}}G^{\text{Liquid}} \quad (3.11)$$

where  $X_i$  and  $X_j$  represent the mole fraction of components  $i$  and  $j$ , respectively. The first two terms on the right-hand side of the equation represent the Gibbs free energy of the mechanical mixture of the components; the third term is the ideal Gibbs free energy of mixing; and the last term refers to the excess Gibbs free energy in the form of Redlich-Kister polynomial equation, as in equation 3.12.

$${}^{\text{ex}} G^{\text{Liquid}} = X_i X_j \sum_{n=0}^m [{}^n L_{i,j}^{\text{Liquid}} (X_i - X_j)^n] \quad (3.12)$$

$$\text{and } {}^n L_{i,j}^{\text{Liquid}} = a_n + b_n T \quad (n=0, \dots, m) \quad (3.13)$$

where,  $a_n$  and  $b_n$  are model parameters to be optimized using experimental data.

### 3.2.3 Stoichiometric compound phase

AlSb is the only stoichiometric compound in the Al-Sb system. In the Mg-Sb system, the present work considers that the low temperature modification of the intermediate phase,  $\alpha\text{-Mg}_3\text{Sb}_2$ , as a line compound. The Gibbs free energy of these compounds is described using the equation 3.14.

$$G^\phi = X_i {}^0 G_i^{\phi_1} + X_j {}^0 G_j^{\phi_2} + \Delta G_f \quad (3.14)$$

$$\text{and } \Delta G_f = a + bT \quad (3.15)$$

where  $\phi$  denotes the phase in question,  $\phi_1$  and  $\phi_2$  denote the reference structure of elements  $i$  and  $j$ , respectively,  ${}^0 G_i^{\phi_1}$  and  ${}^0 G_j^{\phi_2}$  represent the Gibbs free energy of components  $i$  and  $j$  in their standard states, respectively,  $\Delta G_f$  represents the Gibbs free energy of formation of the stoichiometric compound,  $a$  and  $b$  are the model parameters to be optimized using experimental data.

### 3.2.4 Non-stoichiometric phase

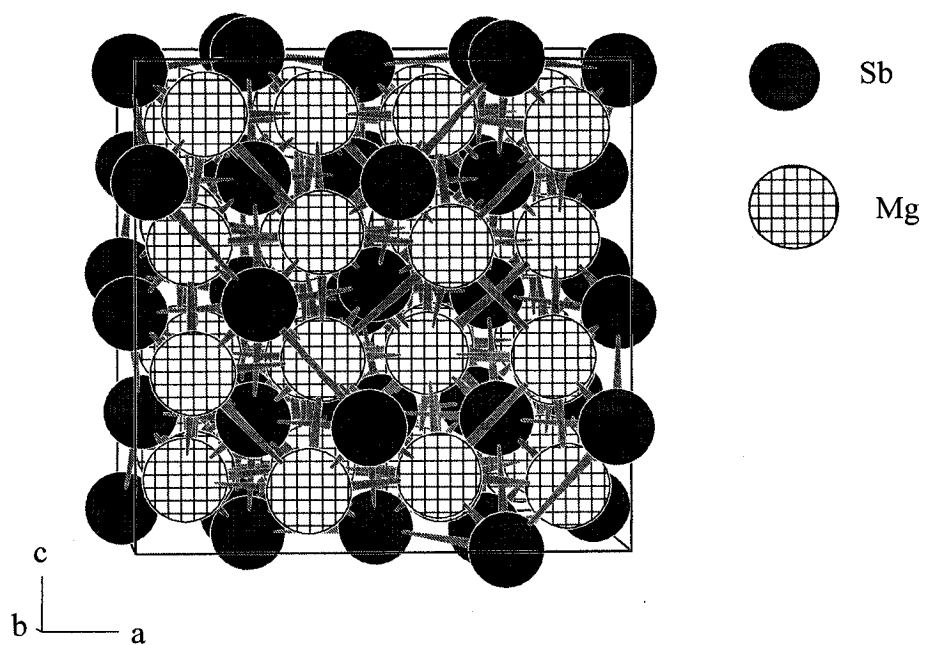
In Mg-Sb system, the present work considers  $\beta\text{-Mg}_3\text{Sb}_2$  as a non-stoichiometric compound. However, there is no information available about the types of defects and the

solubility range of  $\beta\text{-Mg}_3\text{Sb}_2$ . The only available information on this phase in the literature shows a very narrow solubility towards Mg-rich side from the line of stoichiometry. As was mentioned earlier, the crystallographic data of  $\beta\text{-Mg}_3\text{Sb}_2$  is not available. However, according to [12] the prototype of this phase is known to be  $\beta\text{-Mn}_2\text{O}_3$ . In order to have an idea about the possible sublattices, a crystal structure analysis is done on  $\beta\text{-Mg}_3\text{Sb}_2$  by assuming the lattice parameters of  $\beta\text{-Mg}_3\text{Sb}_2$  as that of  $\beta\text{-Mn}_2\text{O}_3$ . Crystal structure data of  $\beta\text{-Mn}_2\text{O}_3$  are given in the Table 3.1.

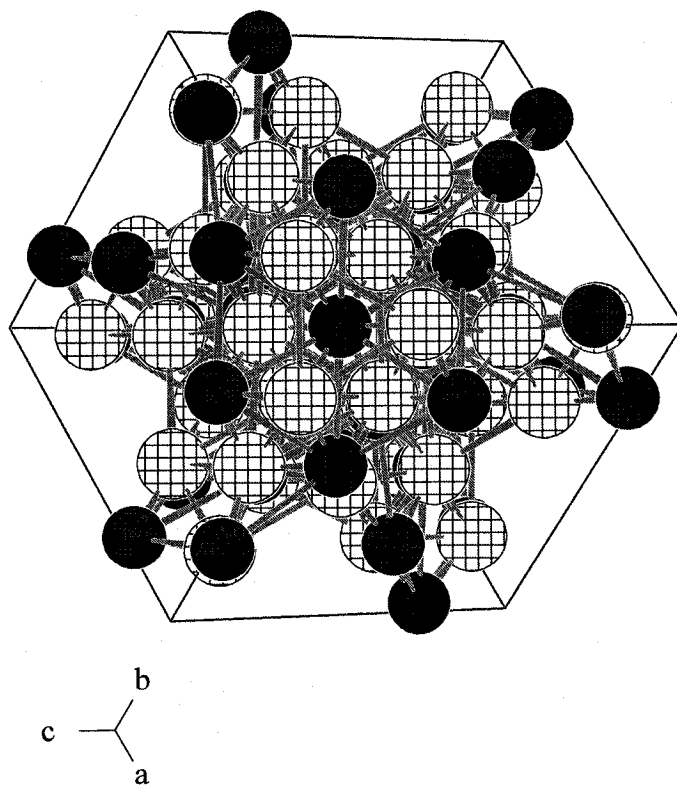
**Table 3.1:** Crystal structure data of  $\beta\text{-Mn}_2\text{O}_3$  [54]

Atom	Atomic position (Wyckoff position)	X	Y	Z
Mn1	8b	0.25	0.25	0.25
Mn2	24d	0.97	0	0.25
O	48e	0.385	0.145	0.380
Space group number: 206				
Lattice parameter: $a = 0.9408 \text{ nm}$				

The following crystal structure analysis of  $\beta\text{-Mg}_3\text{Sb}_2$  assumes Sb on the Mn sites and Mg on the O sites. With these data the crystal structure of  $\beta\text{-Mg}_3\text{Sb}_2$  is generated by Powder Cell software [55]. Figure 3.2 and 3.3 show different views of the  $\beta\text{-Mg}_3\text{Sb}_2$  crystal.

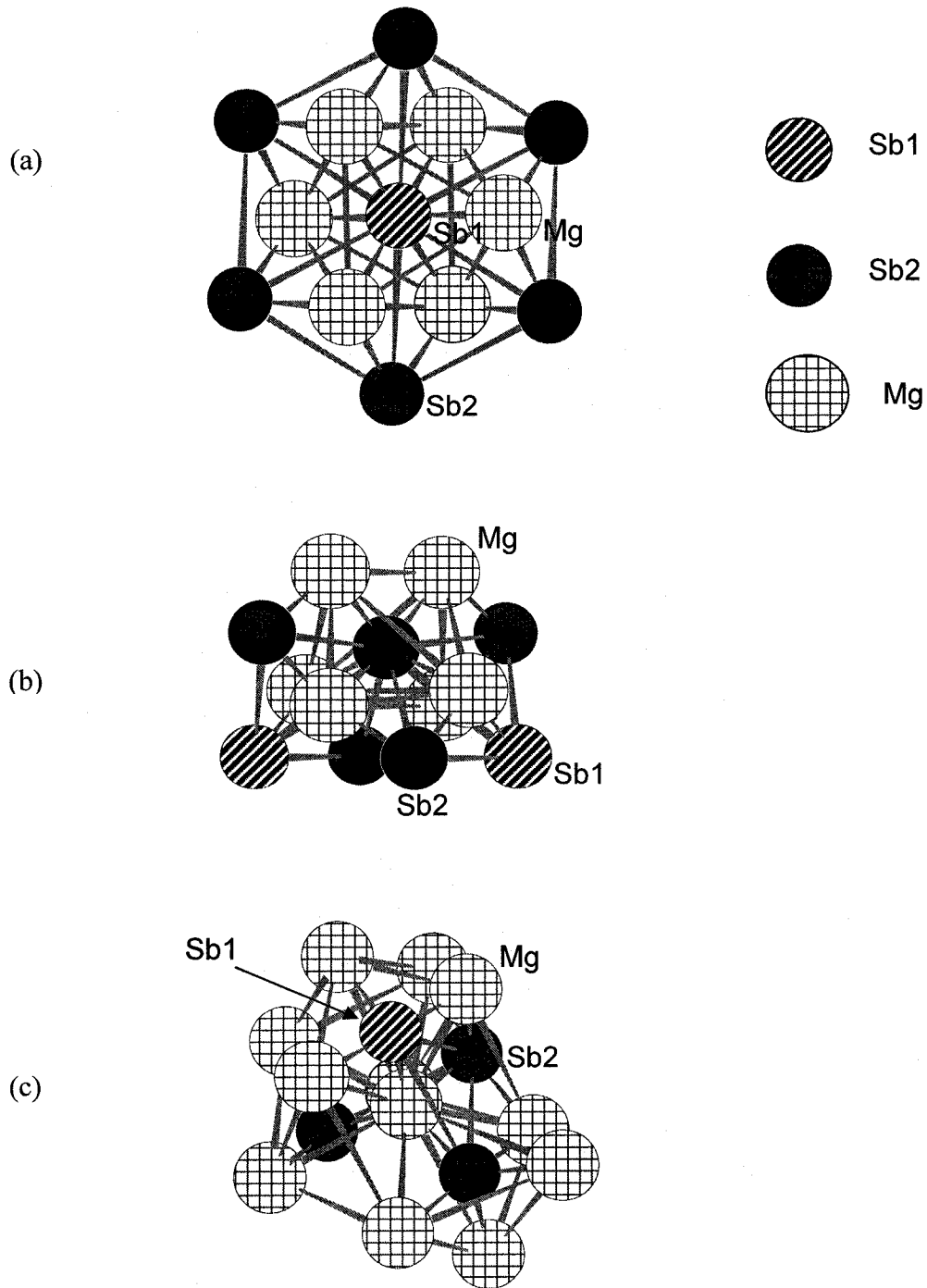


**Figure 3.2:**  $\beta$ - $\text{Mg}_3\text{Sb}_2$  crystal structure projected on (010)



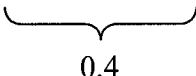
**Figure 3.3:**  $\beta$ - $\text{Mg}_3\text{Sb}_2$  crystal structure projected on (111)

More detailed look at  $\beta$ - $\text{Mg}_3\text{Sb}_2$  crystal structure is shown in Figure 3.4 (a), (b), and (c)



**Figure 3.4:** *Neighboring atoms around Sb1, Sb2, and Mg*

From Figures 3.4 (a), (b), and (c) together with the Wyckoff position of Sb1, Sb2, and Mg atoms, the following can be deduced.

	Sb1	Sb2	Mg
The coordination number	6	6	4
Wyckoff position	8b	24d	48e
Mole fraction	0.1	0.3	0.6
			0.6

According to Harikumar *et al.* [56] the atoms with the same coordination number can be combined and be considered as one sublattice. Hence, the sublattices of Sb1 and Sb2 are combined and considered as sublattice I with the mole fraction of 0.4. The Mg sublattice is named as sublattice II. Since the nature of the defects in the  $\beta$ -Mg<sub>3</sub>Sb<sub>2</sub> is not known, the present study assumes that the substitutional atoms of Mg on Sb sites and Sb on Mg sites as the only defects. Hence, the species in the sublattice I and II are Mg and Sb. During the model parameter optimization of the  $\beta$ -Mg<sub>3</sub>Sb<sub>2</sub>, it was not possible to get the reported homogeneity range of this phase with two sublattices. Hence, 5/6<sup>th</sup> mole of the Mg sublattice is assumed to have defects. It is purely an arbitrary guess, and the remaining 1/6<sup>th</sup> mole is without defects. In other words, the Mg sublattice is divided into two sublattices. They are:

- (1) sublattice II with the mole fraction of 0.5 and with the species Mg and Sb.
- (2) Sublattice III with the mole fraction of 0.1 and with only Mg in it.

As the sublattice III is with pure Mg atoms, there is no mixing in this sublattice and the Gibbs free energy per mole of formula units can be written as in equation 3.16.

$$G_m = y_{Mg}^I y_{Mg}^{II} {}^0G_{Mg:Mg:Mg}^{Mg_3Sb_2} + y_{Mg}^I y_{Sb}^{II} {}^0G_{Mg:Sb:Mg}^{Mg_3Sb_2} + y_{Sb}^I y_{Mg}^{II} {}^0G_{Sb:Mg:Mg}^{Mg_3Sb_2} + y_{Sb}^I y_{Sb}^{II} {}^0G_{Sb:Sb:Mg}^{Mg_3Sb_2} + RT(0.4 \sum_{i=Mg}^{Sb} y_i^I \ln y_i^I + 0.5 \sum_{i=Mg}^{Sb} y_i^{II} \ln y_i^{II}) + y_{Mg}^{II} y_{Sb}^{II} {}^0L_{Mg:Mg,Sb:Mg}^{Mg_3Sb_2} \quad (3.16)$$

$$\text{and } 0.4 \sum_{i=Mg}^{Sb} y_i^I + 0.5 \sum_{i=Mg}^{Sb} y_i^{II} + 0.1 y_{Mg}^{III} = 1 \quad (3.17)$$

where,  $y_{Mg}^I$ ,  $y_{Mg}^{II}$ ,  $y_{Mg}^{III}$  are the site fractions of Mg in lattice I and II respectively,

$y_{Sb}^I$ ,  $y_{Sb}^{II}$  are the site fractions of Sb in lattice I and II respectively,

${}^0G_{Mg:Mg:Mg}^{Mg_3Sb_2}$ ,  ${}^0G_{Mg:Sb:Mg}^{Mg_3Sb_2}$ ,  ${}^0G_{Sb:Mg:Mg}^{Mg_3Sb_2}$ ,  ${}^0G_{Sb:Sb:Mg}^{Mg_3Sb_2}$ , and  ${}^0L_{Mg:Mg,Sb:Mg}^{Mg_3Sb_2}$  are the

parameters to be optimized using experimental data.

### 3.3 METHODOLOGY

The so-called CALPHAD (CALculation of PHase Diagrams) method is used in the present research. In 1970, the foundation for the CALPHAD method was laid by Kaufman and Bernstein [57] with the goal of generating descriptions of binary, ternary, and quaternary systems that can be used for the construction of thermodynamic database. This method is based on the minimization of the free energy of the system. CALPHAD method is a technique by which a variety of experimental values concerning the phase boundaries and the thermodynamic properties are analyzed according to an appropriate thermodynamic model and the interaction energies between atoms are evaluated [58].



From this method phase diagrams outside the experimental range also can be calculated.

The standard methodology in the CALPHAD method is illustrated in Figure 3.5.

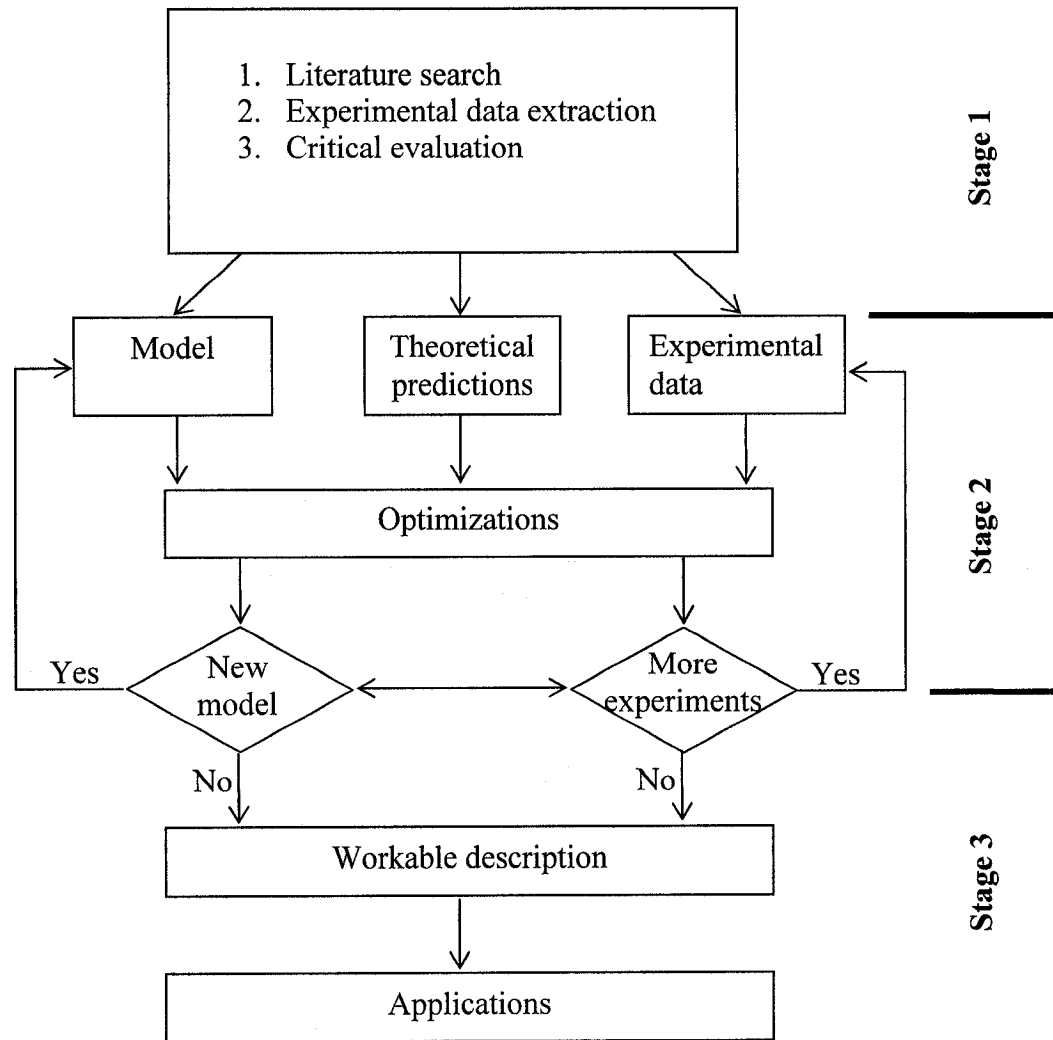


**Figure 3.5:** CALPHAD assessment procedure [59]

There are three different stages in the CALPHAD procedure. In the first stage, the literature is critically evaluated and models are proposed for different existing phases. In

the second stage, the determination of a complete set of the Gibbs free energies of all phases, appearing in the system, is carried out and it can be improved by new data or new modeling. In the final stage, a workable description is obtained such that it satisfies the application requirements.

The main purpose of the CALPHAD method is to calculate (predict) unknown multicomponent phase equilibrium information from the known information available for lower-order systems. The useful strategy for assessment of a multicomponent system is shown in Figure 3.6. As we can see from Figure 3.6, first the thermodynamic descriptions of the constituent binary systems are derived. Then thermodynamic extrapolation methods are used to extend the thermodynamic functions of the binaries into ternary and higher order systems.

Since the present research is carried out on Mg-Al-Sb ternary system, the ternary extrapolation was obtained from the binary subsystems as shown in Figure 3.7.

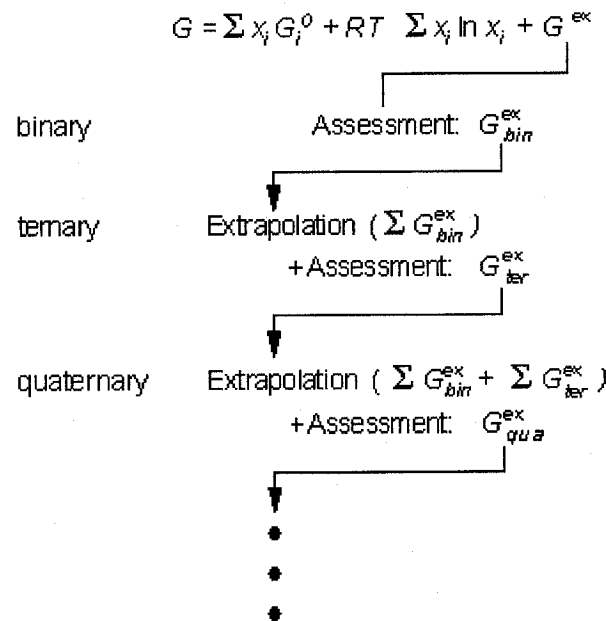


**Figure 3.6:** CALPHAD methodology. The assessed excess Gibbs free energies of the constituent subsystems are for extrapolation to a higher component system [1]

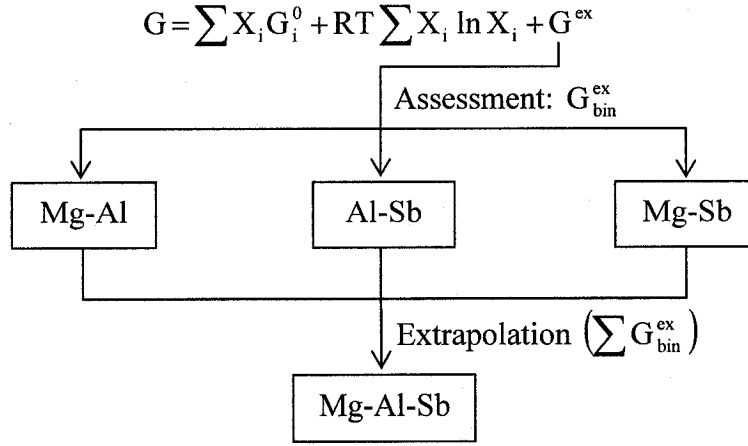


**Figure 3.7:** The assessment strategy of Mg-Al-Sb ternary system

Among the three binaries in Mg-Al-Sb system, the database of Mg-Al is obtained from the COST 507 database [15]. The other two binaries were assessed using the WinPhaD Prgram [60], whereas, the FactSage program [61] was used to construct the thermodynamic database and to calculate the ternary Mg-Al-Sb system.

### 3.4 CONSTRUCTION OF BINARY PHASE DIAGRAM

An alloy phase diagram is a graphical representation of the equilibrium phase limits or phase boundaries as function of temperature and composition. The composition of co-existing phases under equilibrium condition can be obtained by plotting a series of Gibbs free energy-composition curves at different temperatures. For most of the systems there

will be more than one phase and associated Gibbs free energy curve to consider. At a given temperature the most stable phase for a system can vary with composition. Figure 3.8 shows Gibbs free energy curves of a simple eutectic system with terminal solid solutions at different temperatures ( $T_0 > T_1 > T_2 > T_3 > T_4$ ).

At  $T_0$  the Gibbs free energy of the liquid phase is lower than that of the solid phase over the whole composition range. At equilibrium the system exhibits minimum Gibbs free energy. Hence, at  $T_0$  the equilibrium phase is liquid through out the whole composition range. But the system shows different Gibbs energy curves when the temperature is  $T_1$ . At  $T_1$ , within different composition ranges different phases show the minimum Gibbs free energy. That is, when:

- (i)  $X_B < X_1$                        $\rightarrow$        $\alpha$  phase has the lowest Gibbs free energy
- (ii)  $X_1 < X_B < X_2$              $\rightarrow$       both  $\alpha$  and liquid phases have minimum Gibbs free energy
- (iii)  $X_B > X_2$                      $\rightarrow$       liquid phase has the lowest Gibbs free energy

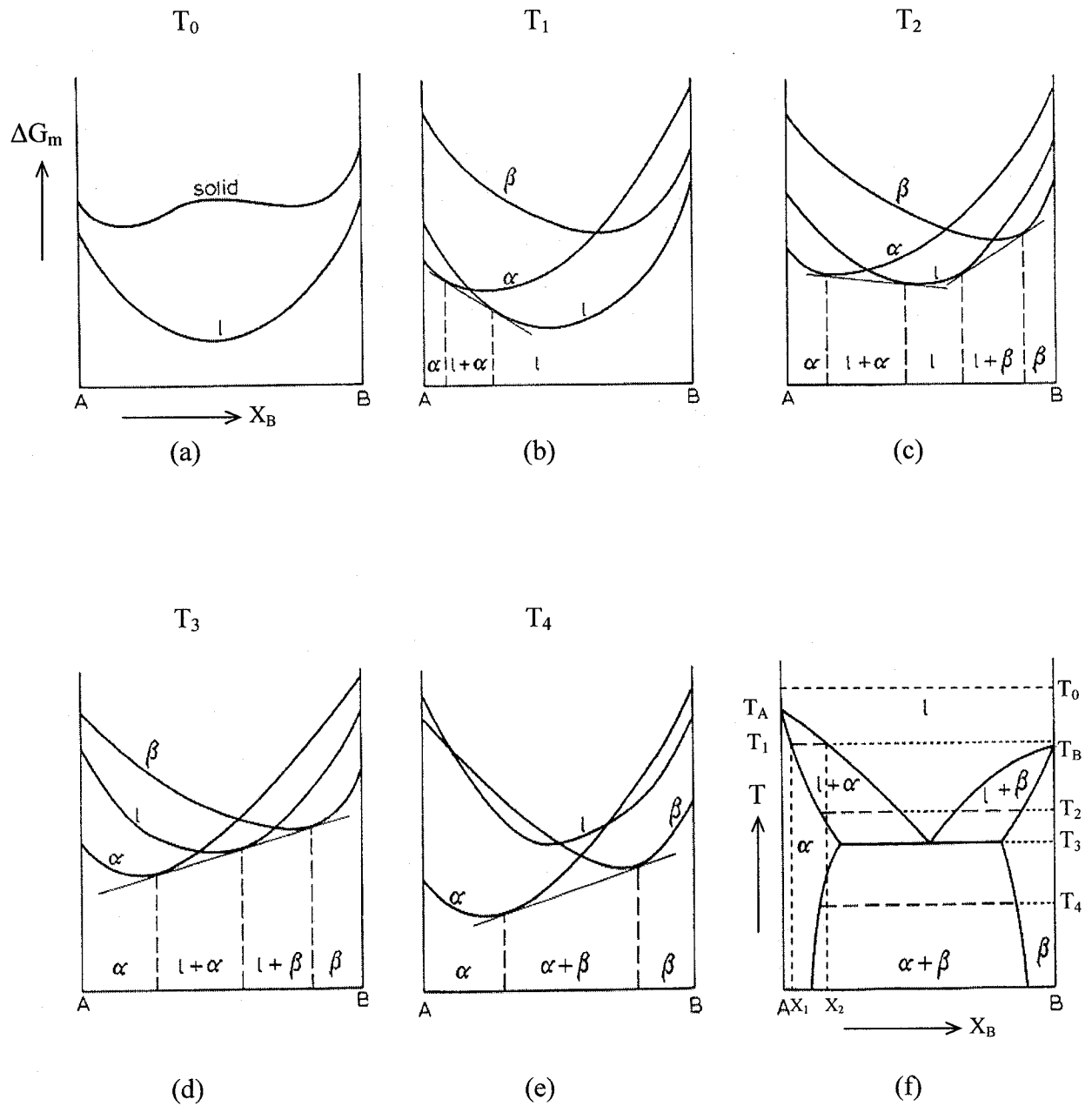


**Figure 3.8:** Derivation of a eutectic phase diagram from the Gibbs free energy curves for the liquid,  $\alpha$  and  $\beta$  phases [62]

Further explanation for the equilibrium condition in the composition range  $X_1 < X_B < X_2$  is shown in Figure 3.9.

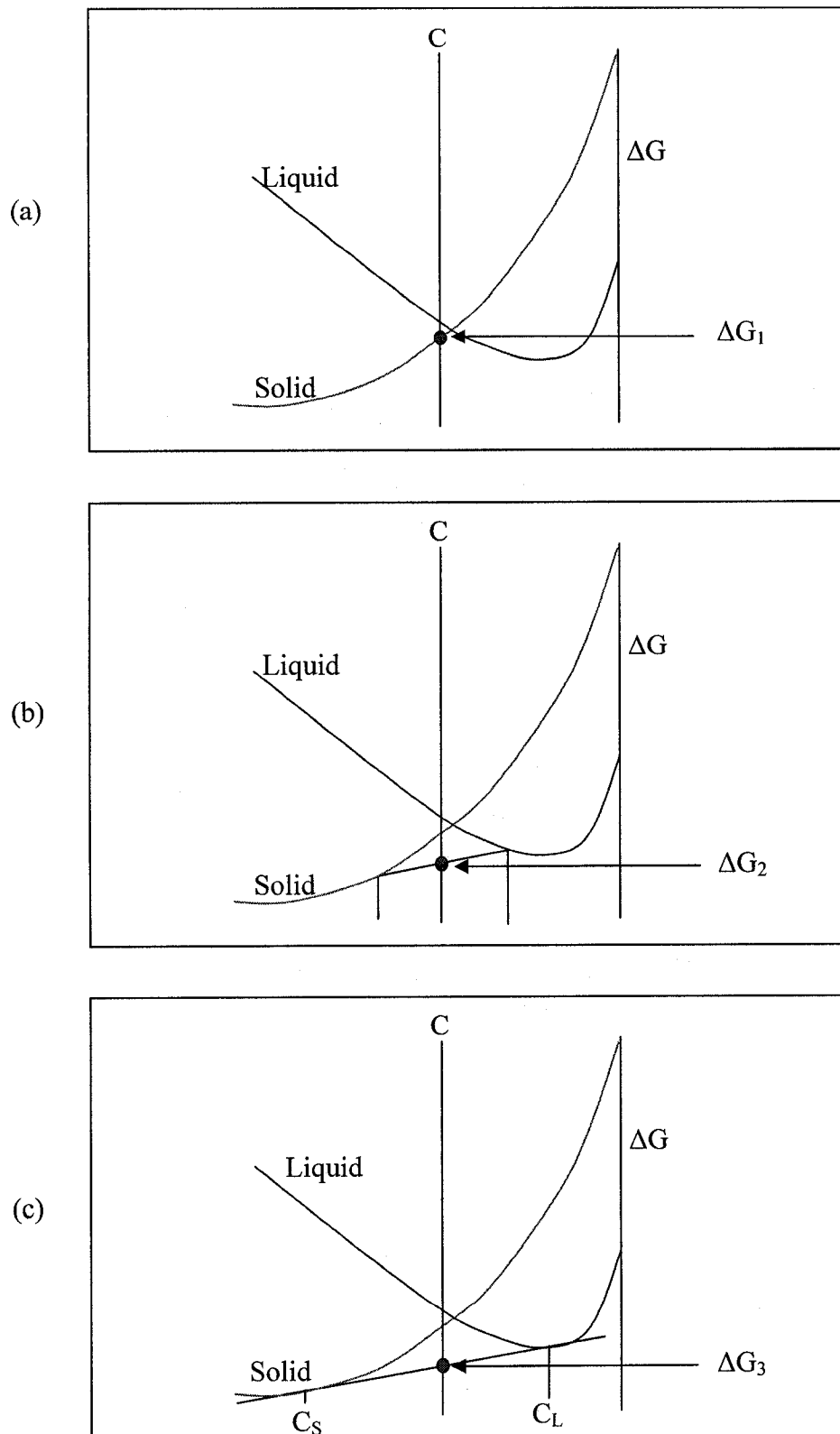


**Figure 3.9:** Common tangent construction in two phase equilibrium

It can be seen from Figure 3.9 (a) that the system is sitting entirely in the phase which is the most stable with the Gibbs free energy of  $\Delta G_1$ . Figure 3.9 (b) shows that by separating into two phases the overall Gibbs free energy of the system can be reduced to  $\Delta G_2$ . In Figure 3.9 (c), the common tangent construction can be seen linking the solid and liquid Gibbs free energy curves to minimize the system's Gibbs free energy for a given overall composition C. This construction also identifies the composition of the solid and liquid phases ( $C_S$  and  $C_L$ ) which are in equilibrium at this temperature.

As it can be seen from Figure 3.9 (a) through 3.9 (c), any composition ( $C_S < C < C_L$ ) on the common tangent of liquid and solid phases minimizes the system's total Gibbs free energy. Hence, in Figure 3.8, at  $T_1$ , the two phase ( $\alpha$  and liquid) equilibrium boundary is identified by constructing the common tangent to the Gibbs free energy curves of  $\alpha$  and liquid. The same principle is used at temperatures  $T_3$  and  $T_4$  and the constructed phase diagram is shown in Figure 3.8 (f).

### 3.5 TERNARY PHASE DIAGRAM

The ideas that have been developed for binary systems can be extended to systems with three or more components [63]. The composition of a ternary alloy can be indicated on an equilateral triangle (the Gibbs triangle) whose corners represent 100% A, B, C as shown in Figure 3.10.

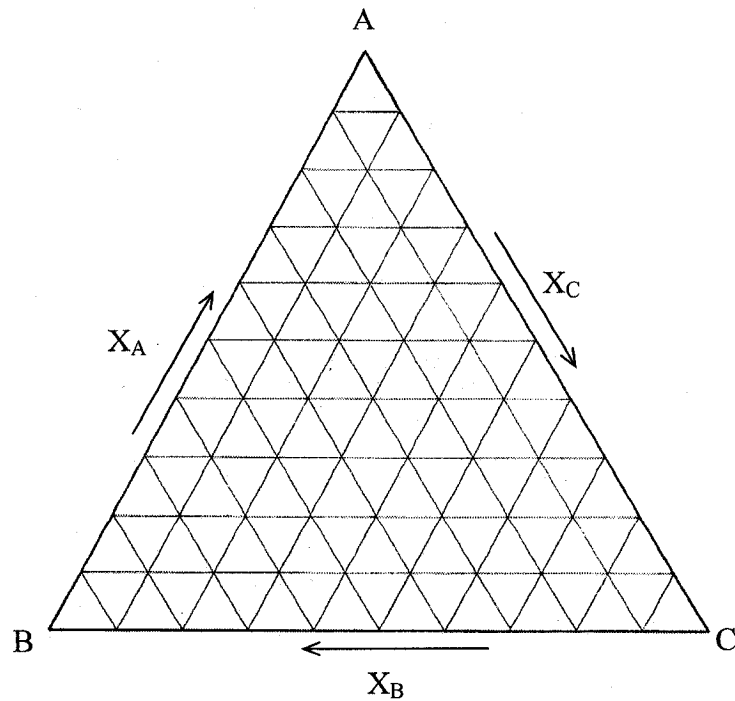


**Figure 3.10:** Gibbs triangle with components A, B and C

A ternary temperature-composition phase diagram at constant total pressure may be plotted as a three-dimensional “space model” within a right triangular prism with the equilateral composition triangle (Gibbs triangle) as base and temperature as vertical axis. Such a space model for a simple eutectic ternary system A-B-C is illustrated in Figure 3.11.



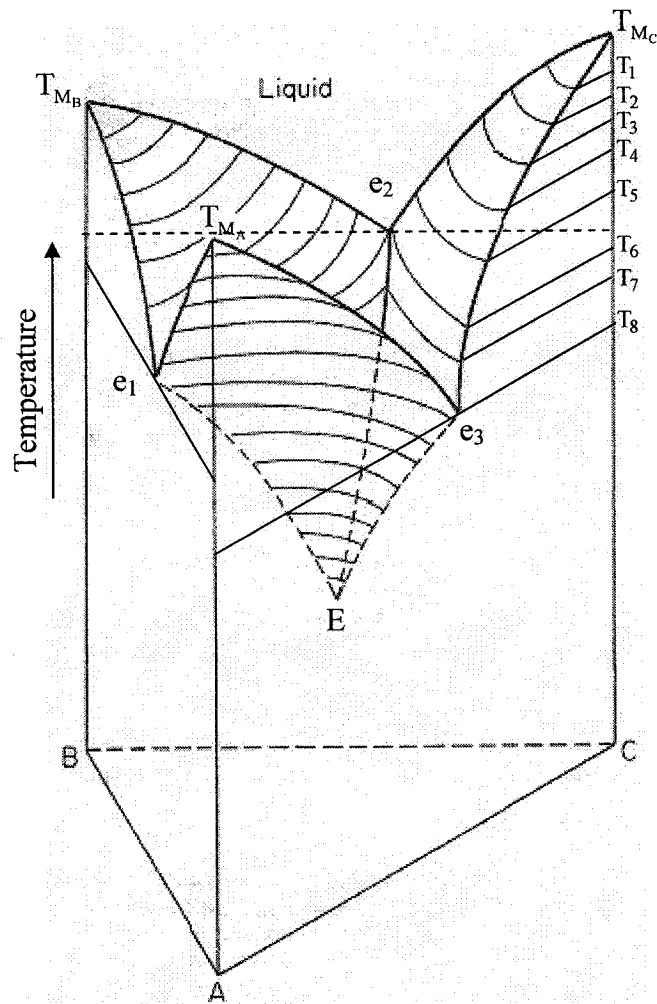


**Figure 3.11:** Diagram of a ternary system containing one ternary eutectic [64]

The three binary subsystems in Figure 3.11 such as A-B, B-C, and C-A, can be seen on the vertical faces of the prism. The three binary eutectic points are  $e_1$ ,  $e_2$ , and  $e_3$ . Within the prism, the three liquidus surfaces descending from the melting points of pure A, B, and C and make the ternary eutectic point E. The lines on the liquid surface are the constant temperature lines called isotherms. The plan view of the ternary space model (Figure 3.11) with the critical points is shown in Figure 3.12.

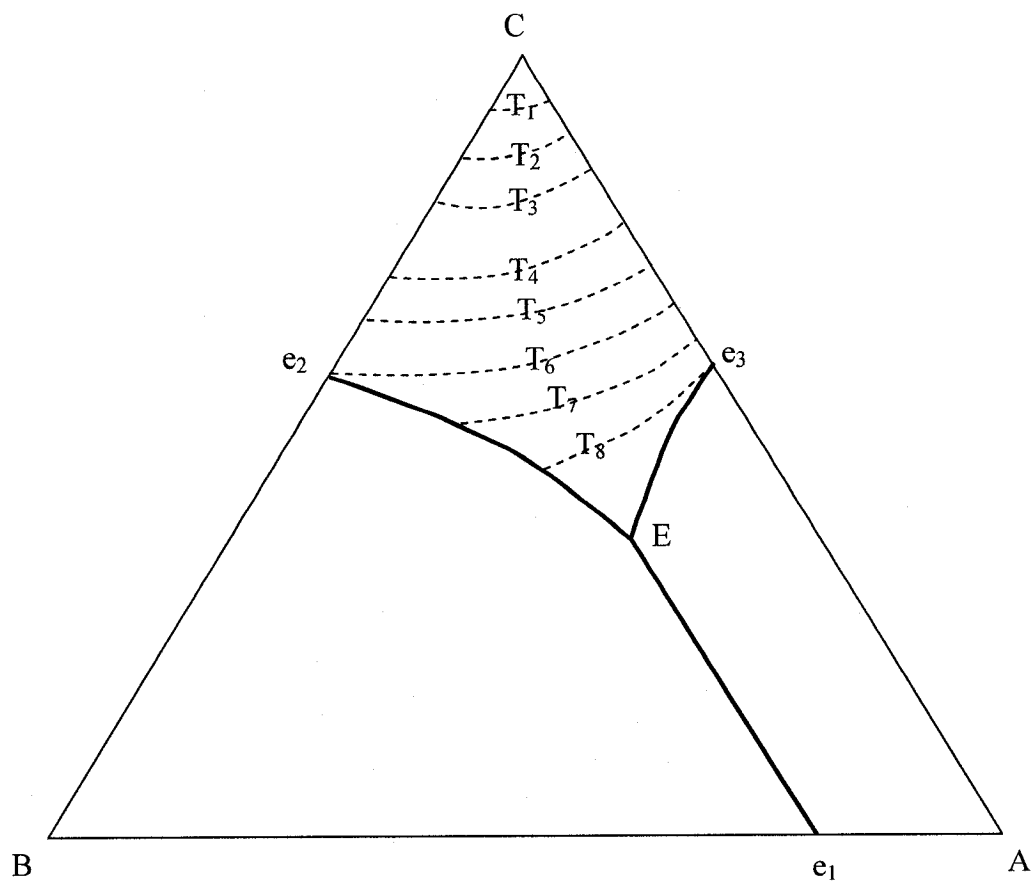


**Figure 3.12:** The plan view of the liquidus surface of the system shown in Figure 3.11

# CHAPTER 4

---

## RESULTS AND DISCUSSIONS

### 4.1 Al-Sb BINARY SYSTEM

The selected experimental phase diagram, enthalpy of mixing, entropy of mixing, Gibbs free energy of mixing and activities of liquid Al-Sb alloys data, which were discussed in section 2.1, were used to optimize the thermodynamic model parameters for the liquid and AlSb phases. The optimization is done using the computer program WinPhaD Pro. [60]. The optimized model parameter values are given in Table 4.1.

*Table 4.1: The optimized model parameters for the liquid and AlSb phases*

Phase	Term	a (J/ mole atom)	b (J/ mole atom.K)
Liquid	L <sub>0</sub>	-13327.934	-5.103
	L <sub>1</sub>	10748.104	0.337
AlSb	$\Delta G_f$	-40636.090	15.847

The reference structure of the Gibbs free energy of the formation of AlSb is considered as Al-Fcc and Sb-Rhombo. In order to maintain the consistency with other systems modeled in our group, no lattice stability values are added to the pure

components Al-fcc and Sb-rhombo. From the optimized model parameters, the phase diagram of Al-Sb and the thermodynamic properties of Al-Sb system are calculated.

#### 4.1.1 Phase diagram

The calculated phase diagram in relation to experimental data from the literature is shown in Figure 4.1. Excellent agreement between the calculated phase diagram and measured liquidus points can be observed in this figure. Values of the optimized parameters are listed in Table 4.1. Only two Redlich-Kister coefficients ( $L_0$  and  $L_1$ ) were used to describe the liquid phase. A comparison between the current results and other works on this system is presented in Table 4.2.

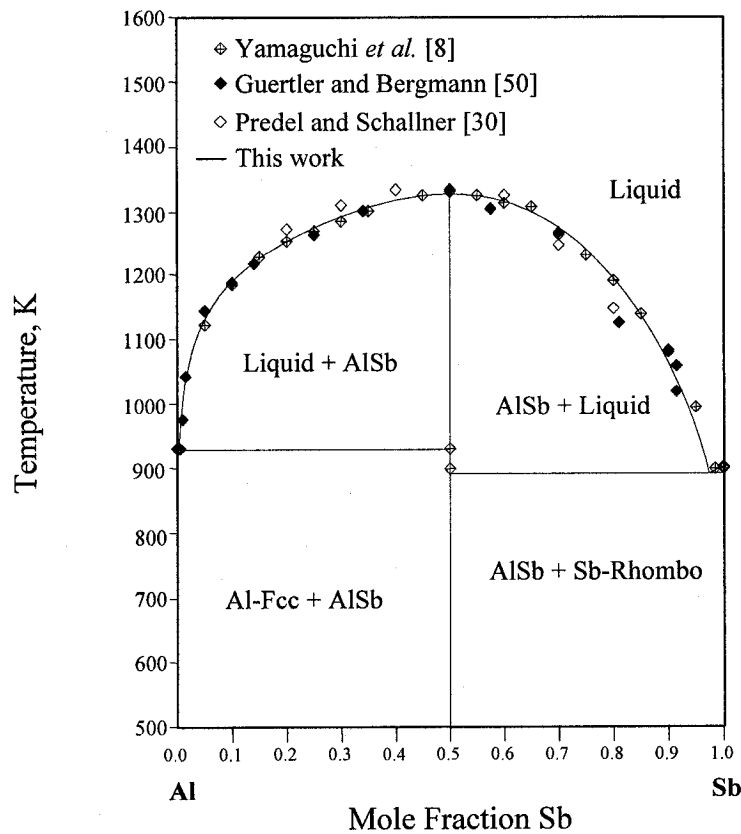


**Figure 4.1:** Calculated Al-Sb Phase diagram with experimental data from the literature

**Table 4.2:** Comparison between different works (calculations) on the equilibria in the Al-Sb system

Reaction	Temp. (K)	Comp. ( $X_{Sb}$ )	Solution Model	Reference
L=(Al)+AlSb	931	-	Redlich-Kister polynomial	[10]
	928	-	Associated solution	[10]
	932	0.004	Redlich-Kister polynomial	[8]
	930.4	0.00476	Associated solution	[11]
	930	0.004	Associated solution	[9]
	931.3	0.0034	Redlich-Kister polynomial	This work
L=(Sb)+AlSb	897	-	Redlich-Kister polynomial	[10]
	897	-	Associated solution	[10]
	901	0.983	Redlich-Kister polynomial	[8]
	898.3	0.9833	Associated solution model	[11]
	899	0.984	Associated solution model	[9]
	893	0.974	Redlich-Kister polynomial model	This work
L=AlSb	1331	0.5	Redlich-Kister polynomial model	[10]
	1333	0.5	Associated solution model	[10]
	1335	0.5	Redlich-Kister polynomial model	[8]
	1336.4	0.5	Associated solution model	[11]
	1332	~ 0.5	Associated solution model	[9]
	1328.4	0.5	Redlich-Kister polynomial model	This work

#### 4.1.2 Thermodynamic properties

As shown in Figure 4.2, the calculated activities of Al and Sb in liquid Al-Sb alloys at 1350 K are in fair agreement with Zajaczkowski and Botor [11] and Predel and Schallner

[30]. The calculated activity of Al shows slight positive deviation from the ideal behavior in the Al-rich side. Zajaczkowski and Botor [11] reported that this was the case in many other works too. In the Al-rich side, it can be observed that our calculated activity of Al lies in between Zajaczkowski and Botor [11] and Predel and Schallner [30]. However, the calculated values of Al in the Sb-rich side agree well with both Zajaczkowski and Botor [11] and Predel and Schallner [30]. The activity of Sb in liquid Al-Sb alloys shows negative deviation from ideal behavior in the whole range of composition. The calculated activity values of Sb from this work closely match with Zajaczkowski and Botor [11].

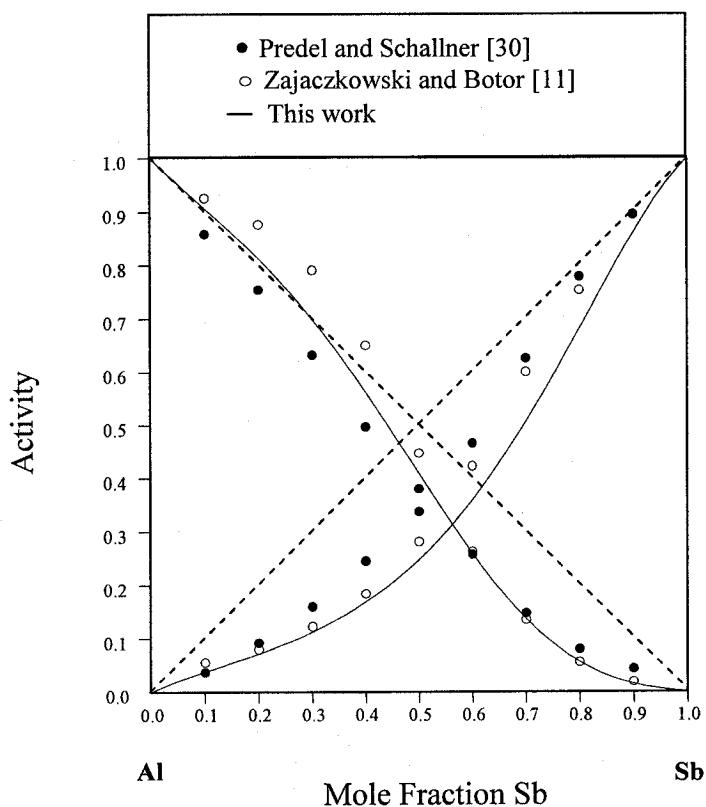


**Figure 4.2:** Activity of components in the liquid Al-Sb alloys at 1350 K: comparison between calculated values and the experimental data

The calculated enthalpy of mixing of liquid Al-Sb alloys at 1350 K in Figure 4.3, shows fairly good agreement with Yamaguchi *et al.* [8]. On the other hand the results of the current research agree with the enthalpy values reported by Batalin *et al.* [29] in the Al-rich side and deviate from those at the Sb-rich side.

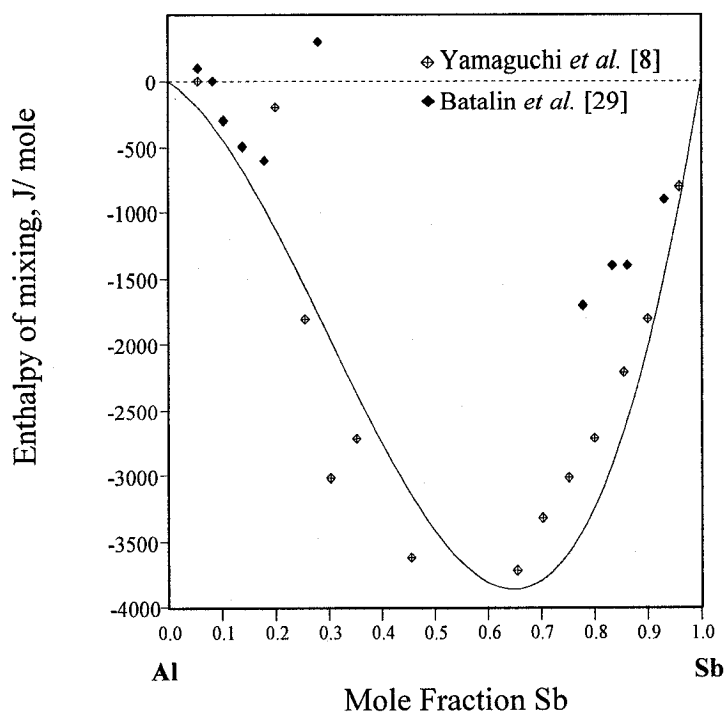


**Figure 4.3:** Enthalpy of mixing of liquid Al-Sb alloys at 1350 K: comparison between calculated values and the experimental data

The calculated entropy of mixing and Gibbs free energy of mixing of liquid Al-Sb alloys at 1350 K are shown in Figure 4.4 and 4.5, respectively. As discussed in section 2.1.2, the work of Yamaguchi *et al.* [8] is the only experimental data available for Gibbs free energy and entropy of mixing of Al-Sb liquid. The results of the current work are in very good agreement with their results.

In the neighborhoods of  $0.2 < X_{\text{Sb}} < 0.3$  and  $0.55 < X_{\text{Sb}} < 0.75$ , the calculated entropy of mixing of liquid Al-Sb shows some deviation from the values of Yamaguchi *et al.* [8].

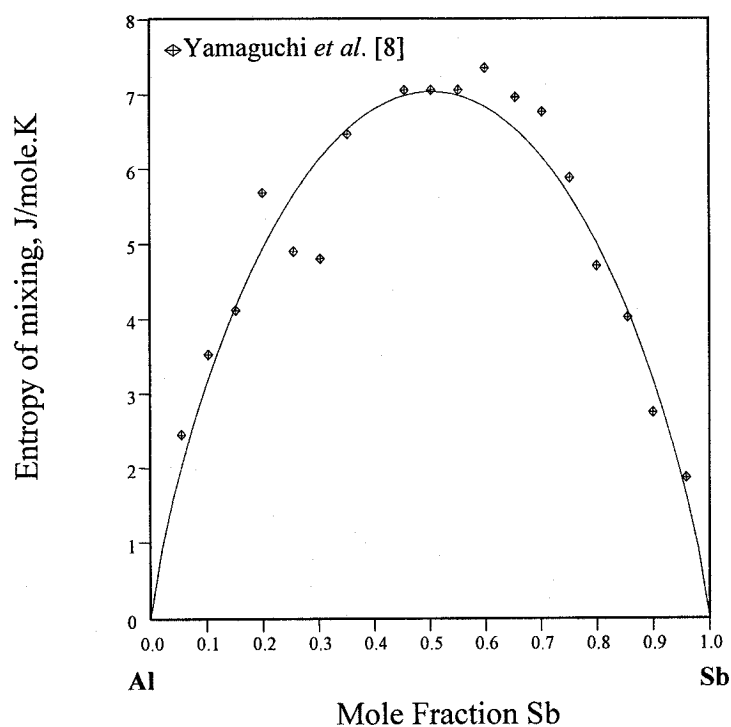


**Figure 4.4:** Entropy of mixing of liquid Al-Sb alloys at 1350 K: comparison between calculated values and the experimental data

Figure 4.5 shows that throughout the whole composition range, the calculated Gibbs free energy of mixing of Al-Sb liquid agrees with the experimental work of Yamaguchi *et al.* [8].



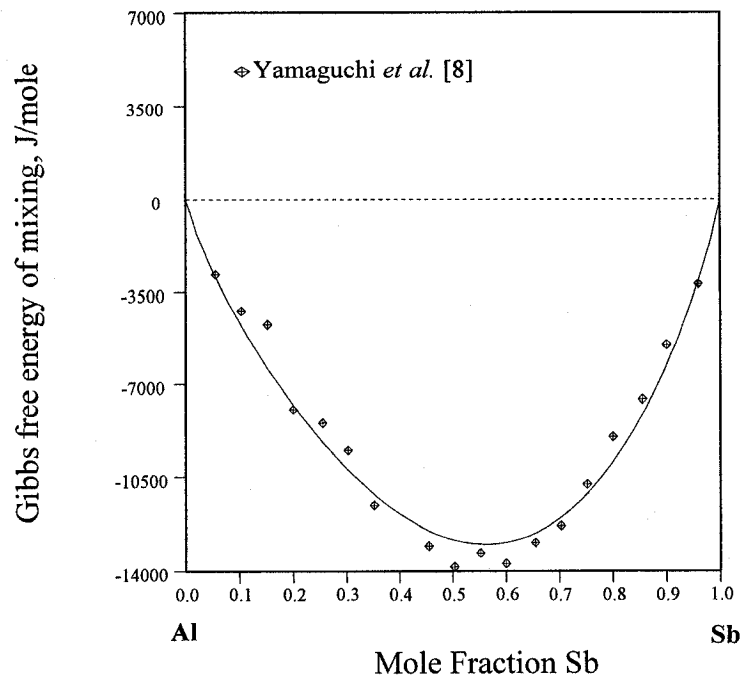


**Figure 4.5:** Gibbs free energy of mixing of liquid Al-Sb alloys at 1350 K: comparison between calculated values and the experimental data

The calculated enthalpy and entropy of formation of the compound AlSb are compared with the reported literature data in Table 4.3.

**Table 4.3:** Calculated enthalpy and entropy of formation of AlSb with the reported data from the literature

Temperature (K)	$\Delta H_f$ (kJ/mol)	$\Delta S_f$ (J/mol. K)	Reference
298	-96.60	-51.60	[9] Cal.
298	-73.49	-36.13	[10] Cal.
298	-84.00		[11] Cal.
298	$-82.00 \pm 2.51$		[27] Exp.
298	-81.27	-42.13	This work

Cal. denotes calculated values by associated solution model  
Exp. denotes experimental value by drop calorimetry

Table 4.3 shows that the calculated enthalpy and entropy of formation of AlSb in the present research is in good agreement with the calculated and experimental results reported in the literature.

#### 4.2 Mg-Sb BINARY SYSTEM

The selected experimental data of phase diagram, enthalpy of mixing, entropy of mixing, Gibbs free energy of mixing and activities of components Mg and Sb in liquid Mg-Sb alloys, which were discussed in section 2.2, were used to optimize the thermodynamic model parameters for the liquid,  $\alpha$ -Mg<sub>3</sub>Sb<sub>2</sub>, and  $\beta$ -Mg<sub>3</sub>Sb<sub>2</sub> phases. The optimized model parameters for the liquid,  $\alpha$ -Mg<sub>3</sub>Sb<sub>2</sub>,  $\beta$ -Mg<sub>3</sub>Sb<sub>2</sub> are given in Table 4.4.

**Table 4.4:** The optimized parameters for the liquid,  $\alpha$ -Mg<sub>3</sub>Sb<sub>2</sub>, and  $\beta$ -Mg<sub>3</sub>Sb<sub>2</sub>

Phase	Term	a (J/ mole atom)	b (J/ mole atom.K)
Liquid	L <sub>0</sub>	-172660.521	44.865
	L <sub>1</sub>	-157139.842	123.000
	L <sub>2</sub>	29500.000	10.637
	L <sub>3</sub>	127386.016	-98.780
$\alpha$ -Mg <sub>3</sub> Sb <sub>2</sub>	$\Delta G_f$	-98006.025	48.795
$\beta$ -Mg <sub>3</sub> Sb <sub>2</sub>	G(Mg:Mg:Mg)	65000.000	
	G(Mg:Sb:Mg)	-37429.535	-2.010
	G(Sb:Sb:Mg)	39651.000	-9.048
	L(Mg: Mg, Sb: Mg)	-150000.000	60.000

The reference structure of the Gibbs free energy of formation of  $\alpha$ -Mg<sub>3</sub>Sb<sub>2</sub> is considered as Mg-Hcp and Sb-Rhombo. No lattice stability values are added to the pure components Mg-hcp and Sb-rhombo. From the optimized model parameters, the phase

diagram and the thermodynamic properties of Mg-Sb system are calculated. Moreover, the obtained database can be combined with other binaries and used to interpolate and extrapolate the thermodynamic properties as well as to calculate meta-stable phase boundaries.

#### 4.2.1 Phase diagram

The calculated phase diagram is shown in Figure 4.6. It shows a fair agreement with the experimental data of Grube [32], Grube and Bornhak [33], Hansen and Anderko [35], and Rao and Patil [37]. A comparison between the results of this work and other works is given in Table 4.5.

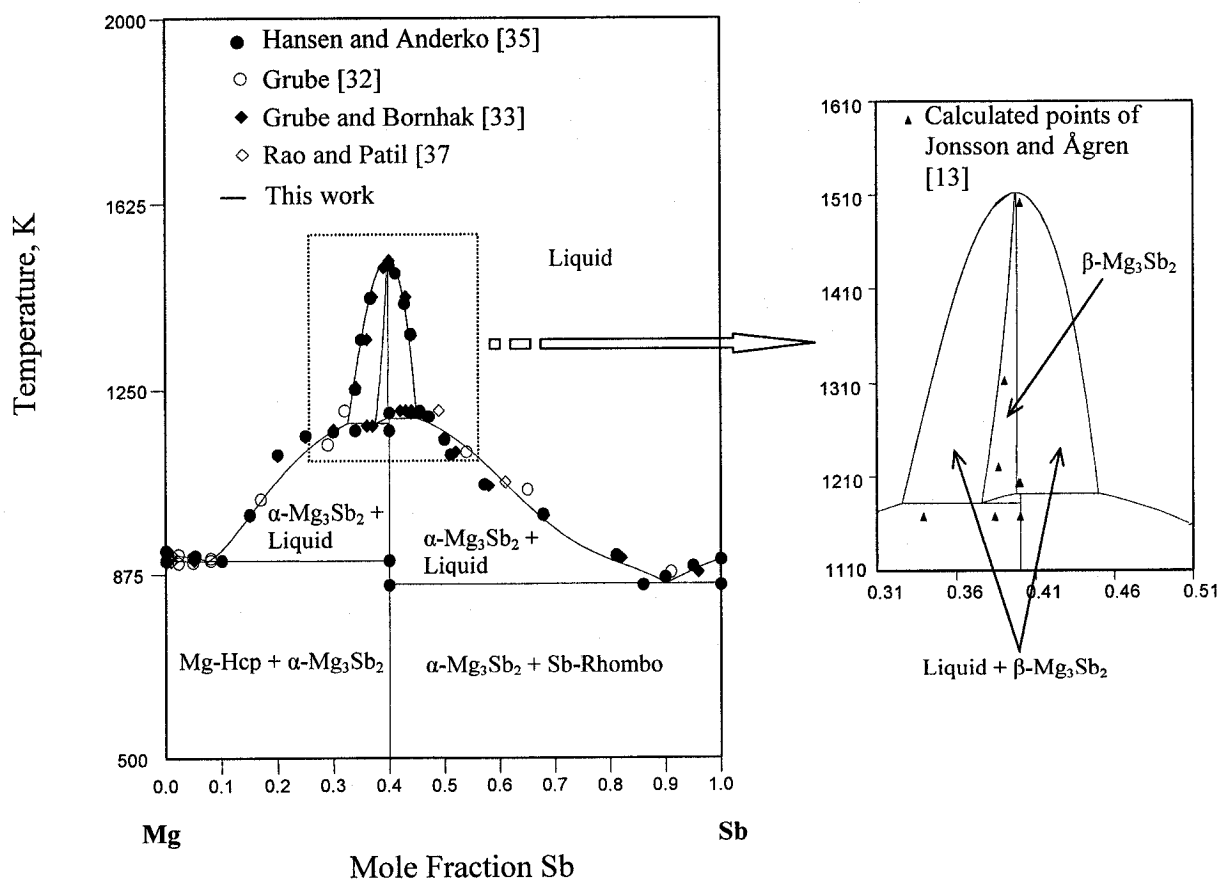


**Figure 4.6:** Calculated Mg-Sb phase diagram with experimental data from the literature

**Table 4.5.** Comparison between different works (calculations) on the equilibria in the Mg-Sb system

Reaction	Temperature (K)	Composition( $X_{Sb}$ )	Reference
$L=(Mg)+\alpha-Mg_3Sb_2$	902	0.026	[13]
	902	0.1	[33]
	902	0.1	[35]
	902	0.1	[40]
	902	0.076	This work
$L=(Sb)+\alpha-Mg_3Sb_2$	852	0.848	[13]
	852	0.86	[33]
	852	0.86	[35]
	852	$\sim 0.87$	[40]
	854	0.9	This work

#### 4.2.2 Thermodynamic properties

The calculated thermodynamic properties are in good agreement with the experimental data reported in the literature. As shown in Figure 4.7, the calculated activity of Mg in liquid Mg-Sb alloys at 1073 K is in fairly good agreement with the experimental data of Rao and Patil [37] and Eckert *et al.* [42].

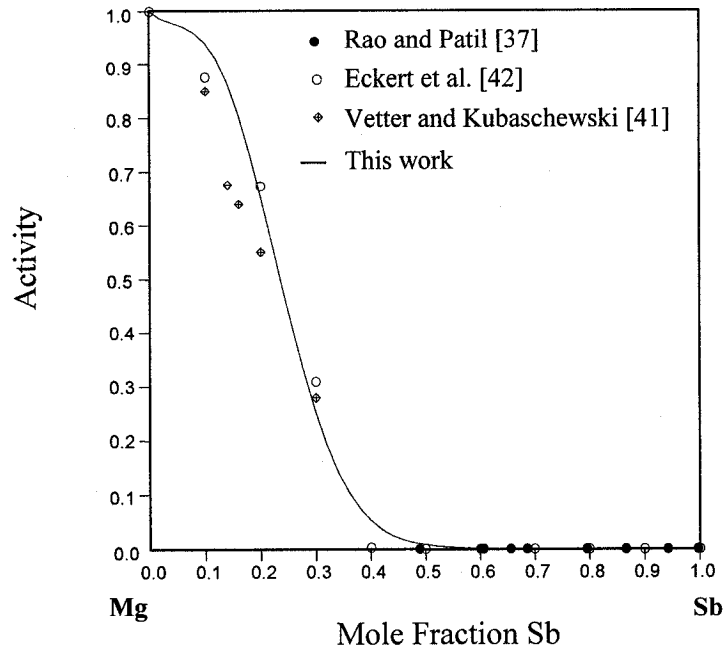


**Figure 4.7:** Activity of component Mg in the liquid Mg-Sb alloys at 1073 K: comparison between calculated values and the experimental data

The calculated entropy of mixing of liquid Mg-Sb alloys at 1073K, Figure 4.8, shows very good agreement with the experimental data of Rao and Patil [37].

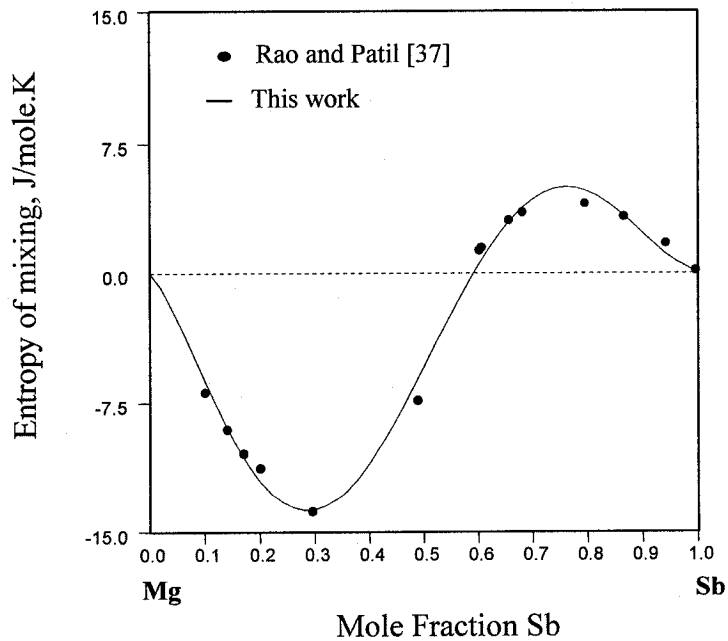


**Figure 4.8:** Entropy of mixing of liquid Mg-Sb alloys at 1073 K: comparison between calculated values and the experimental data

It can be observed from Figure 4.8 that, in the composition range of  $0.2 < X_{Sb} < 0.4$  the liquid Mg-Sb alloys show minimum (-ve) entropy and in the range of  $0.7 < X_{Sb} < 0.85$  they show maximum (+ve) entropy. That is, within the composition range of  $0.2 < X_{Sb} < 0.4$ , the liquid is relatively ordered and in the range of  $0.7 < X_{Sb} < 0.85$  it is highly disordered.

The calculated enthalpy of mixing and Gibbs free energy of mixing of liquid Mg-Sb at 1073K are shown in Figure 4.9 and 5.10, respectively. They also show good agreement with the experimental data from the literature.

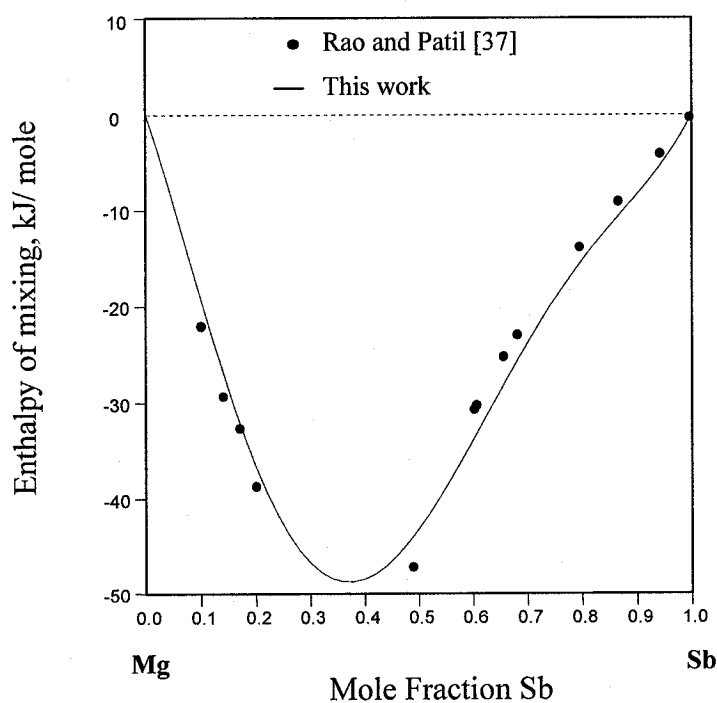


**Figure 4.9:** Enthalpy of mixing of liquid Mg-Sb alloys at 1073 K: comparison between calculated values and the experimental data

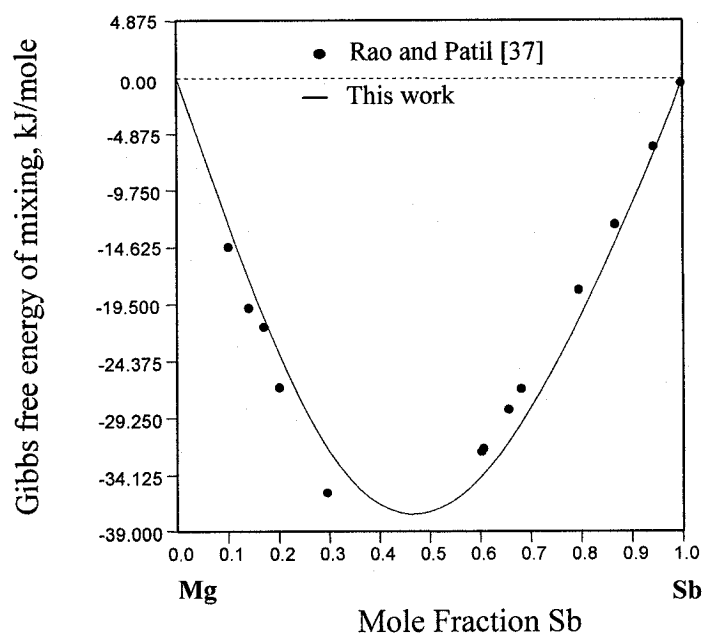


**Figure 4.10:** Gibbs free energy of mixing of liquid Mg-Sb alloys at 1073 K: comparison between calculated values and the experimental data

The calculated enthalpy and entropy of formation of the compound  $\alpha\text{-Mg}_3\text{Sb}_2$  are compared with the data reported in the literature in Table 4.6.

**Table 4.6:** Calculated enthalpy and entropy of formation of  $\alpha\text{-Mg}_3\text{Sb}_2$  with the reported data from the literature.

Temperature (K)	$\Delta H_f$ (kJ/mol)	$\Delta S_f$ (J/mol. K)	Reference
900	$-299 \pm 3^*$	$-59 \pm 5^*$	[37] Exp. 1
773	$-235 \pm 6^*$	$-15 \pm 10^*$	[40] Exp. 1
923	$-285^{**}$		[43] Exp. 2
800	$-320 \pm 40$	$-91 \pm 52$	[45] Cal.
298	-300	-	[46] Cal.
298	-490	-54	This work

Exp. 1 denotes the experimental values by emf measurements

Exp. 2 denotes the experimental value by high temperature calorimeter measurements

Cal. denotes calculated values

It can be observed from Table 4.6 that, the calculated enthalpy value in the present research is some what higher than the experimental values reported in the literature. This may be due to the assumption, that the low temperature modification  $\alpha\text{-Mg}_3\text{Sb}_2$  is a stoichiometric compound.

### **4.3 Mg-Al-Sb TERNARY SYSTEM**

For the first time Mg-Al-Sb system is thermodynamically modeled. A database was constructed for this system by combining the binary thermodynamic descriptions of Mg-Al, Al-Sb, and Mg-Sb. The database is used to calculate polythermal projections of liquidus surfaces, ternary isothermal sections, ternary isopleths (constant composition sections), pseudo-binary phase diagrams, and phase assemblage diagrams.

#### **4.3.1 Polythermal projections of liquidus surfaces**

A two dimensional representation of the ternary liquidus surface is obtained as an orthogonal projection upon the base composition triangle with components Mg, Al, and Sb and shown in Figure 4.11. The dashed lines are the constant temperature lines called liquidus isotherms and the thick continuous lines are the univariant valleys. The arrows indicate the direction of decreasing temperature along the univariant valleys.

There is a ternary liquid miscibility gap in the composition range of  $0.0048 < X_{\text{Sb}} < 0.375$ . Even though the three binaries in the Mg-Al-Sb system do not show any liquid



miscibility gap, it is observed in the ternary system, this is known as closed miscibility gap. The critical points in Mg-Al-Sb ternary phase diagram are

- (1) 6 ternary eutectics:  $E_1$ ,  $E_2$ ,  $E_3$ ,  $E_4$ ,  $E_5$ , and  $E_6$
- (2) 2 peritectics:  $P_1$  and  $P_2$
- (3) 1 saddle point:  $S_1$  and
- (4) 4 plait points: Plait point 1, 2, 3, and 4



Plait points are the maximum or minimum temperature points at which two or three liquid phases exist in equilibrium [65].

Table 4.7 shows the estimated critical points and expected reactions at those points.

**Table 4.7: Calculated invariants points and reactions**

Critical point	X <sub>Sb</sub>	X <sub>Mg</sub>	Temperature (K)	Reaction
E <sub>1</sub>	0.902	0.093	852.6	$L \leftrightarrow \text{AlSb} + \text{Sb} + \alpha\text{-Mg}_3\text{Sb}_2$
E <sub>2</sub>	0.063	0.930	898.8	$L \leftrightarrow \alpha\text{-Mg}_3\text{Sb}_2 + (\text{Mg})$
E <sub>3</sub>	0.1E-7	0.690	708.9	$L \leftrightarrow (\text{Mg}) + \alpha\text{-Mg}_3\text{Sb}_2 + \gamma$
E <sub>4</sub>	0.1E-7	0.424	721.8	$L \leftrightarrow \gamma + \alpha\text{-Mg}_3\text{Sb}_2 + \text{Al}_{140}\text{Mg}_{89}$
E <sub>5</sub>	0.1E-7	0.362	723.4	$L \leftrightarrow \alpha\text{-Mg}_3\text{Sb}_2 + (\text{Al}) + \text{Al}_{140}\text{Mg}_{89}$
E <sub>6</sub>	0.003	0.002	930.2	$L \leftrightarrow \text{AlSb} + (\text{Al}) + \alpha\text{-Mg}_3\text{Sb}_2$
P <sub>1</sub>	0.017	0.959	987.4	$L \leftrightarrow L + (\text{Mg}) + \alpha\text{-Mg}_3\text{Sb}_2$
P <sub>2</sub>	0.075	0.040	1133.2	$L \leftrightarrow L + \alpha\text{-Mg}_3\text{Sb}_2 + \text{AlSb}$
S <sub>1</sub>	0.430	0.398	1136.9	$L \leftrightarrow \alpha\text{-Mg}_3\text{Sb}_2 + \text{AlSb}$
Plait point 1	0.375	0.353	1133.2	$L / L + \text{Liquid \#2} + \alpha\text{-Mg}_3\text{Sb}_2 + \text{AlSb}$
Plait point 2	0.278	0.122	1226.0	$L / L + \text{Liquid \#2} + \text{AlSb}$
Plait point 3	0.037	0.950	901.3	$L / L + \text{Liquid \#2} + \alpha\text{-Mg}_3\text{Sb}_2 + (\text{Mg})$
Plait point 4	0.292	0.472	1164.0	$L / L + \text{Liquid \#2} + \alpha\text{-Mg}_3\text{Sb}_2$

The different phase fields around the plait points 1, 2, 3, and 4 are shown in Figure 4.12 (a), (b), (c), and (d), respectively. The compositions of the plait points are shown by the vertical dashed lines.

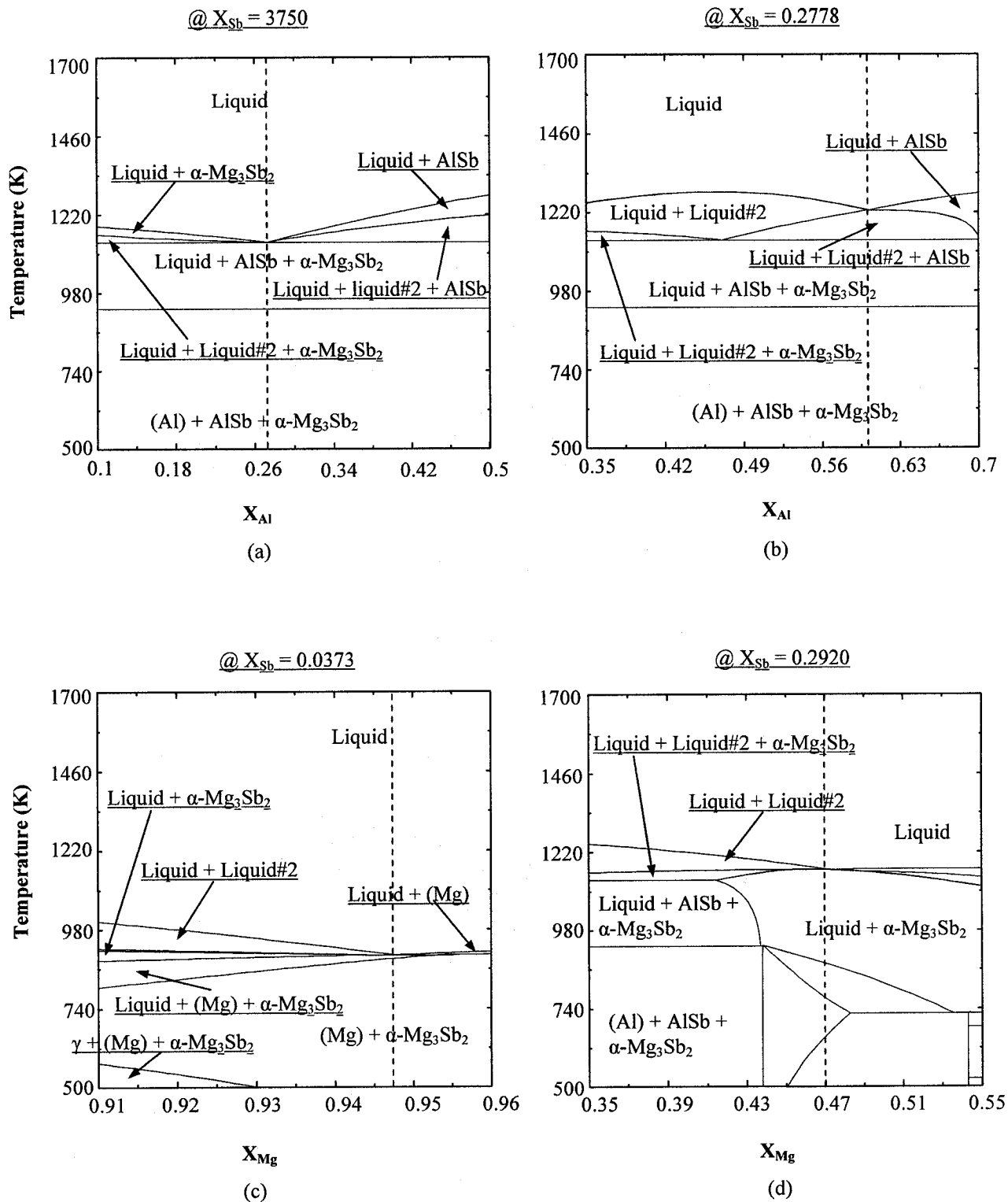
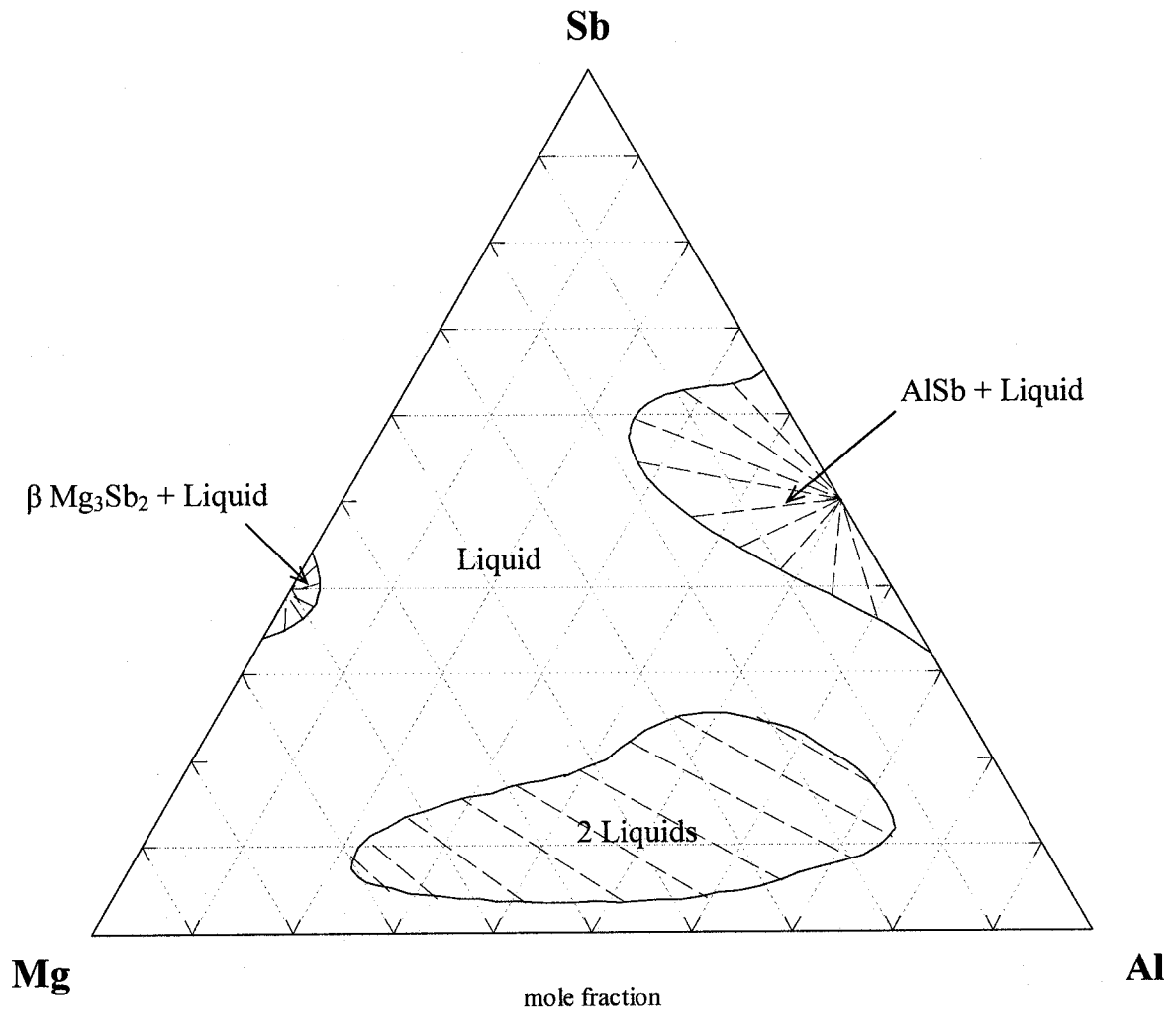


Figure 4.12: Different phase fields around the plait points in the Mg-Al-Sb ternary system

### 4.3.2 Ternary isothermal sections

Polythermal projections of the liquidus surface do not provide information on the compositions of the solid phases at equilibrium. However, this information can be presented at any one temperature on an isothermal section such as that shown for the Mg-Al-Sb system at 1300 K in Figure 4.13.



**Figure 4.13:** Isothermal section of the Mg-Al-Sb system at 1300 K.

The liquidus lines bordering the single phase of Figure 4.13 are identical to the 1300 K isotherms of the projection in Figure 4.11. The dashed lines in the two phase regions in Figure 4.13 are the tie lines. If the overall composition lines within one of the two phase regions, the compositions of the two phases are given by the ends of the tie lines which passes through the overall composition. Figure 4.14 shows another isothermal section of the Mg-Al-Sb system at 1400 K.

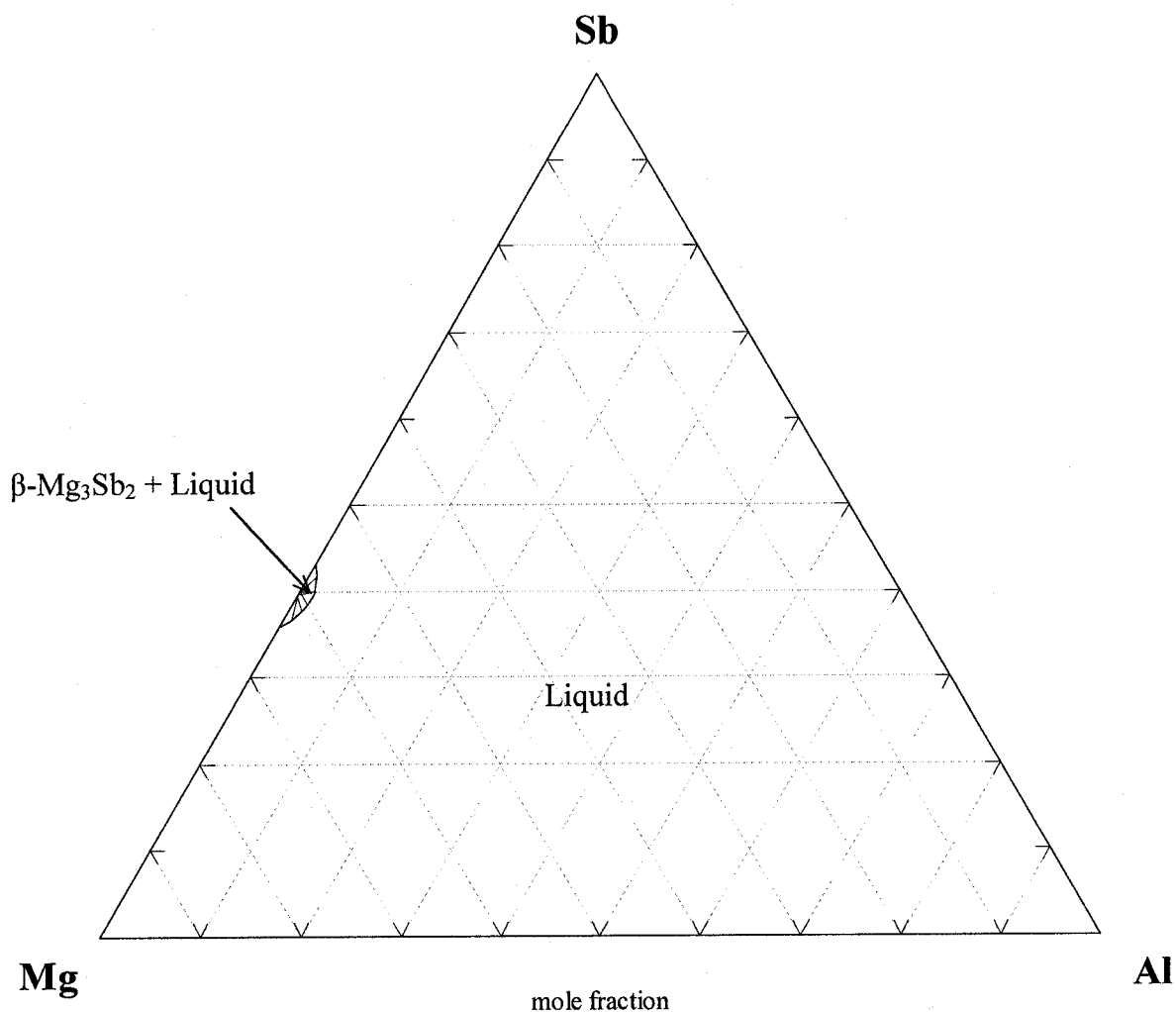


**Figure 4.14:** Isothermal section of the Mg-Al-Sb system at 1400 K.

It can be seen from Figure 4.14 that, at 1400 K: only  $\beta\text{-Mg}_3\text{Sb}_2$  is in equilibrium with homogenous liquid phase, there is no ternary liquid immiscibility. However, at 1300 K (Figure 4.13):  $\beta\text{-Mg}_3\text{Sb}_2$  and  $\text{AlSb}$  are in equilibrium with homogeneous liquid phase, there is ternary liquid miscibility gap.

From this comparison it can be concluded that, the compound  $\beta\text{-Mg}_3\text{Sb}_2$  has the highest melting point in the Mg-Al-Sb system, and the ternary liquid miscibility gap starts below 1400 K namely at 1386.5 K.

### 4.3.3 Pseudo-binary phase diagrams

One of the benefits of establishing thermodynamic database for a multicomponent system is the ability to calculate different types of diagrams in relation to temperature and composition of the components. The Pseudo-binary phase diagram is one of these types of diagrams which can be calculated from a thermodynamic database. It is drawn between two compounds in a system.

In order to see the reliability of the present research work, the obtained thermodynamic database for the Mg-Al-Sb systems is used to predict the pseudo-binary diagrams of Al-AlSb, AlSb- $\text{Mg}_3\text{Sb}_2$ , and Al- $\text{Mg}_3\text{Sb}_2$  and compared with the reported experimental observation in the literature.

As discussed in chapter 2.4, Loofs-Rassow [51] reported that Al-AlSb and AlSb -  $\text{Mg}_3\text{Sb}_2$  systems form a homogeneous liquid phase at high temperature and they do not form miscibility gaps. Hence, to see the reliability of the present thermodynamic model

for the Mg-Al-Sb system, quasi-binary phase diagrams are calculated and drawn for Al-AlSb and AlSb-Mg<sub>3</sub>Sb<sub>2</sub> systems. These diagrams are shown in Figure 4.15 and 4.16.

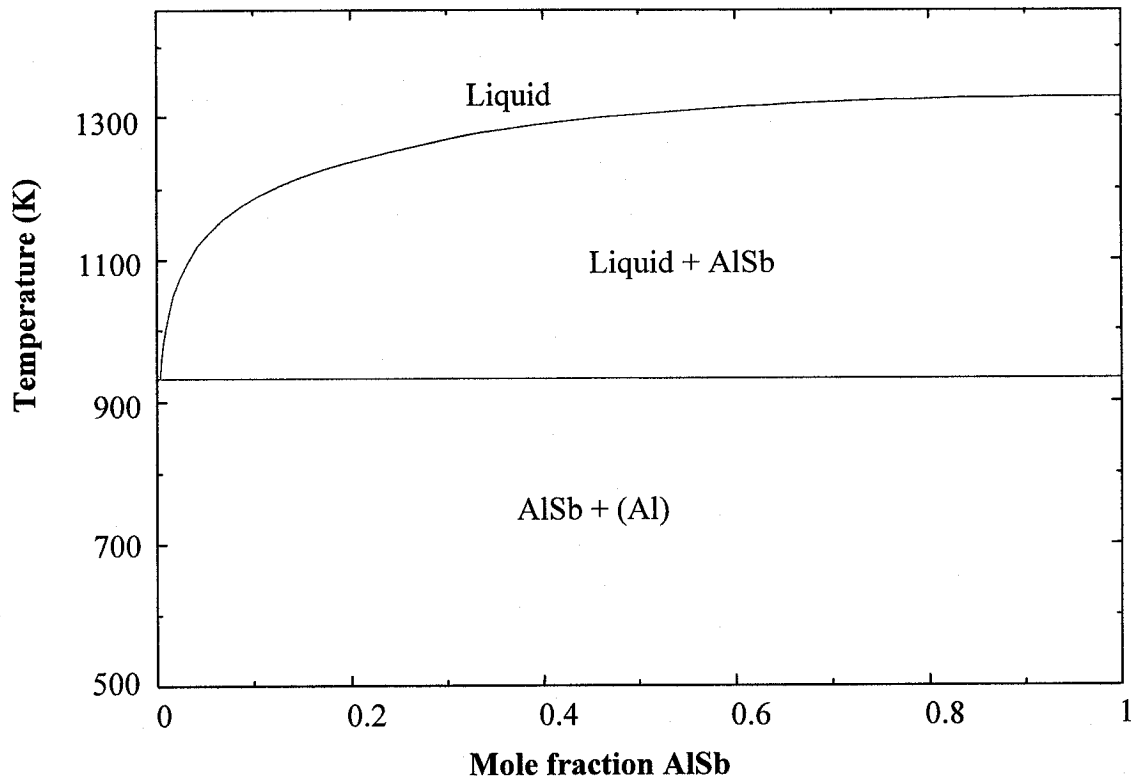


**Figure 4.15:** Pseudo- binary Al-AlSb phase diagram



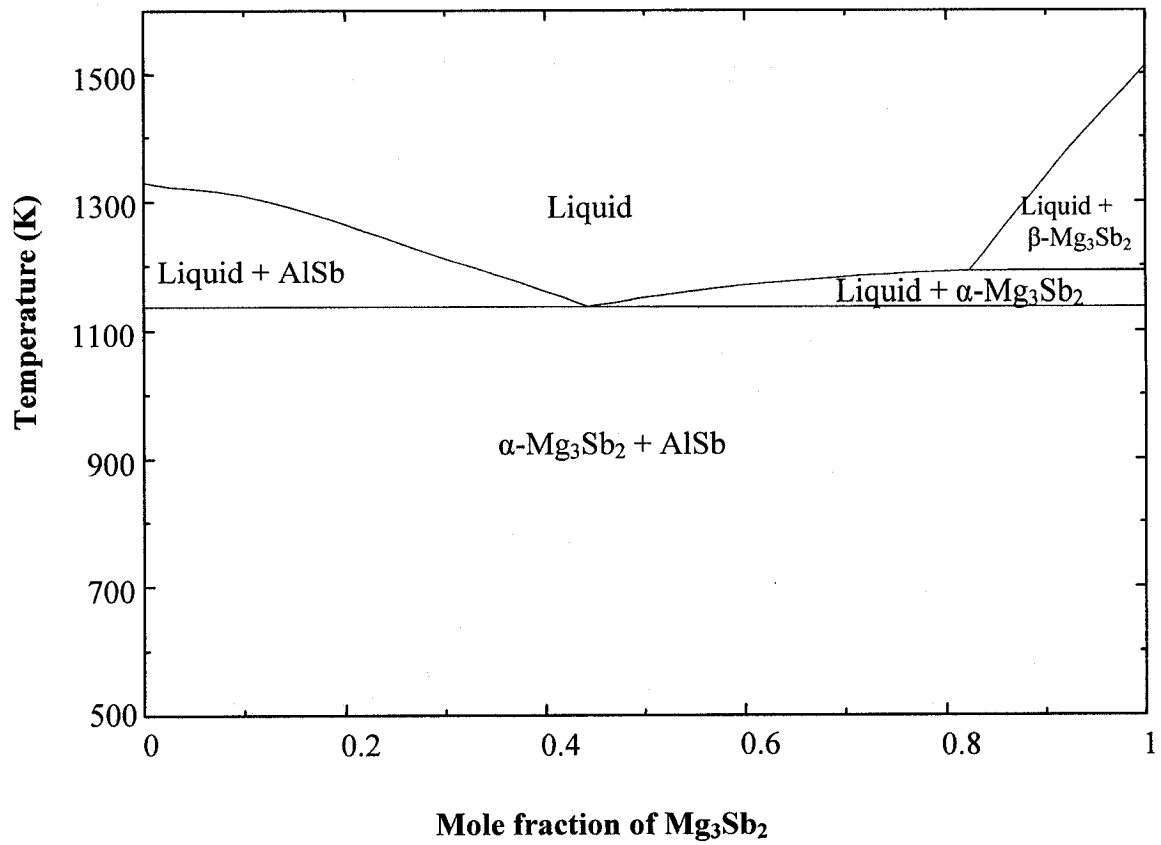


**Figure 4.16:** Pseudo-binary AlSb-Mg<sub>3</sub>Sb<sub>2</sub> phase diagram

Neither Figure 4.15 nor 4.16 show liquid miscibility gaps. This means that the present model is supported by the experimental work of Loofs-Rassow [51]. Moreover Loofs-Rassow [51] and Guertler and Bergman [50] reported that there is a liquid miscibility gap in the binary Al-Mg<sub>3</sub>Sb<sub>2</sub>. This experimental observation was also reproduced in the pseudo-binary Al-Mg<sub>3</sub>Sb<sub>2</sub> calculated from the current thermodynamic model and shown in Figure 4.17.

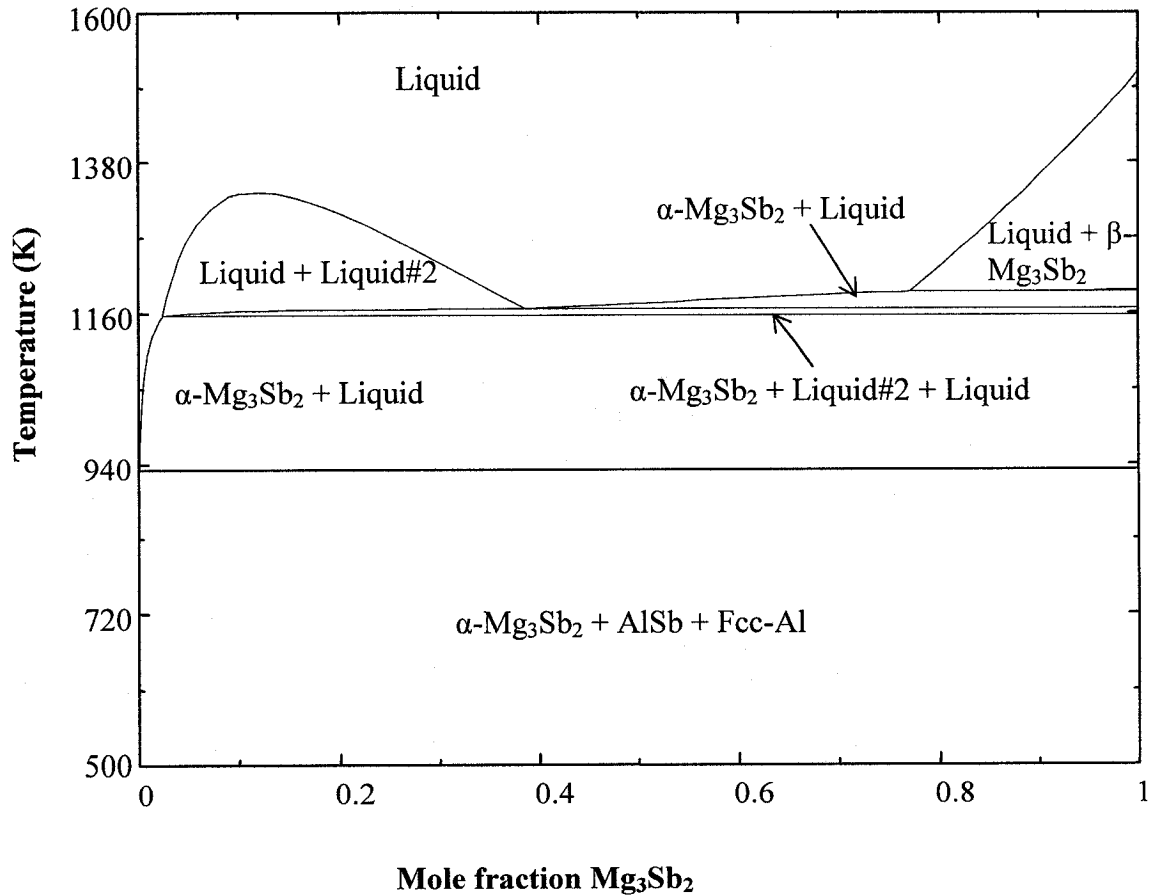


**Figure 4.17:** Calculated pseudo-binary Al-Mg<sub>3</sub>Sb<sub>2</sub> phase diagram

#### 4.3.4 Ternary isopleths (at constant composition of one component)

A vertical isopleth, or constant composition section (ie. composition of one component is fixed) through the space model of the Mg-Al-Sb system is shown in Figure 4.18. The phase fields on Figure 4.18 indicate which phases are present when a set of alloys with overall composition of 0.5A Mg- (0.5-0.5A) Al- 0.5 Sb is equilibrated at any temperature. Here A ranges from 0 to 1. It should be noted that on an isopleth the tie lines do not, in general, lie in the plane of the diagram [2]. Hence, the lever rule cannot be applied on an

isopleth diagram. That is, the isopleth diagram provides information only on which phases are present, not their compositions.

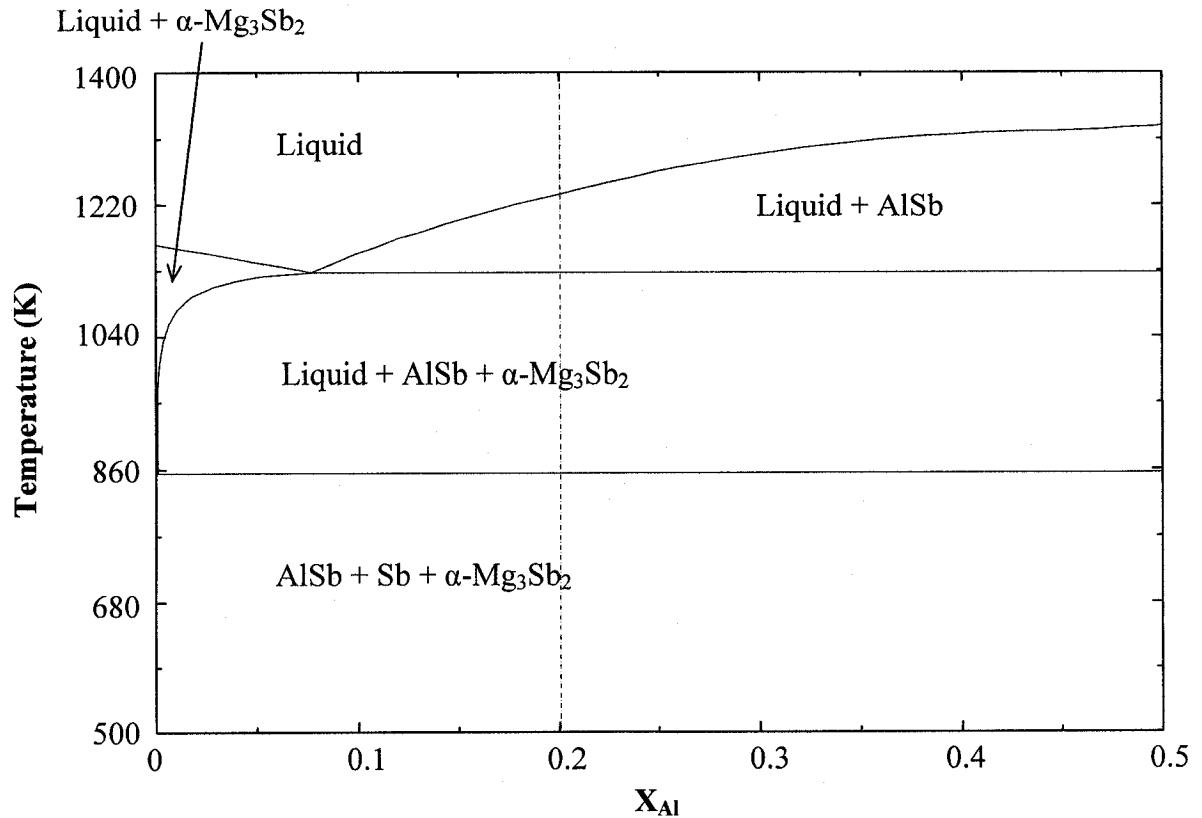


**Figure 4.18:** Isopleth of the Mg-Al-Sb system at  $X_{Sb} = 0.5$

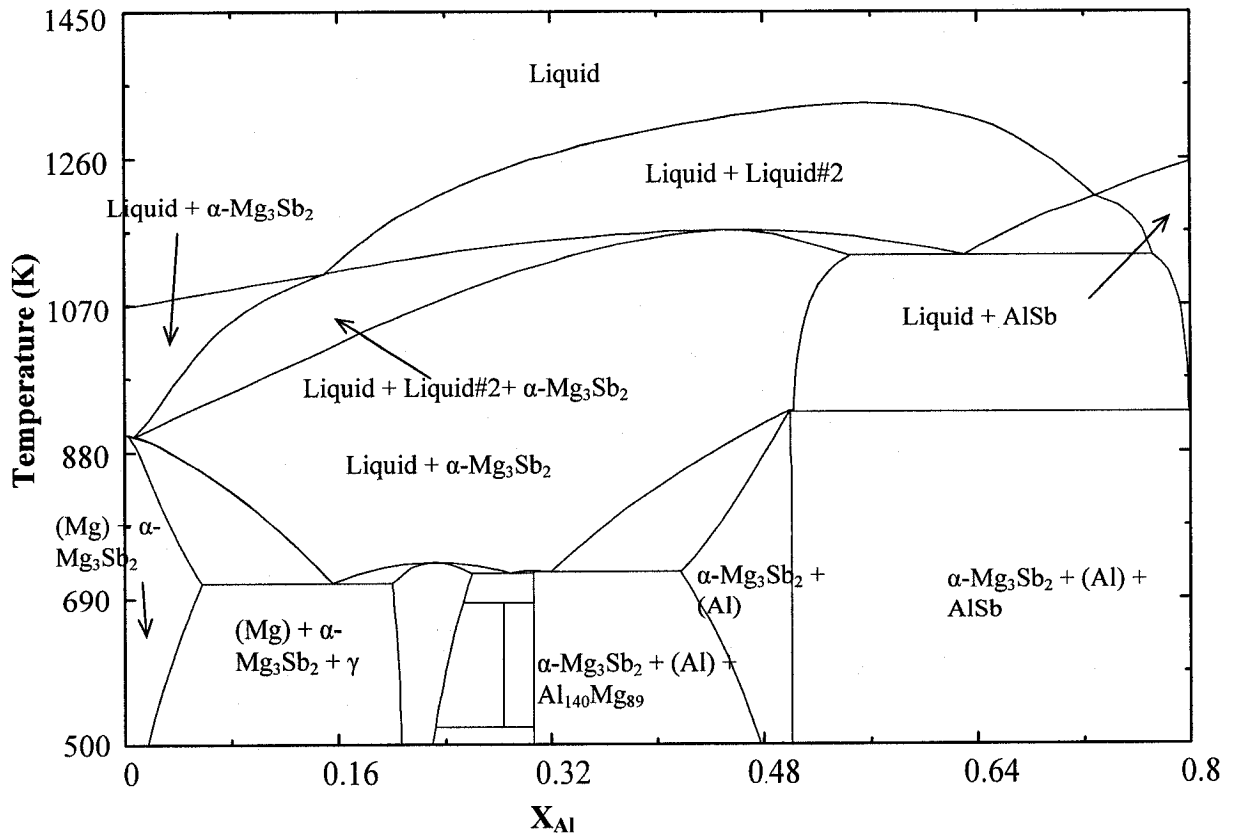
The application of an isopleth can be explained by the following example. Consider an alloy of 0.3 Mg-0.2 Al- 0.5 Sb. The position of this composition is shown in the Figure 4.18 with a vertical dashed line through 0.2 Al. The different phase fields of this alloy during cooling from 1400 K to 500 K are,

From 1400 K to ~ 1234 K: Liquid

From 1234 K to ~ 1127 K: Liquid + AlSb

From 1227 K to ~ 852 K: Liquid + AlSb +  $\alpha$ -Mg<sub>3</sub>Sb<sub>2</sub>

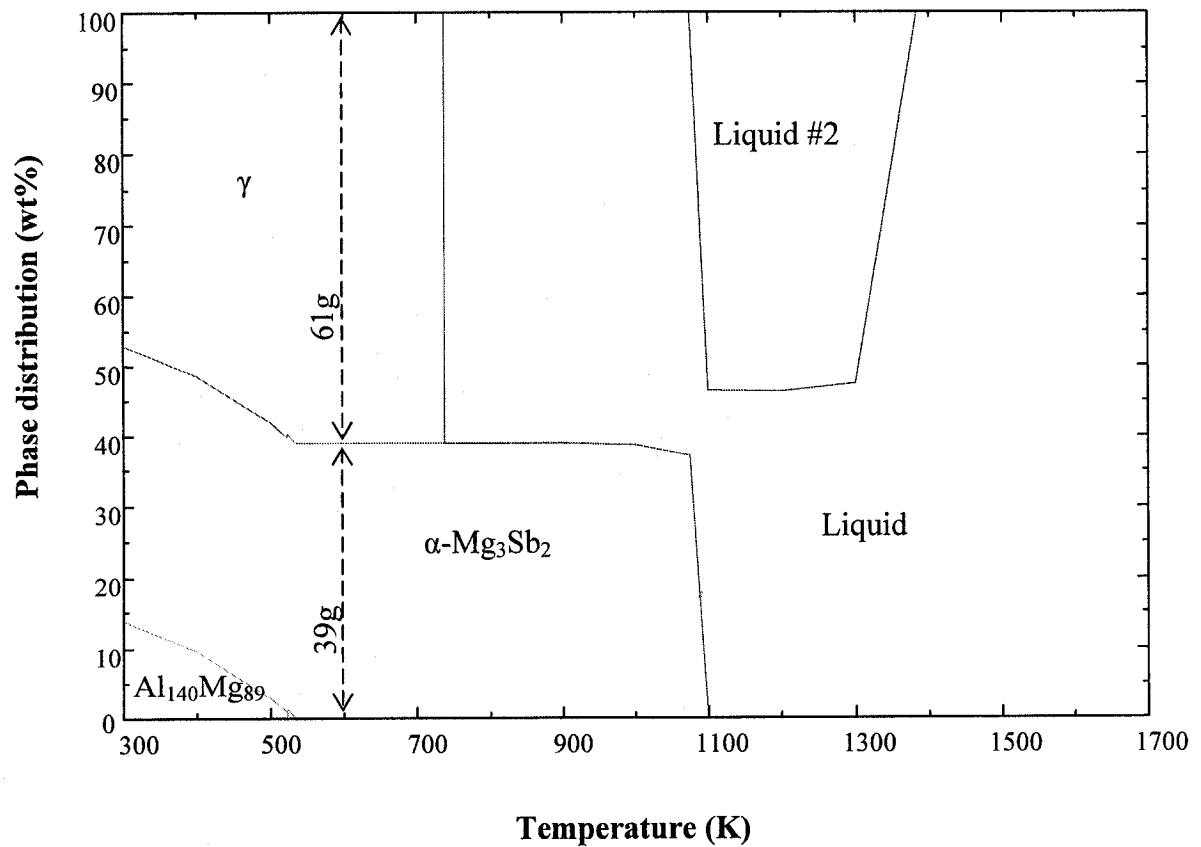
From 852 K to 500 K: AlSb + Sb +  $\alpha$ -Mg<sub>3</sub>Sb<sub>2</sub>



**Figure 4.19:** Isopleth of the Mg-Al-Sb system at  $X_{Sb} = 0.2$

Figure 4.19 is the isopleth of the Mg-Al-Sb system at  $X_{Sb} = 0.2$  which shows the ternary liquid miscibility gap at high temperature. As the isopleth diagram shows different phases that occur during cooling of an alloy, it can also be used to identify the eutectic reaction temperatures in the alloy system.

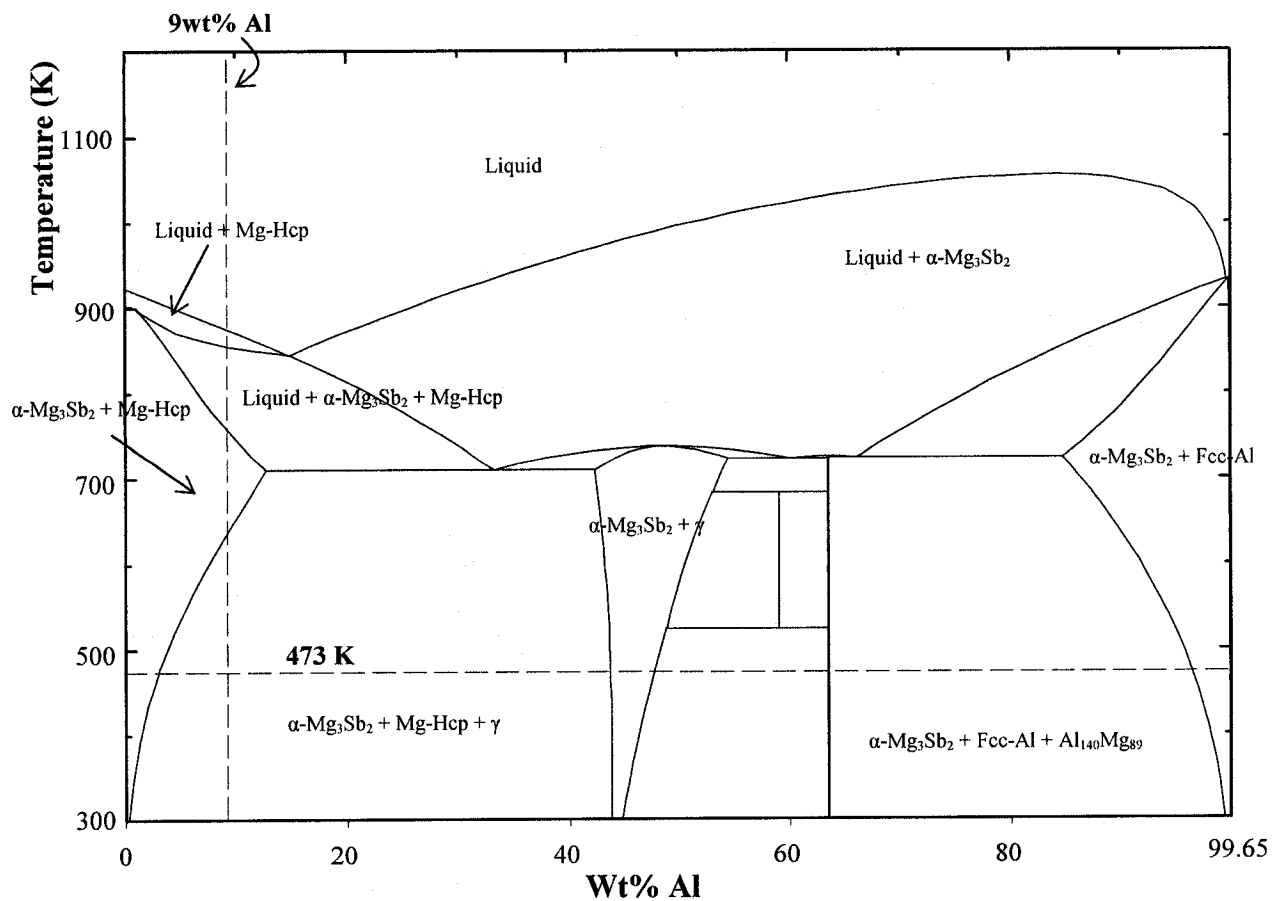
### 4.3.5 Phase assemblage diagrams



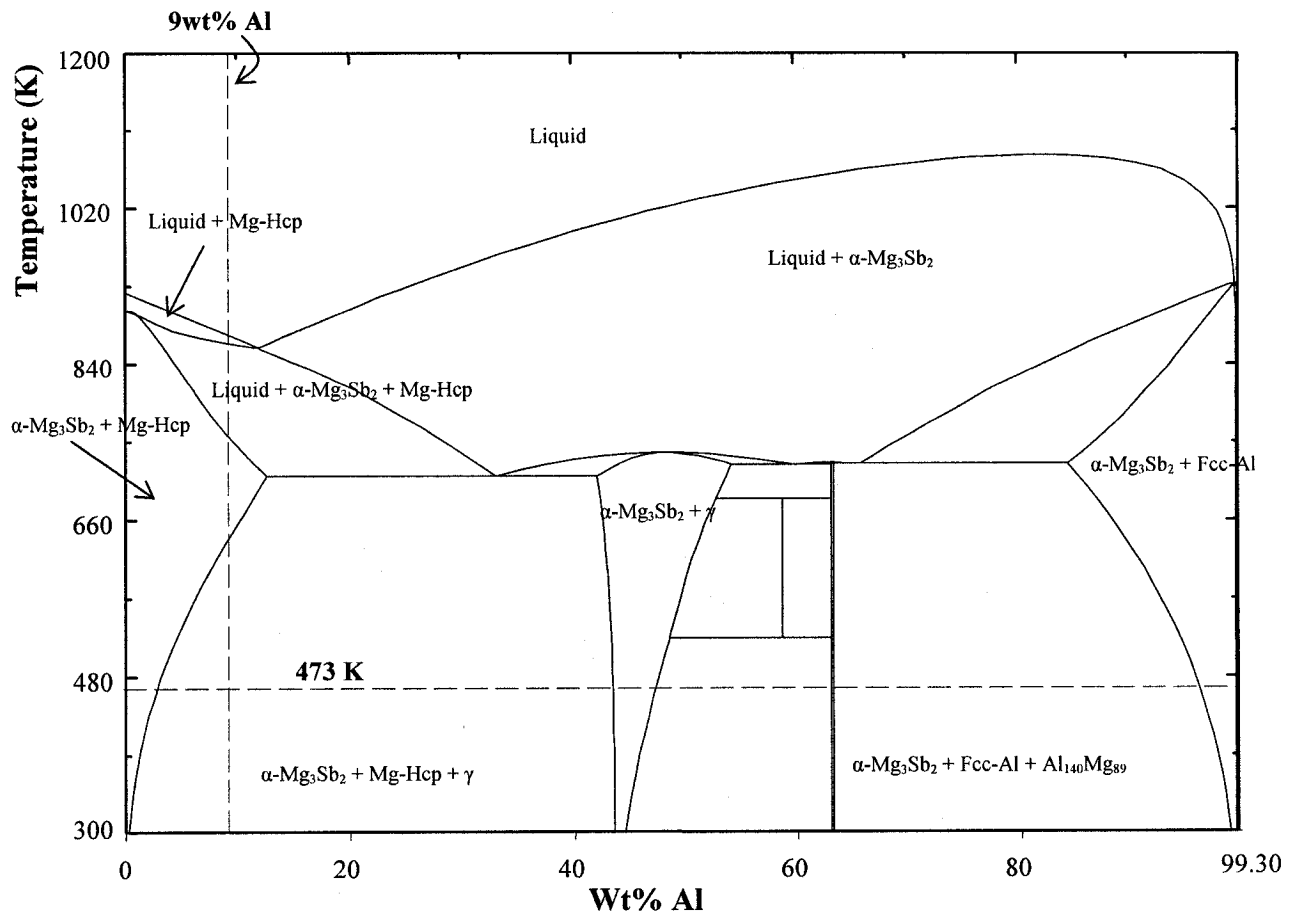
**Figure 4.20:** Phase assemblage diagram of 40wt% Mg, 30wt% Al, and 30wt% Sb

Figure 4.20 shows the phase assemblage diagram of the alloy 40wt% Mg, 30wt% Al, and 30wt% Sb. By drawing this diagram at a specific composition the relative amount of the phases can be calculated. For example, at 600 K, an alloy of this composition with an overall weight of 100g consists of 39g of  $\alpha\text{-Mg}_3\text{Sb}_2$  and 61g of  $\gamma$ . The applications of phase assemblage diagrams and isopleth diagrams are demonstrated in the following examples.

As it can be seen from Figure 1.2, the AZ91 alloy with 0.35wt% Sb shows higher creep resistance than that of 0.70wt% Sb. Also, it was discussed in section 1.2 that the improvement in creep resistance in these alloys is due to the formation of  $\text{Mg}_3\text{Sb}_2$  precipitates. Hence, to have an idea of different phases in these two alloys, by assuming that the presence of Zn and Mn alloying elements do not affect the formation of  $\text{Mg}_3\text{Sb}_2$  precipitates, vertical sections of the Mg-Al-Sb system at constant Sb of 0.35wt% Sb and 0.70wt% Sb are drawn and shown in Figures 4.21 and 4.22.



**Figure 4.21:** Isopleth of the Mg-Al-Sb system at 0.35wt% Sb



**Figure 4.22:** Isopleth of the Mg-Al-Sb system at 0.7 wt% Sb

It can be observed from Figures 4.21 and 4.22 that, during cooling, the alloys Mg-9Al-0.35Sb and Mg-9Al-0.7Sb pass through same phase fields. Hence, it can be deduced that the difference in creep resistance in AZ91 alloys with 0.35wt%Sb and 0.7wt%Sb may be due to the difference in the relative amounts of these phases. In order to obtain the relative amounts of phases, phase assemblage diagrams are drawn for the Mg-Al-Sb system at constant composition of Sb of 0.35 wt% and 0.7 wt%Sb and shown in Figures 4.23 and 4.24, respectively.

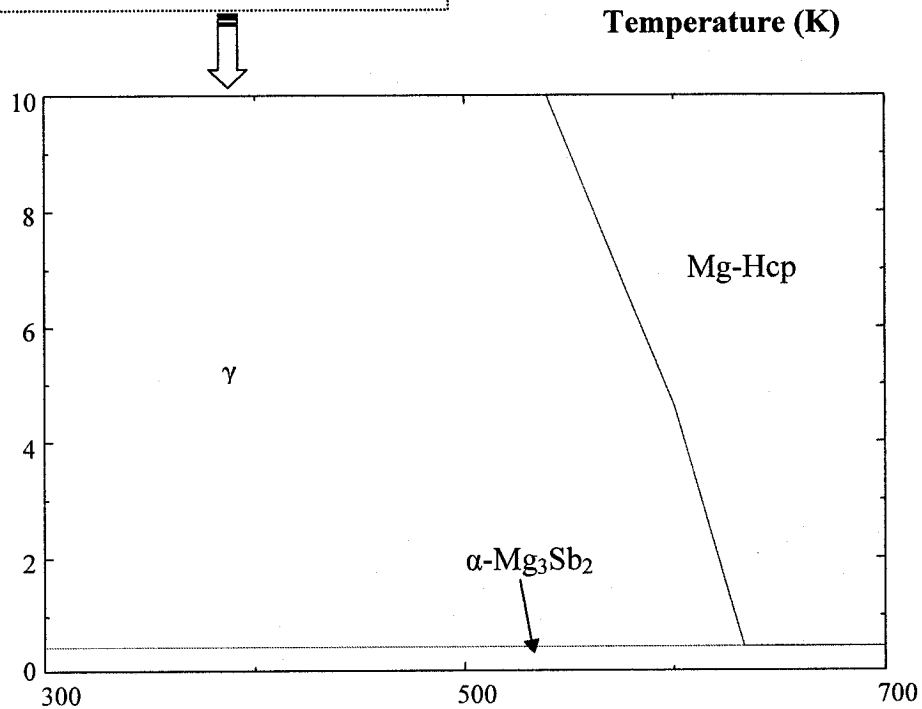
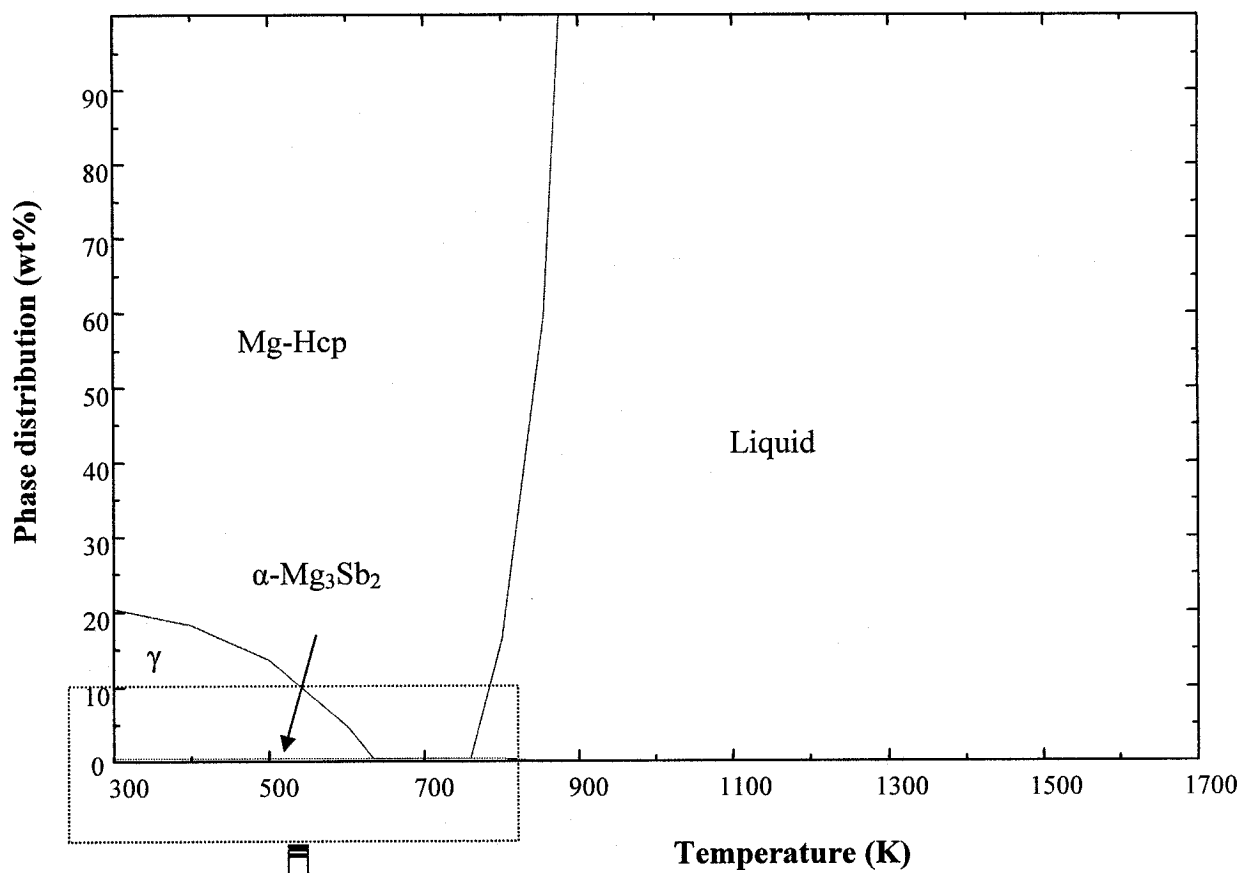


**Figure 4.23:** Phase assemblage diagram of Mg-9Al-0.35Sb



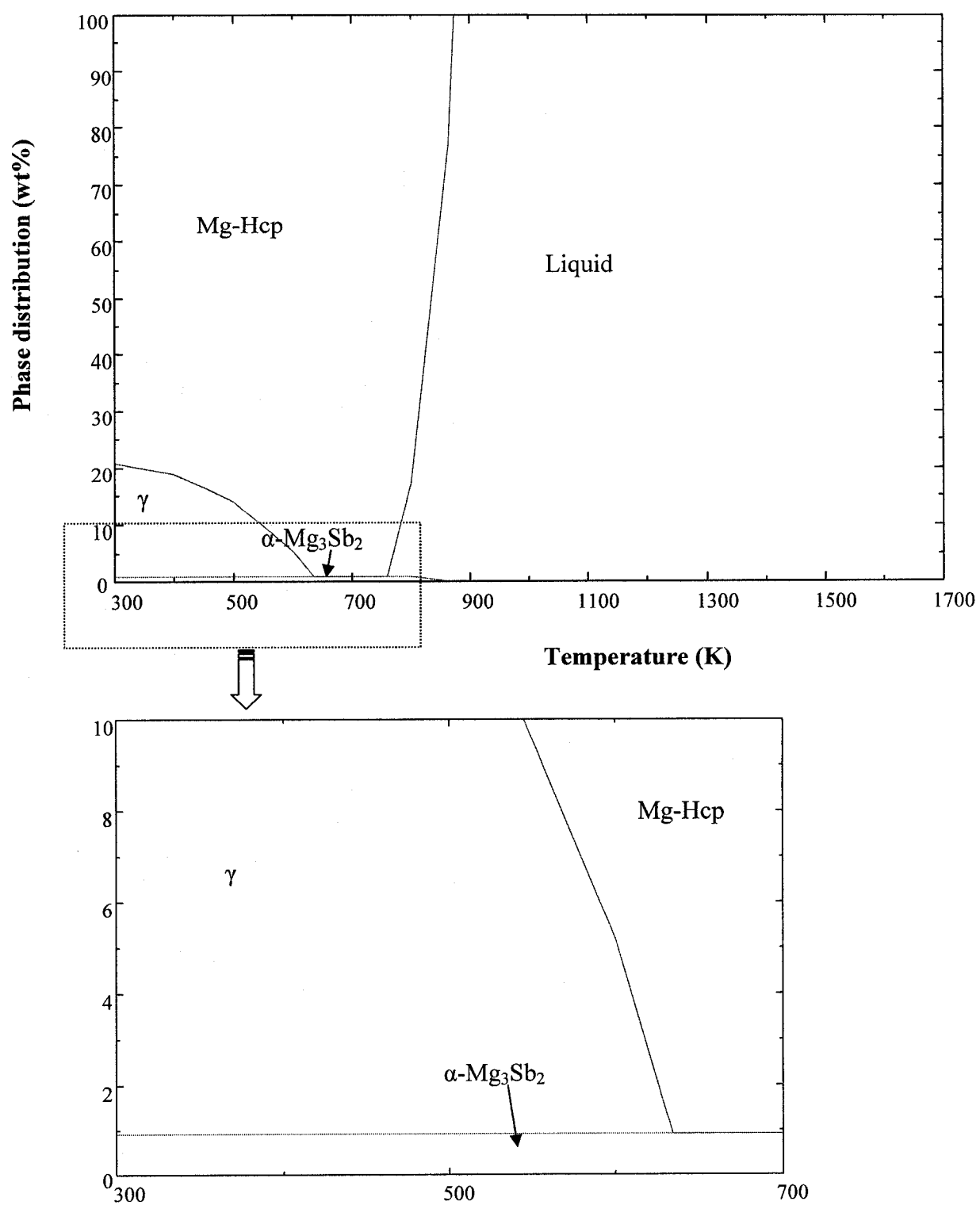


**Figure 4.24:** Phase assemblage diagram of Mg-9Al-0.7Sb

It can be seen from Figures 4.23 and 4.24 that, at 473 K, the amount of  $\text{Mg}_3\text{Sb}_2(\text{s})$  phase varies from 0.4 to 0.9 wt% when Sb addition varies from 0.35 – 0.7 wt%. Hence, in Figure 1.2, the lower creep resistance of alloy 4 than that of alloy 3 may be due to the large precipitates of  $\text{Mg}_3\text{Sb}_2$ .

# CHAPTER 5

---

## CONCLUSIONS, CONTRIBUTIONS AND SUGGESTIONS FOR FUTURE WORK

### 5.1 CONCLUSIONS

In this research, the Mg-Al-Sb system was thermodynamically modeled as part of thermodynamic database construction for Mg-Al based alloys and the following conclusions were drawn:

Optimized thermodynamic model parameters for different phases in the binaries Al-Sb, and Mg-Sb were obtained, where, the liquid phases were described by Redlich-Kister polynomial model and the non-stoichiometric compound  $\beta\text{-Mg}_3\text{Sb}_2$  was described by a sublattice model. The model parameters of different phases were optimized with no added lattice stability values to the pure components Mg-Hcp, Al-Fcc, and Sb-Rhombo.

From the obtained optimized model parameters, phase diagrams of Al-Sb, Mg-Sb and the thermodynamic properties such as enthalpy, entropy, Gibbs free energy, and activity were calculated and compared with the experimental literature data. The calculated phase diagrams and thermodynamic properties were found to be in good agreement with the data reported in the literature.

The thermodynamic database of Mg-Al-Sb system was constructed by combining the databases of the constituent binaries Mg-Al, Al-Sb, and Mg-Sb. From the established thermodynamic database, the Mg-Al-Sb ternary phase diagram was calculated and the critical points were predicted. It was found that Mg-Al-Sb system has six eutectics, two peritectics, one saddle point, and four plait points.

A closed ternary liquid miscibility gap was predicted by the established Mg-Al-Sb thermodynamic database. By drawing isopleth diagrams and pseudo-binary diagrams this ternary liquid immiscibility gap was compared and found consistent with the reported experimental observations in the literature.

The thermodynamic database forms the basis for understanding the existing Mg-Al-Sb alloys and for developing new alloys in this system.

## **5.2 CONTRIBUTIONS**

In this work, the Mg-Al-Sb system was modeled and the database was constructed for the first time.

As the present thermodynamic database of Mg-Al-Sb was constructed without any added lattice stability values to the pure components, it could be easily used in building a multicomponent database of Mg-Al based alloys.

The constructed thermodynamic database of the Mg-Al-Sb system, which is found to be an interesting creep resistant Mg alloy system, allows the researchers to study this system thoroughly and select useful compositions to make key experiments towards finding the optimum creep resistant Mg-Al-Sb alloy for today's needs.

### 5.3 SUGGESTIONS FOR FUTURE WORK

Experimental determination of the crystal structure and the solubility limit of  $\beta$ -Mg<sub>3</sub>Sb<sub>2</sub> phase are still needed. Then, a thermodynamic model based on these findings should be carried out.

The established database is a first step to construct the equilibria in the Mg-Al-Sb system and should be followed by key experiments to determine the exact location of the critical points and the miscibility gap.

Experimental work is to be done on the measurement of thermodynamic properties of the ternary Mg-Al-Sb liquid alloys.

As the predicted Mg-Al-Sb ternary system shows a ternary liquid miscibility gap, experimental work could be done to explore the glass forming possibility in this system.

## REFERENCES

- [1] Kattner U. R., "The thermodynamic modeling of multicomponent phase equilibria", *JOM*, **49**(12), pp. 14-19, 1997
- [2] Pelton A. D., "Material science and technology", Thermodynamics and phase diagrams of materials, 5, Weinheim, New york, pp. 34, 46, 2001
- [3] Bettles C. J., Humble P., and Nie J. F., "The effect of trace additions on the aging behavior of AZ91E", *Proceedings of the third international magnesium conference*, pp. 403-417, 1996
- [4] Emley E. F., "Principles of magnesium technology", Pergamon press, London, pp. 879, 1966
- [5] Raynor G. V., "The physical metallurgy of magnesium and its alloys", Pergamon press, London, p386, 1959
- [6] Robers C. S., "Magnesium and its alloys", John Weily and Sons Inc., New York, pp. 101, 1960
- [7] Guangyin Y., Yangshan S., and Wenjiang D., "Effeects of Sb addition on the microstructure and mechanical properties of AZ91 magnesium alloy", *Scripta materialia*, **43**(11), pp. 1009-1013, 2000
- [8] Yamaguchi K., Yoshizawa M., Takeda Y., Kameda K., and Itagaki K., "Measurement of Thermodynamic Properties of Al-Sb System by Calorimeters", *Materials transactions, JIM*, **36**(3), pp. 432-437, 1995
- [9] Yamaguchi K., Itagaki K., and Chang Y. A., "Thermodynamic Analysis of the In-P, Ga-As and Al-Sb Systems", *Calphad*, **20**(4), pp. 439-446, 1996
- [10] Coughanowr C. A., Kattner U. R., and Anderson T. J., "Assessment Of The Al-Sb System", *Calphad*, **14**(2), pp. 193-202, 1990
- [11] Zajackowski A., and Botor J., "Thermodynamics of the Al-Sb System Determined by Vapour Pressure Measurements", *Zeitschrift fuer metallkunde.*, **86**(9), pp. 590-596, 1995
- [12] Nayeb-Hashemi A. A., and Clark J. B., "The Mg-Sb (Magnesium-antimony) system", *Bulletin of alloy phase diagrams*, **5**(6), pp. 579-584, 1985
- [13] Jönsson B., and Ågren J., "A Theoretical Evaluation of Chemical Ordering and Glass Transition in Liquid Mg-Sb Alloys", *Metallurgical transactions*, **18**(A), pp. 1395-1401, 1987

- [14] Jansson B., Ph.D Thesis, Div. Phys. Met., Royal Inst. Techn., Stockholm, Sweden, 1984
- [15] Ansara I., Dinsdale A. T., and Rand M. H., "COST 507 – Thermochemical database for light metal alloys", European Commission EUR 18499, 1998
- [16] Murray J. L., "The Al-Mg (Aluminum-Magnesium) system", *Bulletin of alloy phase diagrams*, **3**(1), pp. 60-74, 1982
- [17] Saboungi M. L., and Hsu C. C., "Estimation of Isothermal Sections of Ternary Phase Diagrams of Lithium Containing Systems", *Applications of phase diagrams in metallurgy and ceramics proceedings of workshop*, Gaithersburg, pp. 1109-1138, 1977
- [18] Ludecke D., and Hack K., "A Thermodynamic Evaluation of the Al-Mg System", *Zeitschrift fuer metallkunde.*, **77**, pp. 145-161, 1986
- [19] Saunders N., "A Review and Thermodynamic Assessment of The Al-Mg and Mg-Li systems", *Calphad*, **14**(1), pp. 61-70, 1990
- [20] Zuo Y., and Chang Y. A., "Thermodynamic Calculation Of The Al-Mg Phase Diagram", *Calphad*, **17**(2), pp. 161-174, 1993
- [21] Chartrand P., and Pelton A. D., "Critical Evaluation and Optimization of the Thermodynamic Properties and Phase Diagrams of the Al-Mg, Al-Sr, Mg-Sr, and Al-Mg-Sr Systems", *Journal of phase equilibria*, **15**(6), pp. 591-605, 1994
- [22] Moser Z., Zakulski W., Gasior W., Panek Z., Matsuda I., Fukuda Y., Iida T., Zajackowski Z., and Botor J., "New Thermodynamic Data for Liquid Aluminum-magnesium Alloys from emf, Vapor Pressures, and calorimetric Studies", *Journal of phase equilibria*, **19**(1), pp. 38-45, 1998
- [23] Czeppe T., Zakuiski W., and Bielanska E., "Study of the Thermal Stability of Phases in the Mg-Al System", *Journal of phase equilibria*, **4**(3), pp. 249-254, 2003
- [24] Liang P., Su H. L., Donnadieu P., Harmelin M., Quivy A., "Experimental investigation and thermodynamic calculaiton of the central part of the Mg-Al phase diagram", *Zeitschrift fuer metallkunde*, **89**(8), pp. 536-40, 1998.
- [25] Guertler W., and Bergmann A., "Ternary system: aluminum-antimony-magnesium", *Zeitschrift fuer metallkunde*, **25**(4), pp. 81-84, 1933
- [26] Linnebach R., and Benz K. W., "Liquid phase epitaxy of aluminum antimonide from antimony solutions", *Journal of crystal growth*, **55**(3), pp. 531-538, 1981

- [27] Lichter B. D., and Sommelet P., "Thermal properties of  $A^{III} B^V$  compounds- 1: High-temperature heat contents and heats of fusion of InSb, GaSb, and AlSb", *Transactions of the metallurgical society of AIME*, **245**, pp. 99-105, 1969
- [28] Girard C., Miane J. M., Riou J., Baret R., and Bros J. P., "Enthalpy of formation of aluminum-antimony and aluminum-gallium-antimony liquid alloys", *Journal of the less-common metals*, **128**, pp. 101-115, 1987
- [29] Batalin G. I., Sokol'skii V. E., Shimanskaya T. B., "Enthalpies of mixing liquid alloys of aluminum with magnesium and antimony", *Ukrainskii khimicheskii zhurnal*, **37**(4), pp. 397, 1971
- [30] Predel B., and Schallner U., "Thermodynamic investigation of the aluminum-antimony and aluminum-gold systems", *Material science and engineering*, **5**(4), pp. 210-219, 1970
- [31] Botor J., Dziewidek L., Zajaczkowski A., Report No. U-204/I/89, Institute of Non-ferrous metals, Gliwice, 1989 (cited in [9])
- [32] Grube G., "On the alloys of magnesium with cadmium, zinc, bismuth, and antimony", *Zeitschrift fuer anorganische chemie*, **49**(72), pp. 87-91, 1906
- [33] Grube G., and Bornhak R., "Binary diagram of magnesium-antimony", *Zeitschrift fuer elektrochemie und angewandte physikalische chemie*, **40**, pp. 140-142, 1934
- [34] Jones W. R. D., and Powell L., "The effect of antimony on magnesium", *Journal of the institute of metals*, **67**(901), pp. 177-188, 1941
- [35] Hansen M., and Anderko K., "Mg-Sb Magnesium-Antimony", in "Constitution on binary alloys", R. F. Mehl and M. B. Bever, Eds., McGraw-Hill, N. Y., (1958), pp. 915-916
- [36] Zabdyr L., and Moser Z., "Thermodynamic Studies on Mg-Sb System", *Bulletin of the Polish academy of sciences and technical sciences*, **31**(1-12), pp. 37-42, 1983
- [37] Rao Y. K., and Patil B. V., "Thermodynamic Study of the Mg-Sb System", *Metallurgical transactions*, **2**(7), pp. 1829-1835, 1971
- [38] Bolshakov K. A., Bulonkov N. A., and Tsirlin M. S., "New polymorphic transformation of  $Mg_3Sb_2$ ", *Zhurnal neorganicheskoi khimii*, **7**, pp. 1176, 1962
- [39] Egan J. J., "Thermodynamics of Liquid Magnesium Alloys Using  $CaF_2$  Solid Electrolytes", *Journal of nuclear materials*, **51**(1), pp. 30-35, 1974
- [40] Eremenko V. N., and Lukashenko G. M., "Thermodynamic properties of



magnesium antimonide", *Zhurnal neorganicheskoi khimii*, **9**(7), pp. 1552-1555, 1964

- [41] Vetter F. A., and Kubaschewski O., "Vapor pressure of magnesium over its binary liquid alloys with antimony and bismuth", *Zeitschrift fuer elektrochemie und angewandte physikalische chemie*, **57**(4), pp. 243-248, 1953
- [42] Eckert C. A., Irwin R. B., and Smith J. S., "Thermodynamic Activity of Magnesium in Several Highly-Solvating Liquid Alloys", *Metallurgical transactions*, **14**(B), pp. 451-458, 1983
- [43] Kubaschewski O., and Walter A., "Experience and results of high-temperature calorimetry of alloys", *Zeitschrift fuer elektrochemie und angewandte physikalische chemie*, **45**(9), pp. 732-740, 1939
- [44] Kubaschewski O., and Catterall J. A., "Thermodynamic data of alloys", Pergamon press, New York, 1956
- [45] Hultgren R., Desai P. D., Hawkins D. T., Gleiser M., and Kelley K. K., "Selected values of the thermodynamic properties of binary alloys", *ASM international, Metals park*, OH, pp. 1106-1108, 1973
- [46] Barin I., Knacke O., and Kubaschewski O., "Thermochemical properties of inorganic substances", supplement, Springer-Verlag, pp. 385, 1977
- [47] Ganguli A. K., Kwon Y. U., and Corbett J. D., "Three Novel Zintl Phases in the Mg-La-Sb Systems based on Intergrowth of LaSb and  $Mg_3Sb_2$ ", *Inorganic Chemistry*, **32**, pp. 4354-4359, 1993
- [48] Schuermann E., Geissler I., "Phase equilibriums in the solid condition of the aluminum- resp. the magnesium-rich corner of the ternary system of aluminum-lithium-magnesium. Part 3. Phase equilibriums in the solid condition of the binary system of aluminium-magnesium", *Giessereiforschung*, **32**(4), pp. 167-170, 1980
- [49] Goel N. C., Cahoon J. R., and Mikkelsen B., "An experimental technique for the rapid determination of binary phase diagrams", *Metallurgical transactions*, **20**(A), pp. 197-203, 1989
- [50] Guertler W., and Bergmann A., "Ternary system: aluminum-antimony-magnesium", *Zeitschrift fuer metallkunde.*, **25**(5), pp. 111-116, 1933
- [51] Loofs-Rassow E., "Microscopical and thermal examination of aluminum-antimony-magnesium alloys", *Hauszeit V. A. W. Erftwerk A. G. Aluminium*, **3**, pp. 20-32, 1931
- [52] Porter D. A., Easterling K. E., "Phase transformations in metals and alloys", First

edition, T. J. Press ltd., Great Britain, pp. 1, 1981

- [53] Dinsdale A. T., "Thermodynamic data of the elements", *Calphad*, **15**(4), pp. 317-425, 1991
- [54] Hahn T., "International tables for crystallography", Volume A- space group symmetry, Third edition, Kluwer academic publishers, 1992
- [55] "PowderCell", programmed by W. Kraus, and G. Nolze, BAM Berlin
- [56] Harikumar K. C., Ansara I., and Wollants P., "Sublattice modeling of the  $\mu$ -phase", *Calphad*, **22** (3), pp. 323-334, 1998
- [57] Kaufman L., Bernstein H., "Computer calculation of phase diagrams with special reference to refractory metals," Academic Press, New York, NY, 1970. (Cited in [52])
- [58] Nishizawa T., "Progress of CALPHAD", *Materials transactions, JIM*, **33**(8), pp. 713-722, 1992
- [59] Fries S. G., Jantzen T., "Compilation of CALPHAD formation enthalpy data binary intermetallic compounds in the COST 507 Gibbsian database", *Thermochimica acta*, **314**, pp. 23-33, 1998
- [60] "WinPhad 2.0 – Phase diagram calculation engine for binary systems," CompuTherm LLC, Madison, WI, USA, 2000.
- [61] "FactSage 5.3", Thermfact (Centre for research in computational thermochemistry), Montreal, QC, Canada, 2004.
- [62] Prince A., "Alloy phase equilibria", Elsevier publishing company, p. 66, 1966
- [63] Hillert M., "Phase transformations", American society for metals, Ohio, Chapter 5, 1970
- [64] Bergeron C. G., Risbud S. U., "Introduction to phase equilibria in ceramics", The American ceramic society, Ohio, p. 77, 1984
- [65] Ownby P. D., "Course notes: Crystallisation paths through immiscibility domes", <http://web.umn.edu/~ownby/2000%20Tutorials/>